Defining a solid approach for designing a bridge landing against fatigue

Panagiotis Moragiannis

Defining a solid approach for designing a bridge landing against fatigue

Master of Science Thesis

For the degree of Master of Science in Offshore and Dredging Engineering
at Delft University of Technology

Panagiotis Moragiannis

February 27, 2019

Graduation committee:

Ir. P.G.F. Sliggers	TU Delft – graduation chairman
Ir. C. Keijdener	TU Delft – university supervisor
Dr. Ir. K.N. van Dalen	TU Delft
Ing. R. Voets	Iv-Offshore & Energy B.V. – company supervisor

Acknowledgments

The fulfilment of this graduation thesis signifies the accomplishment of all the requirements for obtaining the Master of Science Degree in Offshore and Dredging Engineering, from the Delft University of Technology. However, besides that, it is also the end of a cycle and the beginning of a new one. It is apparent that, during this tough but instructive period, several people played an important role and their contribution deserves to be acknowledged.

First and foremost, I would like to express my gratitude to Stefan Beukers, the manager of the structural department within Iv-Offshore and Energy. He is the one who gave me the opportunity to work upon this topic and get a feeling of how it is working inside a big company. Honestly speaking, it is a unique experience that I will never forget.

I would also like to thank Richard Voets, my supervisor inside the company and the one who had the biggest impact in this thesis by means of supervising step by step all the work done. The amount of time that he spent on helping me, reviewing my work and guiding me is greatly appreciated. Moreover, I can't overlook the fact that, besides his busy daily schedule, he always found the time to be present to all the meetings that were performed at the university.

Special thanks also go to Frank Sliggers, the chairman of my graduation committee. I have to admit that I wasn't expecting that he would be involved so actively in the whole procedure. On the contrary, Frank refuted me entirely. He was not just a chairman, but mainly an essential member of the process and an endless source of inspiration and knowledge.

Many thanks also go to Chris Keijdener. He was my university supervisor and I appreciate the amount of time that he spent on my thesis. I can't neglect that, besides guiding me, he also had to fulfil his PhD studies, supervise other students and give lectures. His guidance and suggestions throughout all these months were really helpful for me and contributed to the final outcome.

It would be shame, of course, not to mention my colleagues and friends here. Regarding my colleagues inside Iv-Groep, I would like to thank them all for their help and support. Some of them were closer than others, but all deserve my respect. However, I will distinguish Denny van Soest since he became a real friend for me and I feel that he supported me significantly. Concerning my friends, both from Greece and the Netherlands, I don't want to be unfair and distinguish someone in particular. All of them supported me in the best way they could and this is highly appreciated.

Lastly, it goes without saying that my family and my girlfriend provided me the most valuable support during, not only the period of my thesis, but along the entire period of my studies overseas. There are not enough words to describe my gratitude to them. Without my family, this diploma could have never been accomplished. Their support, both economically and psychologically was more than essential. Without my girlfriend, this degree would also not be possible to be obtained. The reasons are numerous and of any kind. Just considering what she has been through for me is enough to be grateful to her for ever.

Abstract

Offshore oil and gas projects usually require the presence of more than one facilities in the same location. These facilities need to be connected with each other in order to enable the transfer of personnel among each other. As a result, bridges are implemented for such purposes with their ends being positioned at extensions of the two connected platforms, known as the bridge landings.

Such a bridge should be able to follow the excitations that are imposed at its two ends from the response of the connected platforms due to the applied environmental loads. Thus, in its longitudinal direction, the bridge should be pinned-supported at one platform and sliding-supported at the other. Such a configuration enables the bridge to adapt to the continuously varying relative movement that is induced by the motion of the two connected platforms. This results in the generation of friction at the sliding end of the bridge.

Similarly to any other offshore structure, a bridge landing should be able to withstand the maximum operating loads and its configuration should be checked against the different limit states. Although a jacket substructure is commonly analysed against the serviceability, ultimate and fatigue limit states, a bridge landing is checked against only the first two states. However, the generated friction at the sliding bridge supports results in varying stresses at the corresponding bridge landing. This indicates that the fatigue limit state should also be examined and thus investigation is required in order to highlight its significance in the design of such a structure.

This is the motivation behind the certain thesis, which intends to clarify the sensitivity of a bridge landing into the varying dynamic load of the generated friction. In order to do so, a specific case is examined, with real information about the structure and the environmental details. The analysis comprises examining three limit states (SLS, ULS, FLS), concluding into the governing one for the case of the bridge landing. The structural analyses were performed using the SACS software, which enables performing all the SLS and ULS checks. Regarding fatigue, though, the whole analysis was conducted independently, using a simplified approach that enables to deal with the issue in a quick way. This comprises the base case approach, through which assumptions are made regarding the wave and friction main characteristics.

After verifying the significance of the fatigue limit state in the design, an assessment of the base case approach follows. This is performed through the examination of the main sensitivity parameters that influence the simplified approach through which the fatigue assessment was conducted. The results of the sensitivity analyses are then incorporated in order to review the method and conclude into any possible improvements.

Finally, enhancement of the structure is examined through four different ways, aiming to turn it to be sufficient against the fatigue requirements. The improvement actions consist of improving the existing weld details, modifying the existing structure and reinforcing of members.

It should be noted that the problem was also approached through a numerical approach that was generated using the Matlab software. Through this, it was intended to capture the behaviour of friction in a more realistic way before incorporating it in the fatigue assessment, something that was not possible to be done inside SACS. However, the model didn't show rational results and thus it could not be used in the fatigue analysis. The whole procedure and theory, though, are described in detail since it is possible that they can set a useful background for further investigation.

Table of contents

List of figures

List of tables

List of symbols

Symbol	Definition
a	crack depth
β_w	correlation factor depending on steel grade
γ_f	partial action factor
γ_M	material factor
γ_{Mw}	material factor used for fillet welds
ΔK	range of stress intensity factor during a fatigue cycle
$\Delta\sigma$	stress range
$\Delta\sigma_{hot\ spot}$	hot spot stress range
$\Delta\sigma_{nom}$	nominal stress range
$\Delta\sigma_\perp$	normal to the throat plane stress range
$\Delta\tau_{||}$	shear stress range at the plane of the throat, parallel to its longitudinal axis
$\Delta\tau_\perp$	shear stress range at the plane of the throat, normal to its longitudinal axis
$\delta_{allowable}$	allowable vertical deflection
δ_{max}	maximum induced vertical deflection
μ	friction coefficient
μ_d	coefficient of kinetic/dynamic friction
μ_s	coefficient of static friction
ρ	material density
$\sigma_{\perp d}$	normal to the throat plane design stress
$\sigma_\perp{}^{flange}$	normal to the throat plane stress in the flange welds of a section
$\sigma_\perp{}^{web}$	normal to the throat plane stress in the web welds of a section
σ_{M_y}	normal stress due to the applied moment over the y-axis
σ_{M_z}	normal stress due to the applied moment over the z-axis
$\sigma_{hot\ spot}$	hot spot stress
$\sigma_{nominal}$	nominal stress
σ_{tot}	total applied normal stress
σ_{vM}	von Mises resultant stress
τ	shear stress
$\tau_{||}$	design shear stress in the throat plane, parallel to the longitudinal axis of weld
$\tau_{||}{}^{flange}$	shear stress in the throat plane of flange welds, parallel to the weld axis
$\tau_{||}{}^{web}$	shear stress in the throat plane of web welds, parallel to the weld axis
$\tau_{||}{}^{y-welds}$	shear stress on the welds along the y-axis of bearing pad, parallel to the weld axis
$\tau_{\perp d}$	design shear stress in the throat plane, perpendicular to the longitudinal axis of weld
$\tau_{\perp d}{}^{flange}$	shear stress in the throat plane of flange welds, perpendicular to the weld axis
τ_{yz}	shear stress in the y-z section plane
A	cross section area
A_{HEA}	area of the certain HEA section
A_f	area of flange welds

A_{flange}	area of section's flange
A_{plate}	area of plate
A_{tot}	area of total section or total area of weld
A_w	area of web welds
A_y	area of the welds along the y axis of the bearing pad
a_f	throat size of fillet welds used in the flange connections
a_w	throat size of fillet welds used in the web connections
a_y	throat size of fillet welds used along the y axis of the bearing pad
b	section width
b_{HEA}	width of the certain HEA section flange
b_{flange}	width of section's flange
b_{plate}	width of plate
C	material constant
C_s	shape coefficient
CoG	center of gravity
D	accumulated fatigue damage or diameter
DFF	design fatigue factor
da/dN	crack growth rate
E	Young's modulus of elasticity
F_{app}	applied force
F_c	Coulomb friction force
F_N	normal force
F_{wind}	wind load
F_x	axial force
F_y	horizontal shear force
F_z	vertical force
FLS	fatigue limit state
Fr	friction force
Fr_{kin}	kinetic friction force
Fr_{max}	maximum static friction force
$Friction$	friction force
f_u	ultimate tensile strength
$HSSR$	hot spot stress range
H_C	characteristic wave height
H_s	significant wave height
h	section height
h_{HEA}	height of the certain HEA section
h_{bridge}	bridge height
$\log \bar{a}$	characteristic of a certain S-N curve
I_t	torsional moment of inertia of a section over its centroid axis
I_t^{HEA}	torsional moment of inertia of the certain HEA section over its centroid axis
I_t^{plate}	torsional moment of inertia of plate over its centroid axis
I_y	moment of inertia over y-axis

I_y^{HEA}	moment of inertia of the certain HEA section over its y centroid axis
I_y^{flange}	moment of inertia of flange over its y centroid axis
I_y^{plate}	moment of inertia of plate over its y centroid axis
I_z	moment of inertia over z-axis
I_z^{HEA}	moment of inertia of the certain HEA section over its z centroid axis
I_z^{flange}	moment of inertia of flange over its z centroid axis
I_z^{plate}	moment of inertia of plate over its z centroid axis
$I_u(z)$	turbulence intensity at elevation z
$\underline{\underline{K_{coef}}}$	stiffness coefficients matrix
k	characteristic of a specific detail class
k_v	viscous coefficient
l_f	length of the welds used in the flanges of a section
l_{seg}	segmented length
l_w	length of the welds used in the web of a section
l_y	length of the welds used along the y axis of the bearing pad
M_t	torsional moment
M_y	bending moment over the y-axis
M_z	bending moment over the z-axis (out-of-plane)
m	material constant / characteristic of a certain S-N curve
N	number of cycles until fatigue failure
n	number of applied cycles during service life
ODE	ordinary differential equation
$PTFE$	Polytetrafluoroethylene (synthetic polymer)
q_{wind}	distributed vertical load due to wind
$q_x(x,t)$	axial distributed load
r	weld grounding radius or distance of a location from the section's CoG
SCF	stress concentration factor
SLS	serviceability limit state
T_C	characteristic wave period
T_p	peak wave period
T_z	mean zero-crossing wave period
t	thickness
t_0	time period for basic mean wind speed
t_f	thickness of section's flange
t_{plate}	plate thickness
t_{ref}	reference thickness
t_w	web thickness
$U(z)$	1-hour mean wind speed at elevation z
U_0	1-hour mean wind speed at 10 m above mean sea level
ULS	ultimate limit state
$u(x,t)$	longitudinal deformation at position x and time t
$u(z,t)$	wind speed at elevation z for an average time period t

$u_{pin}(t)$	horizontal excitation of the pinned end
$u_{slid}(t)$	horizontal excitation of the sliding end
V	vertical force
v_r	relative sliding velocity between two surfaces
v_s	Stribeck velocity
W	width of the continuous member in a crossing point of two members
Y_{CoG}	y-coordinate of center of gravity with respect to the specified system of axes
y_{rel}	relative displacement
y_{rel}^{limit}	relative displacement resulting in the maximum static friction
y_{rel}^{max}	maximum relative displacement induced in a wave cycle
Z_{CoG}	z-coordinate of center of gravity with respect to the specified system of axes
z	elevation
z_f	leg size of fillet welds used in the flange connections
z_w	leg size of fillet welds used in the web connections
z_y	leg size of fillet welds used along the y axis of the bearing pad
$O(l_{seg}^2)$	truncated error

1 Introduction

1.1 Problem introduction

The facilities that are required for the exploration, extraction, storage and process of hydrocarbons in an offshore environment usually consist of a number of units. These units are often spread into more than one platforms. In such a case, the multiple structures need to be connected, allowing the transfer of personnel and equipment between each other.

This is something that is achieved through the construction of bridges in between. Such steel bridges are single-span and mainly of truss type. Their ends are supported at the two connected platforms, whereas their length is usually more than 30 meters. In order to accommodate the bridge supports, extension of the connected platforms, at the level of the bridge base, is required. This comprises the so-called bridge landing, having the purpose to facilitate the supports of the bridge.

Regarding the type of the supports, it should be noted that these need to comply with the kinematic requirements that are imposed by the connected platform movements. Due to the environmental loads applied, the two platforms deform, resulting to certain imposed displacements at the supports of the bridge. As a result, the bridge needs to be able to follow these induced deformations, something that is performed through its supports. Hence, its one end is usually sliding supported, being able to accommodate the induced platform deflections in the longitudinal to the bridge direction while the other one is pinned supported in order to allow for some horizontal rotation. Figure 1-1 provides a typical illustration of the bridge support points that are located at the two bridge landings.
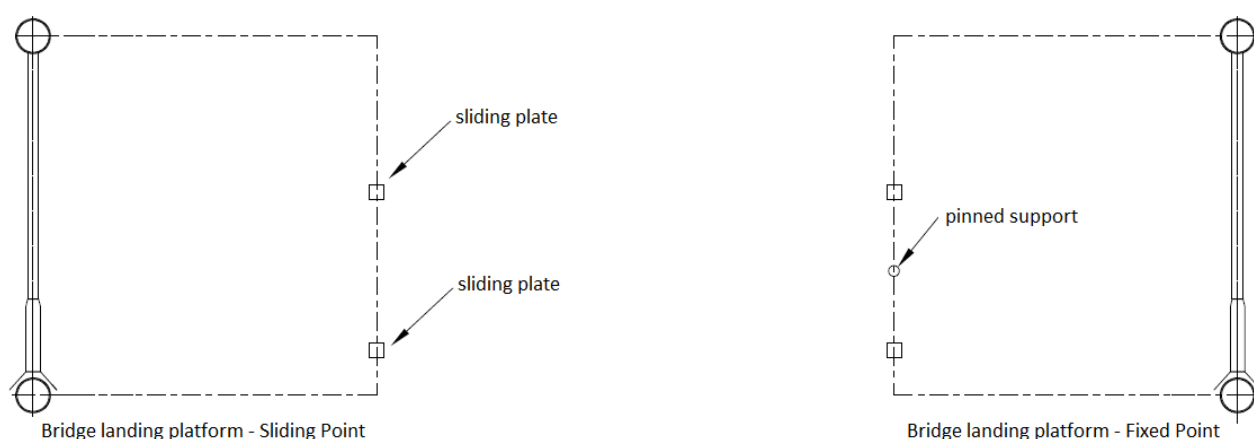
Figure 1-1 – Bridge supports at the two bridge landings

1.2   Problem description

Consequently, the bridge landing should be able to withstand a number of loads, applied directly or transferred through the bridge. More specifically, these consist of dead, live and wind loads acting on the bridge and the landing. Besides these, there is also a generated friction load that acts on the interface between the bridge's sliding end and the corresponding landing, induced by their relative movement.

The friction load is not a static one. Its magnitude and direction vary continuously, depending on the connected platform deflections. Therefore, friction generates varying stresses at the bridge landing members and due to that fatigue damage is induced. Whether such accumulated damage is able to cause the failure of a member or not is something that depends on the specific case conditions and needs to be examined through a fatigue analysis.

Normally, a fatigue analysis is conducted for the entire substructure due to the applied environmental loads, but not for the examination of the bridge landing due to the generated friction. The specific case that will be investigated in the certain thesis seems to be prone to that issue and thus particular attention needs to be paid on the design of the bridge landings against fatigue.

1.3   Organization and scope of the thesis

The present graduation thesis is related to a real situation and its targets are practical and very specific. The whole investigation lies in examining the bridge landing of an existing platform and conclude into any recommendations regarding its current design, mainly focused to its fatigue strength. The analysis consists of examining the bridge landing against the ultimate, serviceability and fatigue limit states. However, the main focus is on the fatigue assessment due to the varying generated friction load at the sliding supports of the bridge, which is the driving force of the thesis.

The fatigue assessment of the bridge landing is first performed in a simplified and quick way, making several assumptions for the incoming wave loading. This will form the "base case" and its amount of conservatism, or not, will be determined after examining the effect of the following sensitivity parameters:

- directionality of the incoming wave
- the coefficient of friction to be used

After having analysed the effect of the main influencing parameters, possible improvements in either the weld or the construction details of the landing configuration will be concluded, wherever this is feasible. Consequently, design recommendations for the specific configuration will be derived.

It should be noted that in the above described analysis, the friction load is considered to be of a constant magnitude. This is not reality and forms an assumption that was made for the sake of

simplicity. The actual behaviour of friction is a much more complicated phenomenon, since it has neither a constant magnitude nor a constant friction coefficient. These comprise also points that were investigated in the certain thesis.

1.4 Objectives

The goals of the thesis can be summarized in the following:

- Review the existing simplified method of analysis concerning the fatigue design of the bridge landing structure
- Derive possible recommendations for improving the existing methodology and verify its level of applicability
- Strengthen the structure to be adequate against the fatigue requirements

In order to achieve the above-mentioned goals, several key steps were followed. These are:

- Reassess the structure against the serviceability and ultimate limit states
- Perform a fatigue analysis following the simplified methodology
- Examine the sensitivity of the main parameters that influence the method that was followed
- Incorporate the main characteristics of friction in the fatigue assessment
- Review the weld and construction details of the structure in order to finally improve its behaviour

1.5 Thesis outline

In this section, a brief description of the thesis' structure is provided. The investigation begins with explaining the theory behind fatigue design and the main parameters that influence it, in chapter 0. The two different methods that can be followed are described, with the main focus being on the S-N curves approach which is the one that was followed in this case. The chapter ends with a reference to the main types of welded connections that can be encountered and their influence on the fatigue strength of a detail.

Chapter 3 introduces the characteristics of the bridge landing structure that was examined during this thesis. Its detailed configuration, member properties and the different acting loads considered are demonstrated. The section ends with a list of the different states to be examined and the codes to be followed for that purpose.

In chapter 4, examination of the serviceability and the ultimate limit states is performed. The multiple loads and load combinations are demonstrated and their derivation is described in detail. The structural analysis was conducted by using the SACS software and the final results for the two limit states are presented. Finally, the strength of the fillet weld connections need also to be checked, forming the last part of this chapter.

After showing that the present structure is adequate against the ultimate and serviceability limit states, its fatigue assessment is performed in chapter 5. This is performed through a simplified approach the assumptions of which are listed in the beginning of the section. The different locations that were examined are highlighted and the classification of the most sensitive details is explained. Finally, the results of the fatigue assessment are listed, indicating the inadequate locations of the bridge landing for which the criterion is not satisfied.

Having performed the fatigue analysis through the method described, an assessment of the main parameters that influence the design follows. This is performed in chapter 6 and concerns the directionality of the incoming wave and the friction coefficient value. Regarding the coefficient of friction, reference is also made in the specifications of manufacturer's commercial brochure regarding sliding bearing pads, whereas when examining the directionality issue the fundamentals of friction load are incorporated in the analysis.

Chapter 7 consists of examining 4 different options to improve the structure's fatigue behaviour. First, improvement of the existing welds is examined, in order to identify what is the maximum improvement that can be achieved through achieving the best possible detail category per location identified. The second option concerns modifying the existing layout of the structure through the addition of new members in such a way that the applied stresses would be reduced in the inadequate locations. The last two options comprise strengthening the section of the member where the fatigue requirement was not satisfied. This is done in two ways, by welding a plate at the beam's top flange and by welding a plate vertically to the two flanges of the section. The required plate dimensions are determined for both these options.

Chapter 8 is dedicated into the numerical model that was created to derive the applied friction load with time, as a result of the applied induced displacements at its two support points. This was done by considering the bridge as an one-dimensional continuous rod member. The section begins with describing the actual behaviour of friction and listing some friction models that have been generated so far by other researchers. A detail description of the numerical approach that was applied follows, with the obtained results being listed and commented.

The conclusions that were derived from the analysis are presented in chapter 9. This consists of remarks upon the different limit states examined, the sensitivity analysis performed and the improvement options that were studied. Finally, recommendations upon the way to effectively conduct the fatigue analysis of the bridge landing are derived.

The overview of the thesis is also demonstrated in the block diagram that follows.

Chapter 2

- Theoretical background of fatigue design
- The design approaches
- Local stress concentration
- Damage calculation
- Acceptance criteria
- Weld types

Chapter 3

- Layout of examined situation
- Member sections
- Concerning loads
- Limit states to be examined

Chapter 4

- Software used for structural analysis
- Material properties
- Design codes
- Calculation of acting loads
- SLS, ULS load combinations
- SLS and ULS results

Chapter 5

- Assumptions of the base case approach
- Critical locations to be examined
- Applied stress ranges
- Classification of details
- Fatigue assessment

Chapter 6

- Review of base case through sensitivity studies
- Sensitivity 1: friction coefficient
- Sensitivity 2: Wave directionality

Chapter 7

- Improve structure's fatigue behaviour
- Option 1: weld improvements
- Option 2: modify the structure
- Option 3: Section reinforcement 1
- Option 4: Section reinforcement 2

Chapter 8

- Actual behaviour of friction
- Different existing numerical models
- The numerical model generated
  - Purpose and description
  - Approach and equations
  - Results

Chapter 9

- Conclusions
- Recommendations
- Study proposals

2 Theory of Fatigue Design

In this section, the theory behind the fatigue assessment of a structure is provided. This comprises listing the different applicable methods, the main parameters that influence the analysis and the criteria that determine whether a structure is adequate against fatigue or not.

Fatigue is a phenomenon related to crack propagation due to applied dynamic loads. Cracks may initiate as a result of an applied static force and are not necessarily a problem for a structure's integrity. Under a cyclic load, though, cracks grow due to continuous variations in the applied stresses. This growth can reach a limit, after which the amount of degradation results into failure of the specific detail. This material degradation is stated as cumulative damage when designing against fatigue.

Fatigue is a mechanism that depends on the variation of the applied stresses rather than on their maximum value. According to this, a section may fail under stresses much lower than its yield limit, after a certain number of load cycles, as can be seen in the Figure 2-1 below. Therefore, unlike the Ultimate Limit State, designing against fatigue is independent of the material yield strength and the grade of steel used.
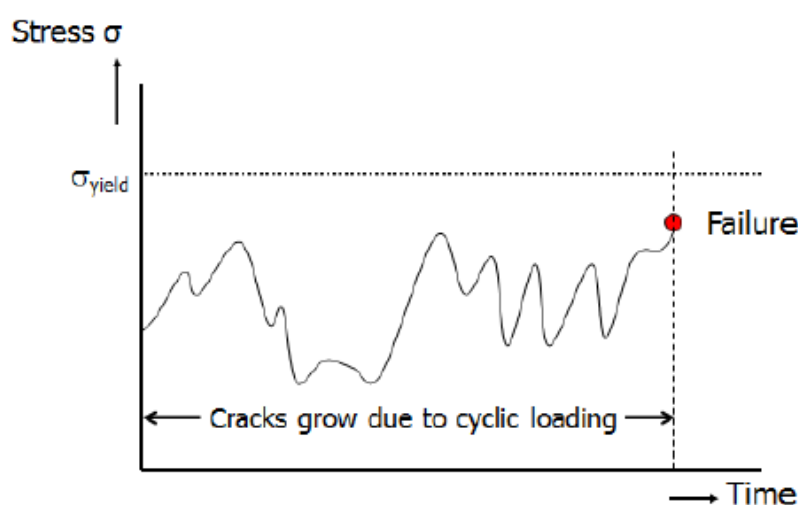
Figure 2-1 – Time-varying stress until failure [5]

Fatigue depends on the following main parameters:
- amount of stress ranges applied due to the applied dynamic load
- number of applied stress cycles
- local details characteristics (member connection details)

It should also be noted that fatigue is a highly localized phenomenon and not any location in a structure is sensitive to it. The most prone locations are areas with material or geometric discontinuities, where high stress concentrations are generated. These mostly consist of:

- welded connections
- locations with abrupt changes of the section geometry
- hole positions

2.1 The different approaches

Designing against fatigue can be performed in two ways, as the relevant codes and guidelines propose. These are:
- the fracture mechanics approach
- the S-N curve method

2.1.1 Fracture mechanics approach

This approach is based on fracture mechanics and utilizes the Paris' crack propagation law in order to define the crack growth due to the applied stress variation. This method is more complicated due to its dependence on the characteristics of the crack itself (crack geometry, length). It is expressed through the following equation [1], [27]:

$$\frac{da}{dN} = C \cdot \Delta K^m$$

where: a is the crack depth, in $[m]$

N is the number of cycles to failure [-]

da/dN denotes the crack growth rate (the crack growth in a load cycle), in $\left[m/cycle\right]$

C is constant dependent on the material, in $\left[\frac{m}{cycle \cdot MPa \cdot \sqrt{m}}\right]$

m is material constant [-]

ΔK is the range of the stress intensity factor during the fatigue cycle, in $\left[MPa \cdot \sqrt{m}\right]$

2.1.2 The S-N curve method

This is the most frequently used method when performing a fatigue analysis and is the one that was followed here as well. The reason why it was chosen proceed with this approach lies in its ease of applicability and understanding. The amount of research upon this method has set a clear approach regarding fatigue, which is well described in the different corresponding codes like DNV RP-C203 [1] and part 1-9 of Eurocode 3 [6].

Fatigue design according to the S-N curves method is based on predefined curves that relate the magnitude of the applied stress range (S) with the number of load cycles (N) that a certain detail can withstand per stress range level. These curves have been defined by using experimental data from representative cyclic load fatigue tests for multiple classes of welded plated and tubular connections. These tests were performed by using a constant amount of stress range until crack failure was reached for the examined specimen. Crack failure can be encountered in different

modes (through the weld root, through the weld toe or into the base material) and is defined as an extensive amount of crack growth that is reached. The results are plotted in logarithmic scale, as depicted in Figure 2-2. It should be noted that, inside the DNV standard [1], distinction is made between the S-N curves to be used for details in air and inside the seawater.
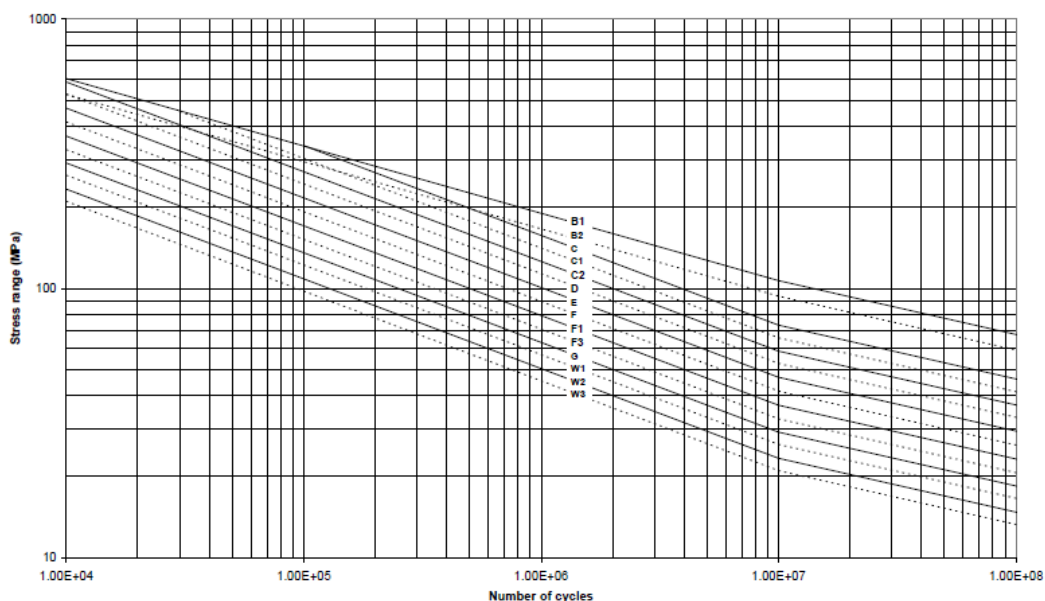
Figure 2-2 – Typical S-N curve for details in air [35]

The classification of the details into different categories depends mainly on its configuration, but also on the applied stress direction and the type of inspection. All the S-N curves are represented by the following form of equation:

$$\log N = \log \bar{a} - m \cdot \log \Delta\sigma$$

where: N: is the number of cycles that lead to failure of the detail for the stress range Δσ
$\log \bar{a}$ and m: are characteristics of the certain curve
$\Delta\sigma$: is the applied stress range (in MPa)

The above formula for the S-N curves does not take into account the thickness of the welded plate. This can be incorporated by using the following expression:

$$\log N = \log \bar{a} - m \cdot \log \left(\Delta\sigma \left(\frac{t}{t_{ref}} \right)^{k} \right)$$

in which: t is the plate thickness inside which the crack will grow ($t \geq t_{ref}$)
t_{ref} is a reference thickness dependent on the type of the connection (i.e. welded plate, tubular joint, bolted connection)
k is a characteristic of the specific detail classification

As can be seen from the shape of the S-N curves, they don't have a constant slope. Depending on the specific code (DNV, Eurocode 3, IIW), there is one or two points where the slope changes. The position of this point(s) is defined at a certain number of cycles value (N) defined by the certain code. According to DNV, the slope changes at one point (knee point), specified at 10^7 cycles. This point also serves as an indication of when a detailed fatigue analysis can be omitted and is called the fatigue limit. It should be noted that the fatigue limit should be reduced, based on the design fatigue factor (DFF) to be applied for the specific case. The amount of this reduction is $DFF^{-0.33}$ [1].

If all the stress ranges defined are below the fatigue limit stress, then it can be assumed that the applied stress ranges will not result in fatigue failure for the examining detail, independent of the applied number of cycles. Hence, no further analysis is required and the fatigue assessment can stop at that point. On the other hand, if at least one of the defined applied stress ranges is above that limit, a detailed fatigue assessment must be performed, considering all applied stress ranges (even the ones below that limit). These two occasions are illustrated at the next figure.
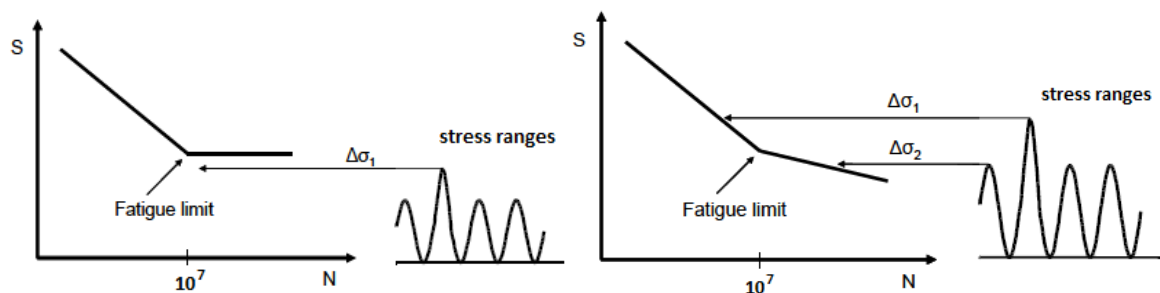
Figure 2-3 – When performing a detailed fatigue analysis can (left) and cannot (right) be omitted [1]

2.1.3   Safety factors

The exact methodology and any specifications may have small differences depending on the design code to be followed, like DNV [1], ISO [27] or Eurocode 3 [6]. Similarly to the other limit states, a safety factor is considered when designing against fatigue as well, in order to reduce the probability of fatigue failure. According to the DNV provisions, this is achieved through the design fatigue factor (DFF) and is specified based on the significance of each component examined. It can be taken into account through either the calculated damage or the derived fatigue life [2].

2.2   Local stress concentration

It has already been mentioned that fatigue is a local phenomenon and that the most sensitive locations are the ones where high stress concentrations are developed. The S-N curves methodology depends on the amount of the applied stress range on the examined detail. In order to properly define the stress range applied in the local detail under consideration, it is important that the local stresses are determined properly.

This means that the local geometry of the detail needs to be considered in the calculation of stresses. This can be achieved through the application of a stress concentration factor (SCF) to magnify the nominal stresses and finally derive the hot spot ones. Nominal stresses are the ones derived by classical beam theory, without taking into account any local geometrical properties of the detail. The hot spot stresses are the ones to be considered for the fatigue design, thus the ones to be considered in the S-N curve of the specific detail. The relation between hot spot and nominal stresses is illustrated in the Figure 2-4 below and is defined through the following equation.

$$\sigma_{hot\ spot} = SCF \cdot \sigma_{nominal}$$
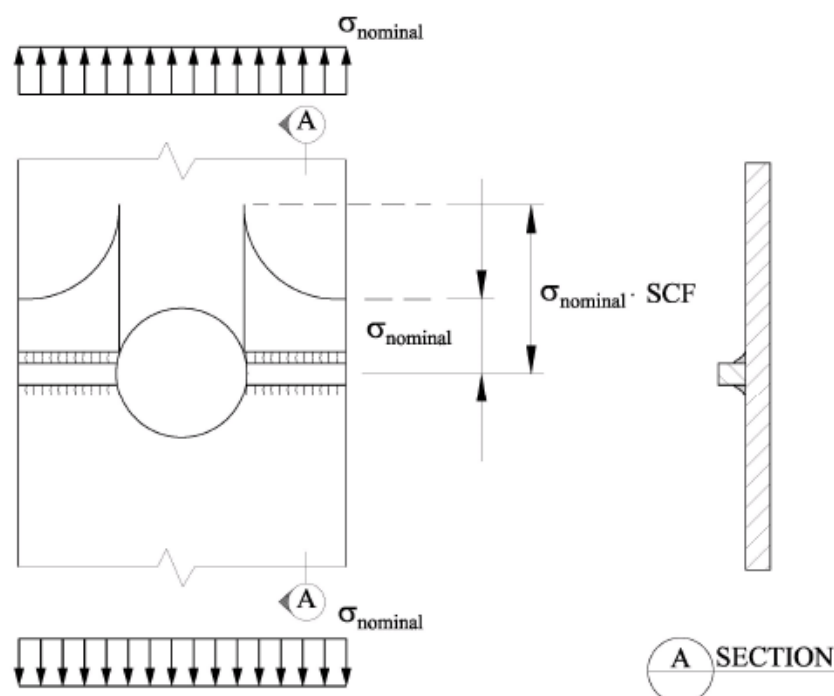
Figure 2-4 – Nominal and hot spot stress in a local detail [1]

Calculation of the stress concentration factor to be applied depends on the characteristics of the detail and is specified according to the code that is followed through parametric equations. These are defined for both plated structures and tubular connections. Another way of defining the local stresses is through finite element analysis. Figure 2-5 illustrates the difference between the local detail stresses in a welded joint and the nominal one. These refer to the weld toe position (hot spot), where a gradual increase of the nominal stress is expected due to the geometric discontinuity (geometric or structural stress). Moreover, an additional stress rise is observed at the corner of the weld (notch), due to the profile and the local geometry of the weld itself. The last type of stress increase is incorporated into the S-N curves and don't need to be considered in the stress range calculation.
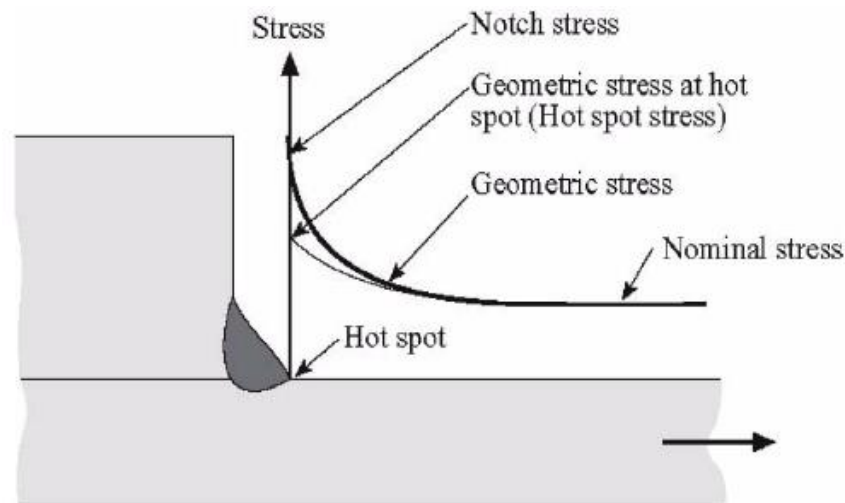
Figure 2-5 – Local stresses in a weld detail

2.3   Fatigue damage assessment

Having determined the stress ranges, the applied number of cycles and the cycles until failure at a specific stress range, the expected degradation of the detail can be defined. This is characterized by the accumulated fatigue damage induced. In order to compute this amount of damage, the so called Palmgren-Miner rule is applied. The damage can be defined by linearly combining the impact of each stress range level defined. The following formula demonstrates this.

$$D = \sum_{i=1}^{k} \frac{n_i}{N_i}$$

where: D is the accumulated fatigue damage

k is the number of different stress ranges ($\Delta\sigma_i$) considered

n_i is the number of applied cycles for the stress range $\Delta\sigma_i$

N_i is the number of cycles of stress range $\Delta\sigma_i$ that results to failure

If the fatigue damage is defined, the corresponding fatigue life can easily be derived, by:

$$fatigue\ life = \frac{service\ life}{D}$$

where D corresponds to the damage induced for the service life considered

2.4   Acceptance criteria

According to the S-N curve method for examining fatigue, the requirements for determining whether a structure is adequate or not concern the following:

- If all the applied stress ranges ($\Delta\sigma$) are below the fatigue limit of the examined detail (reduced by $(DFF)^{-0.33}$), then the detail can be considered to be adequate against fatigue. Thus, the FLS for a detail is satisfied if: $\Delta\sigma < fatigue\ limit \cdot (DFF)^{-0.33}$.

- If at least one of the several applied stress ranges is above the fatigue limit of the examined detail, then the accumulated damage of the detail must be calculated (as described in section 2.3), in order to derive a conclusion. A detail is identified to be sufficient when: $D \cdot (DFF) < 1$.

- An alternative in checking the accumulated damage of a detail is through comparing the resultant fatigue life with the service life of the structure. The requirement is satisfied if: $fatigue\ life > (service\ life) \cdot (DFF)$

2.5 The main types of welded connections

Welded connections are the most common type of connection in the offshore industry. Nevertheless, they form sensitive locations by means of fatigue resistance. Therefore, a brief description of the most commonly used types of them seems to be worthwhile to be stated in the present section.

The two most frequent welding joint types are butt and tee joints. These also comprise the types of welding joints encountered in the problem of the present thesis, hence the description is limited into these two types only.

2.5.1 Butt welds

A butt weld can be simply described as a welded connection of two members side by side. Different kinds of butt welds exist, distinguished by the type of weld preparation, such as square, V-type, bevel, U-type, or J-type ones. Figure 2-6 illustrates the different types of butt welds [8].

Single bevel butt weld   Double bevel butt weld

Single V butt weld   Double V butt weld

Single J butt weld   Double J butt weld

Single V butt weld   Double V butt weld
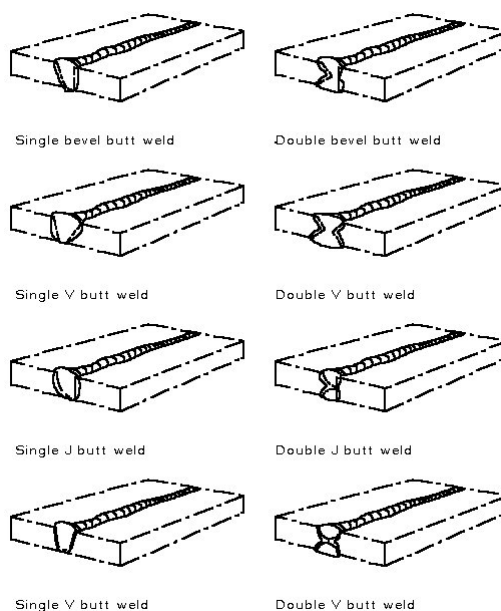
Figure 2-6 – Different types of butt welds

2.5.2 Fillet welds

Fillet welds are tee joint welds, connecting two members perpendicular or at an angle to each other. They can be single or double-sided and are characterized by their leg or throat dimension. Figure 2-7 depicts a typical fillet weld and its main characteristics.

Leg length = $\sqrt{2}$ x Throat thickness
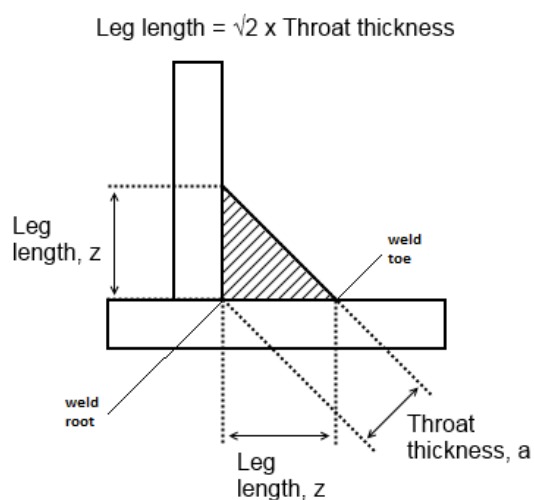
Figure 2-7 – A typical fillet weld [9]

2.5.3 Weld symbolism

Each weld is characterized by a certain symbol in a technical drawing. The main symbols for the butt and fillet ones are presented in Figure 2-8.

◸	Fillet weld
‖	Square Butt
V	Single V Butt
U	Single U
⌐	Single Bevel Butt
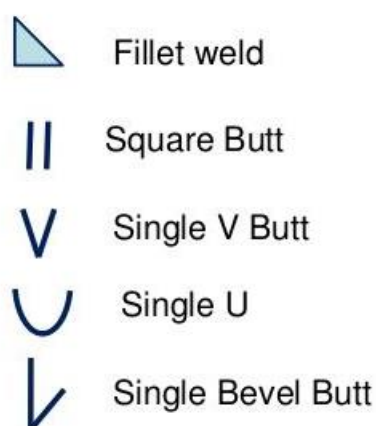
Figure 2-8 – Symbols used for butt and fillet welds [36]

2.5.4 Influence of weld characteristics on fatigue strength

From a fatigue point of view, the type of weld that is used to perform a connection of two members influences its fatigue strength. The weld details determine the classification of the detail and thus the appropriate S-N curve and the amount of stress concentration to be applied at that location. The main weld characteristics that have impact on the fatigue strength are the following:

- direction of loading with respect to direction of welding: Welds loaded at their transverse direction are expected to have larger fatigue strength than the ones that are loaded parallel to their longitudinal direction

- continuity of weld: Continuous welds are stronger than those that have intermediate gaps

- smoothness of transition: The smoother the weld transition is, the smaller the amount of stress concentration that is generated. A smooth weld end transition can be achieved by locally grinding the weld or by smoothing it through hammer peening. Figure 2-9 shows such a smooth weld transition at cruciform joint weld connection

- level of penetration: Partial penetration welds result in smaller fatigue strength than the full penetration ones

- number of sides welded: Double-sided welds enhance the fatigue strength of the detail and have better fatigue characteristics than one-sided welds
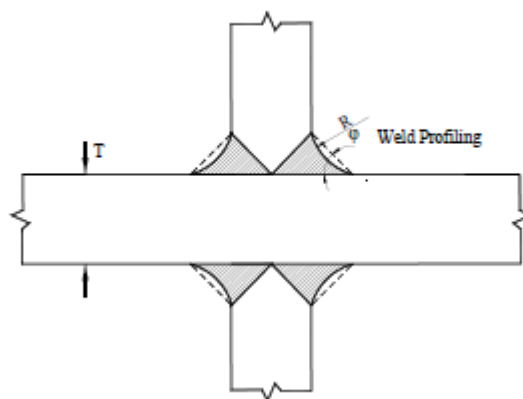
Figure 2-9 – Example of smooth weld transition [1]

3 The specific case

Inside this thesis, an actual case was examined. This consists of the bridge landing design of an existing offshore platform. The main platform is a 6-leg one, located in southern North Sea and is connected with another platform through a single-span truss bridge.

3.1 Detailed configuration

The support system of the bridge differs among its 3 principal directions (horizontal longitudinally to the bridge, horizontal transverse to the bridge and vertical directions), thus it needs to be specified for each direction individually:

  a) vertical direction: The bridge is vertically supported at 4 points, 2 at each of its ends located at the connected platforms

  b) horizontal longitudinally to the bridge: In the horizontal plane, the bridge should be able to follow the horizontal deformations induced by the relative movements of the connected platforms due to the applied environmental loads. For this reason, its one end's supports are free to slide in the longitudinal bridge direction, whereas its other end is pinned supported in order to allow for some rotation in the horizontal plane

  c) horizontal transverse to the bridge: In its transverse direction, the bridge is supported at all its 4 end points

The supports of the bridge are located at an extension platform of the main facility, which is known as the bridge landing. The bridge sliding supports consist of bearing pads, in order to reduce the generated friction, whereas at the other bridge landing, the pin connection is formed through a pivot at an intermediate point between the two end support points at that location. Figure 3-1 below illustrates a layout of the two bridge landings, the sliding and the pinned one. Their main dimensions as well as the bearing locations are depicted.
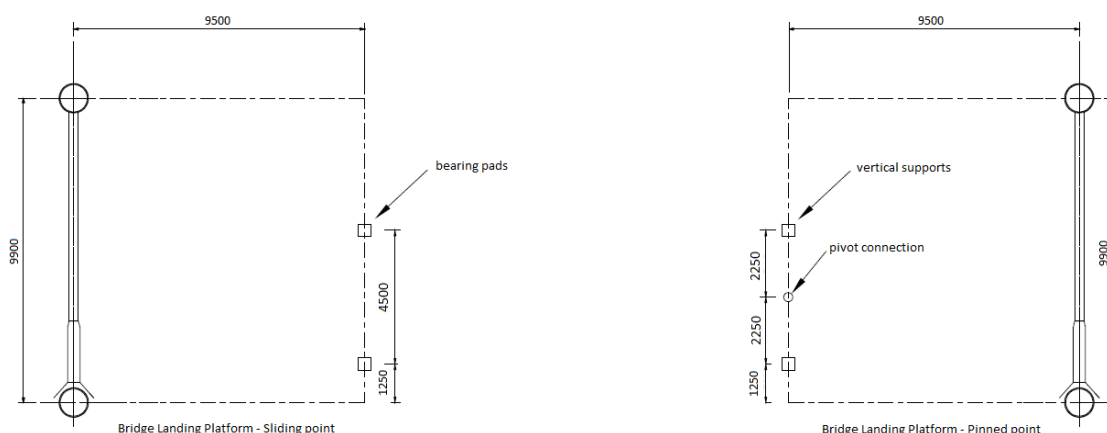
Figure 3-1 – Layout of the two bridge landings

The bridge landing that is examined in this thesis is the sliding one, in which the bearing pads are placed and friction is generated. The following figures demonstrate the detail configuration of this bridge landing, that will be examined from now on.
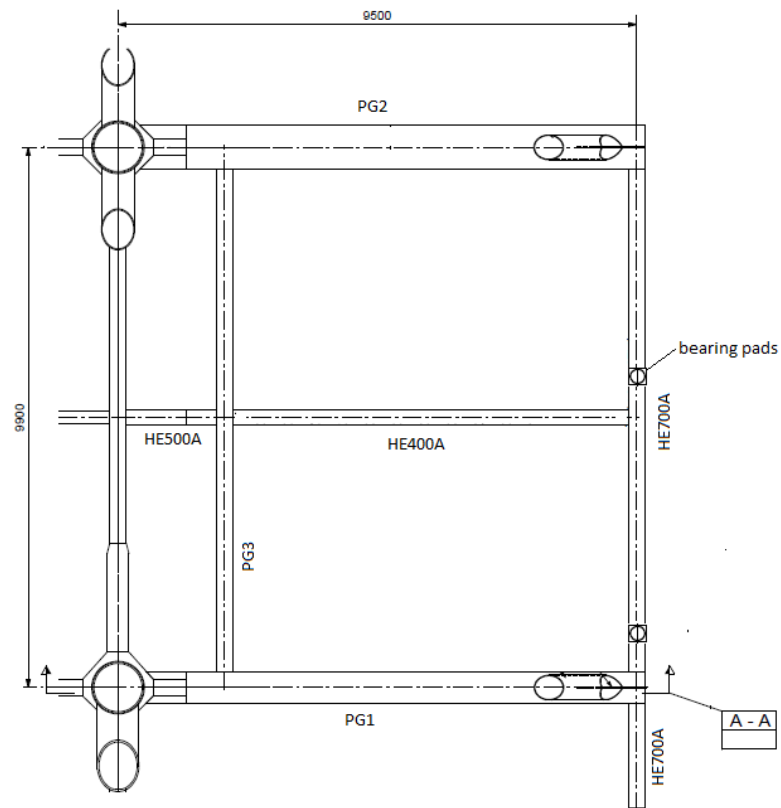
Figure 3-2 – Top view of the bridge landing
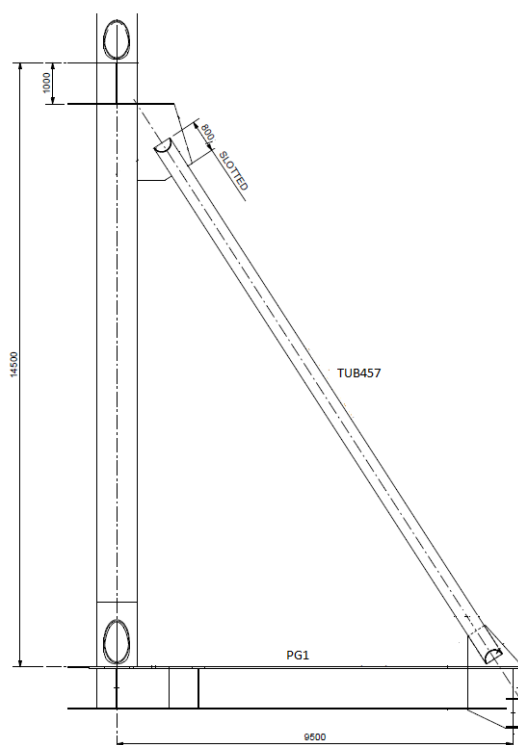
Figure 3-3 – Section A-A of bridge landing

Table 3-1 below lists the main dimensions of the member sections that are used in the bridge landing configuration, where the symbols are explained in Figure 3-4.

Table 3-1 – Member cross section details

Section label	Section type	h [mm]	b [mm]	t_w [mm]	t_f [mm]	D [mm]	t [mm]
PG1	plate girder	1000	600	20	30	-	-
PG2	plate girder	1000	800	20	30	-	-
PG3	plate girder	1000	300	20	30	-	-
HE400A	wide flange	390	300	11	19	-	-
HE500A	wide flange	490	300	12	23	-	-
HE700A	wide flange	690	300	14.5	27	-	-
TUB457	tubular	-	-	-	-	457	10
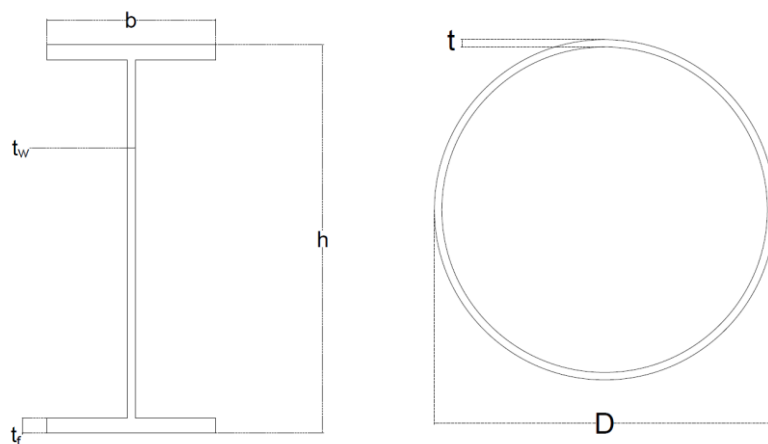
Figure 3-4 – Wide flange (left) and tubular (right)member sections

Regarding the structural configuration of the bridge landing, it is considered to be fixed to the main platform at the corresponding joint locations. The whole landing was modelled in SACS [3] in order to perform a structural analysis. The following figures illustrate the structural model of the structure, as it was derived from the SACS software. Figure 3-5 comprises a 3D view of the model with the member sections labelled, whereas in Figure 3-6 the end supports of the structure are indicated.
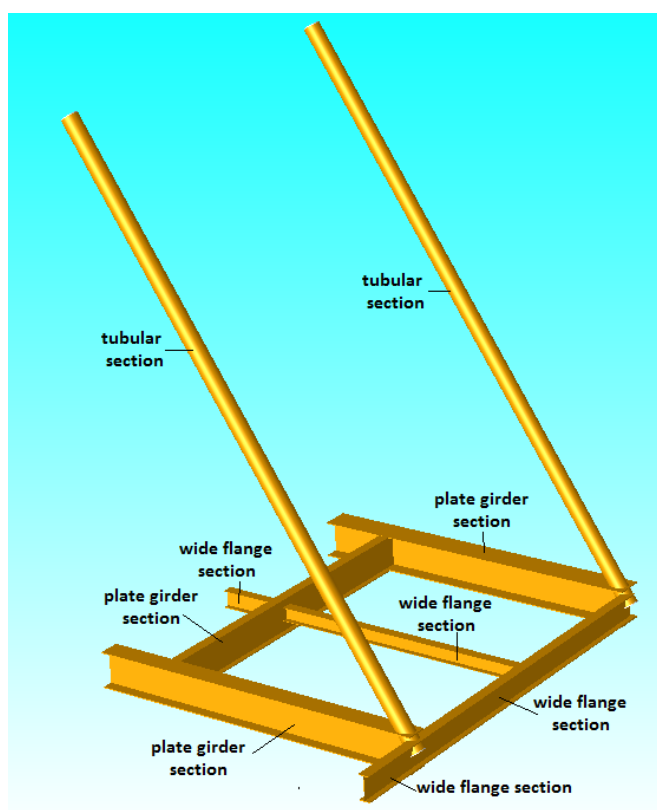
Figure 3-5 – 3D model with member section type labels
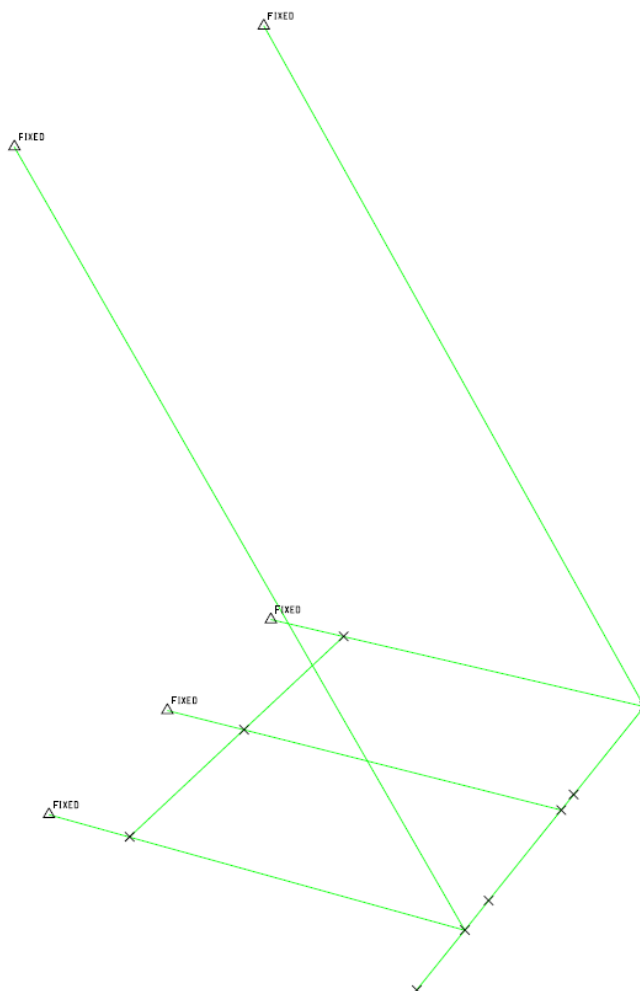
Figure 3-6 – SACS structural model with indication of its end supports

3.2 The multiple acting loads

A bridge landing is exposed to a number of loads. These consist of the following:

1) loads transferred from the bridge through its supports
2) loads directly applied at the bridge landing
3) the friction load that is generated between the sliding end of the bridge and the corresponding landing

All these loads must be combined accordingly, resulting in multiple load cases that will be considered for the required analyses.

3.2.1   Loads transferred from the bridge to the bridge landing

Regarding the loads acting on the bridge, a distinction can be made among the different load directions and the corresponding reaction forces that will be the transferred at the support locations of the bridge with the landing. These concern the following:

i.   The vertical loads that will be transferred to the 2 landings through the 4 bridge supports. These comprise the dead weight loads of the bridge (structural, appurtenance and equipment weight) and the live load acting on it

ii. The horizontal loads applied in the longitudinal to the bridge direction. These are all transferred at the pinned end support

iii. The horizontal loads applied in the transverse to the bridge direction. These are transferred at both bridge landings through their supports and consist of the applied wind force in the transverse direction of the bridge

3.2.2   Loads directly applied at the bridge landing

Regarding the loads acting on the bridge landing, a distinction can be made based on their directions. These consist of:

i.   The vertical loads of the landing's own weight and the live load acting on it

ii. The longitudinal to the bridge horizontal loads that are applied at the landing, consisting of the wind load at that direction

iii. The transverse to the bridge direction loads applied at the landing. These consist of the wind load acting at that direction

3.2.3   The generated friction load

Regarding the friction load that is generated between the sliding end of the bridge and the corresponding landing, this acts at the locations of the two sliding bearings. It opposes the relative motion between the two connecting platform facilities, which is mainly induced from their excitation due to the applied wave load. Friction acts at the longitudinal to the bridge direction, the direction that sliding is performed.

3.3   The situations to be examined

In order to check the bridge landing configuration, multiple limit states should be examined. Specifically, the serviceability (SLS), the ultimate (ULS) and the fatigue (FLS) limit states will be analysed in the following sections. These will be performed considering the relevant to each case acting loads, following the code provisions. Regarding the codes to be instructed, the SLS and ULS will be examined following the NORSOK N-004 [4] and Eurocode 3 [28] provisions, whereas for the FLS design DNVGL RP-C203 [1] was applied.

4 Serviceability and Ultimate limit state checks

```
                    ┌──────────────────────────┐
                    │  Determine the acting loads │
                    └──────────────────────────┘
                              │
                              ├──────►┌──────────────────┐
                              │       │  Permanent loads │
                              │       └──────────────────┘
                              │
                              ├──────►┌──────────────────┐
                              │       │    Live loads    │
                              │       └──────────────────┘
                              │
                              ├──────►┌──────────────────────┐
                              │       │ 1-yr, 100-yr wind loads │
                              │       └──────────────────────┘
                              │
                              ├──────►┌──────────────────┐
                              │       │   Friction load  │
                              │       └──────────────────┘
                              │
                              ▼
                    ┌──────────────────────────┐
                    │ Define the load combinations │
                    └──────────────────────────┘
                              │
                              ├──────►┌──────────────────┐
                              │       │ SLS combinations │
                              │       └──────────────────┘
                              │
                              ├──────►┌──────────────────┐
                              │       │ ULS combinations │
                              │       └──────────────────┘
                              ▼
                    ┌──────────────────────────┐
                    │     Run analyses in SACS │◄──────────┐
                    └──────────────────────────┘           │
                              │                             │
                              ▼                             │
                    ┌──────────────────────────┐           │
                    │ Perform the member checks │           │
                    └──────────────────────────┘           │
                              │                             │
                              ├──────►┌────────────────────┐  NO   ┌──────────────┐
                              │       │ SLS checks satisfied ?│─────►│              │
                 YES          │       └────────────────────┘      │ Change member│
                              ├──────►┌────────────────────┐      │   sections   │
                              │       │ ULS checks satisfied ?│─────►│              │
                              │       └────────────────────┘  NO   └──────────────┘
                              ▼
                    ┌──────────────────────────┐
                    │        members OK        │
                    └──────────────────────────┘
                              │
                              ▼
                    ┌──────────────────────────┐
                    │ Perform the ULS weld checks │◄──────────┐
                    └──────────────────────────┘             │
                              │                               │
                              ▼                               │
                    ┌──────────────────────────┐   NO   ┌──────────────────┐
                    │   weld checks satisfied ? │───────►│ Change weld details │
                    └──────────────────────────┘        └──────────────────┘
                              │ YES
                              ▼
                    ┌──────────────────────────┐
                    │ construction OK against SLS, ULS │
                    └──────────────────────────┘
```

In this chapter, the structure is checked against the serviceability limit state (SLS) for its deflections and against the ultimate limit state (ULS) for its strength. The last limit state concerning fatigue is examined in chapter 5.

4.1 Software used, material properties and codes followed

4.1.1 Structural analysis software used

The Offshore Structural Analysis and Design Software SACS [3] was used to perform the structural analysis. It is a finite element method program using beam element theory. It enables performing global analyses in accordance to most of the available design code provisions. However, local detail connection checks cannot be performed through the software, hence wherever this was the case hand calculations were performed. Figure 4-1 illustrates the bridge landing as modelled in SACS, with its joint names highlighted and the indication of the north direction with respect to the bridge landing.
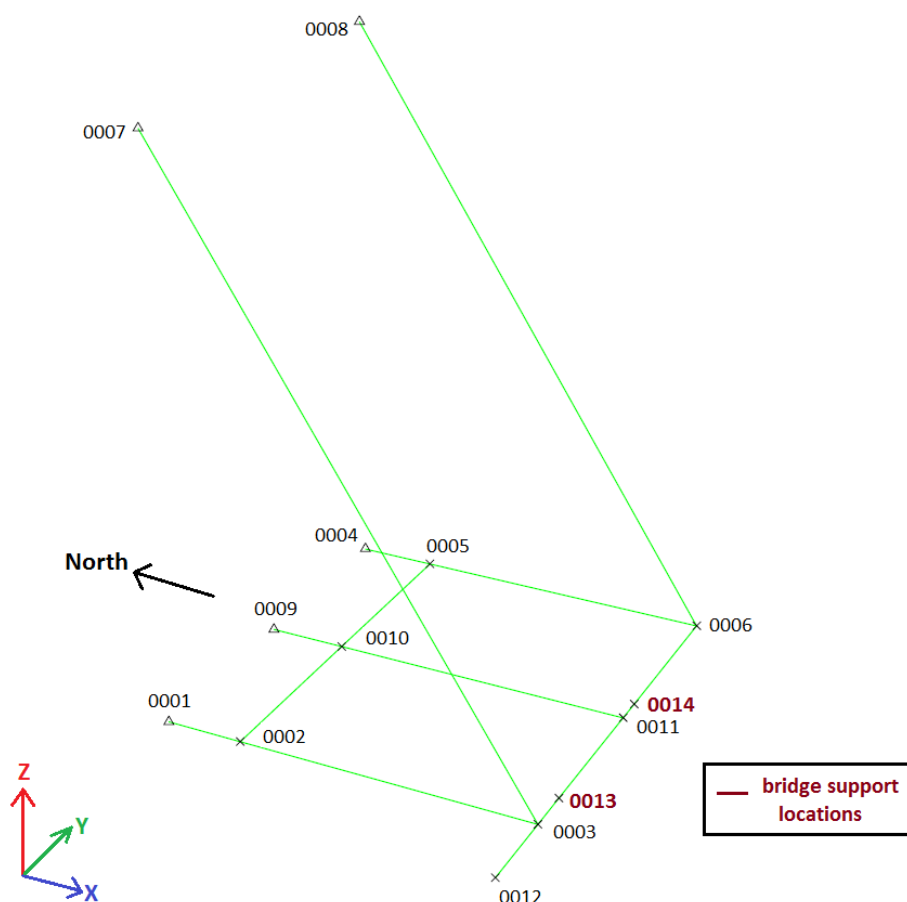
Figure 4-1 – The bridge landing platform [3]

4.1.2 Material properties

The following table lists the material properties that were used for the design.

Table 4-1 – Material properties

Steel quality grade	Material density (tonnes/m³)	Young modulus (GPa)	Shear modulus (GPa)
S355	7.85	210	81

4.1.3 Code checks

The design checks were performed according to NORSOK N-004 [4] for the tubular members and according to Eurocode 3 [28] for the other types of members. These comprise satisfying the requirements that are set by the code provisions, for each of the limit state that is examined. The type of method that was followed is the Load and Resistance Factor Design method (LRFD), which implies satisfying a number of requirements for the different limit states.

The general safety requirement is that the design action must not exceed the design resistance of the examined member. This is performed by factoring the loads through the incorporation of appropriate safety factors, for both the action forces and the member resistances. The factors that regarding the acting loads are called action factors, whereas the ones concerning the member's resistance are stated as material factors.

4.2 Design loads

4.2.1 Analysis assumptions
The following assumptions were made when defining the loads that are applied at the bridge landing:
- the friction coefficient of the bearing pads is considered equal to 0.4
- the loads acting on the bridge are equally transferred to the 2 landings
- only the wind load acting in the direction perpendicular to the bridge is taken into account (direction Y in Figure 4-1). In the direction longitudinally to the bridge, no wind is considered because of the existence of the bridge. Due to its presence, the relevant open area of the bridge landing is very small and any wind load at that direction is neglected.

4.2.2 Acting loads

The loads that act on the bridge landing consist of those that are transferred from the bridge at its support locations and the ones that are applied directly to the bridge landing. They can be divided into permanent, live and environmental ones.

4.2.2.1   Permanent loads

The permanent loads that concern the design consist of vertical applied ones. These are:

- the bridge's structural weight
- the appurtenances weight on the bridge
- the equipment weight on the bridge
- the dead weight of the bridge landing

The loads that act on the bridge are transferred equally to the 4 support points at the two bridge landings. Therefore, these are represented by two concentrated vertical loads at the support points of each bridge landing. The dead weight of the bridge landing consists of distributed vertical loads based on the member section dimensions. Figure A. 1 on Appendix A illustrates the way they act. They are summarized in the following table.

Table 4-2 – Permanent loads

Load description	Total	Per bridge landing	Per support
	[kN]	**[kN]**	**[kN]**
Dead loads from the bridge	-752.9	-376.45	-188.23
Dead weight of bridge landing	-190.95	-	-

4.2.2.2   Live loads

Live loads are varying temporary loads that change over time. In this case, these comprise vertical loads caused from the presence of people at a part of the bridge landing and at the bridge. The bridge ones are equally transferred at the four support points of the two bridge landings as concentrated forces, whereas the ones acting on the bridge landing are distributed vertical loads at specific areas and are applied at the relevant members. Figure A. 2 on Appendix A illustrates the way they act. Table 4-3 and Table 4-4 summarize them.

Table 4-3 – Live load from the bridge

Load description	Total	Per bridge landing	Per support
	[kN]	**[kN]**	**[kN]**
Live load from the bridge	-112.5	-56.25	-28.13

Table 4-4 – Live load at the bridge landing

Load description	Members	Distributed load
		[kN/m^2]
live load at the bridge landing	(0001-0002), (0009-0010), (0004-0005)	-2.50

4.2.2.3 Environmental loads

The environmental loads that concern the design of the bridge landing against the SLS and ULS consist of the wind loads that are transferred from the bridge and the wind load that is applied directly at the bridge landing itself. The wind load that act on the bridge is transferred to the bridge landing at the four support locations. This comprises both concentrated horizontal forces and a couple of vertical ones due to the out-of-plane bending moment that is introduced. The wind load acting directly at the bridge landing is a distributed horizontal load that is applied at the corresponding member. Figure A. 3 and Figure A. 4 on Appendix A illustrate the way they act.

The coupled vertical forces that are generated by the out-of-plane bending moment are calculated according to the following relation, assuming that the wind load acts at half of the bridge's height:

$$F_z = \frac{\frac{F_{wind}}{2} \cdot \frac{h_{bridge}}{2}}{d}$$

where: F_{wind} is the total wind load acting on the bridge
$h_{bridge} = 4m$ is the height of the bridge
$d = 4.5m$ is the distance between the 2 bearing locations

Two cases of mean wind speeds are examined, the 1-year and the 100-year extreme ones. Table 4-5 lists the corresponding wind speeds considered.

Table 4-5 – 1-hour mean wind speeds at 10 m above mean sea level

situation	1-hour mean wind speed U_0 [m/s]
1-year extreme wind	22.7
100-year extreme wind	28.9

The wind load was calculated according to API RP 2A-WSD provisions [29] , through the following formula:

$$q_{wind} = (\rho/2) \cdot u(z,t)^2 \cdot C_s$$

where: q_{wind} is the distributed load due to wind $\left(N/m^2\right)$
ρ is the air density, equal to 1.22 Kg/m^3
C_s is the shape coefficient, equal to 1.5 for non-tubular beams
$u(z,t)$ is the wind speed at elevation z for an average time period t

The wind speed $u(z,t)$ is determined from the following formula [29]:

$$u(z,t) = U(z) \cdot \left[1 - 0.41 \cdot I_u(z) \cdot \ln\left(\frac{t}{t_0}\right)\right]$$

where: $U(z)$ is the 1 hour mean wind speed at elevation z
$I_u(z)$ is the turbulence intensity at elevation z
t is the average time period, equal to 60 s
t_0 is the time period for basic mean wind speed, equal to 3600 s

The 1-hour mean wind speed at elevation z is defined from the 1-hour mean wind speed at 10 m above mean sea level, through the equation [29]:

$$U(z) = U_0 \cdot \left(1 + C \cdot \ln\left(\frac{z}{32.8}\right)\right)$$

where: U_0 is the 1-hour mean wind speed at 10 m above mean sea level
       C is a factor defined from the value of U_0
       z is the elevation, set in feet. Here the elevation of the bridge landing at the level of the bridge is 24.5 m

The turbulence intensity at elevation z is calculated according to [29]:

$$I_u(z) = 0.06 \cdot [1 + 0.0131 \cdot U_0] \cdot \left(\frac{z}{32.8}\right)^{-0.22}$$

in which: U_0 is inserted in $feet/_s$ and z in feet

In this case, the relevant elevation above mean sea level is 24.5 m for the wind acting on the bridge landing (at half of the members height). The resultant wind force is a distributed load at the corresponding members. For wind acting in y-direction (Figure 4-1), this concerns members (0001-0002-0003) and (0004-0005-0006), depending on its direction.

The resultant area load q_{wind} was finally transformed into a line load, applied at half of the member's height. This was done by multiplying the q_{wind} with the height of the corresponding member. Both members (0001-0002-0003) and (0004-0005-0006) have sections of 1m height. The resultant distributed wind loads for the different wind cases are listed in Table 4-6.

Table 4-6 – Wind loads acting on the bridge landing

Load description	Design wind speed at elevation z $u(z,t)$	Members	Distributed load
	[m/s]		[kN/m]
West 1-year wind	29.3	(0001-0002), (0002-0003)	0.78
West 100-year wind	38.3	(0001-0002), (0002-0003)	1.34
East 1-year wind	29.3	(0004-0005), (0005-0006)	-0.78
East 100-year wind	38.3	(0004-0005), (0005-0006)	-1.34

Regarding the wind that acts on the bridge, the situation that was examined concerns a bridge with the following characteristics (Figure A. 6 in Appendix A illustrates it):

- $L = 16.55\ m$
- $H = 4\ m$

The wind load was calculated following the procedure as described above, with considering it as a concentrated load acting at half of the bridge's height, so at elevation $z = 26.5m$ from the mean sea

level. The bridge area was considered as a closed rectangle area ($A = L \cdot H$) and the defined distributed load q_{wind} was transformed into a concentrated force acting at the bridge supports. Table 4-7 lists the obtained results.

Table 4-7 – Wind Loads transferred from the bridge to the bridge landing

Load description	design wind speed at elevation z $u(z, t)$	Horizontal force				Vertical forces	
		distributed	Total	Per bridge landing	Per support (joints 0013,0014)	Per support	
	[m/s]	[kN/m²]	[kN]	[kN]	[kN]	Joint	[kN]
West 1-year wind	32.4	0.96	63.55	31.78	15.89	0013	14.12
						0014	-14.12
West 100-year wind	42.9	1.69	112	56	28	0013	24.89
						0014	-24.89
East 1-year wind	32.4	-0.96	-63.55	-31.78	-15.89	0013	-14.12
						0014	14.12
East 100-year wind	42.9	-1.69	-112	-56	-28	0013	-24.89
						0014	24.89

4.2.3 Friction load

Finally, there is also the generated friction that needs to be considered for the strength and deformation checks of the structure. This is generated at the locations of the bearing pads, thus in the joints 0013 and 0014, as depicted in Figure 4-1. Friction acts at the direction longitudinally to the bridge (global direction x) and its magnitude depends on the vertical load that acts at these locations. This concerns the vertical support reaction, not only due to the dead and live loads acting on the bridge, but also due to the moment that is generated because of the applied wind load that acts transversely to the bridge. The generated friction was calculated, assuming a friction coefficient equal to 0.4, based on the formula $Friction = \pm \mu \cdot F_z$. Figure A. 5 on Appendix A illustrates the way they act. The following table illustrates the friction load that is generated at each bearing pad, for the most conservative wind cases (100-year cases).

Table 4-8 – Largest friction applied at the bearing pads

Load description	Joints	F_z from vertical loads	F_z from wind	Resultant vertical load F_z	Generated friction F_x
		[kN]	[kN]	[kN]	[kN]
with 100-year wind form west	0013	-216.35	24.89	-192	±76.58
	0014		-24.89	-241.78	±96.50
with 100-year wind from east	0013	-216.35	-24.89	-241.78	±96.50
	0014		24.89	-192	±76.58

4.3   Load combinations

Since the strength checks were performed following the NORSOK [4] provisions, the different load combinations for the ULS and SLS checks were accordingly defined. More specifically, the different combinations were defined by applying the action factors (γ_f) for the several combinations. Concerning the serviceability limit state, no action factors are required, whereas for examining the ultimate limit state the relevant loads are factored in two different ways as demonstrated in the following table, obtained from section 6.2.1 of the NORSOK Standard N-001 [11].

Table 4-9 – Action factors for the ULS and SLS conditions [11]

State	Permanent actions	Variable actions	Environmental actions
SLS	1.0	1.0	1.0
ULS (a)	1.3	1.3	0.7
ULS (b)	1.0	1.0	1.3

The applicable material factors (γ_M) to be used for the SLS and ULS checks are listed in Table 4-10. They were obtained from sections 7.2.3 and 7.2.4 of the NORSOK Standard N-001 [11].

Table 4-10 – Material factors for the case of steel structures [11]

State	Material factor (γ_M)
SLS	1.0
ULS	1.15

The combinations that need to be examined are presented in the following tables. Table 4-11 lists the ones concerning serviceability limit state and Table 4-12 those regarding ultimate limit state.

Table 4-11 – SLS load combinations

Load case	Dead loads	Live loads	Friction load	1-yr west wind	100-yr west wind	1-yr east wind	100-yr east wind
Load combination							
SLS1	1.00	1.00	1.00				
SLS2	1.00	1.00	1.00	1.00			
SLS3	1.00	1.00	1.00			1.00	
SLS4	1.00				1.00		
SLS5	1.00						1.00

Table 4-12 – ULS load combinations

Load case	Dead loads	Live loads	Friction load	1-yr west wind	100-yr west wind	1-yr east wind	100-yr east wind
Load combination							
OP1A	1.30	1.30	1.30	0.70			
OP2A	1.30	1.30	1.30			0.70	
EX1A	1.30				0.70		
EX2A	1.30						0.70
OP1B	1.00	1.00	1.00	1.30			
OP2B	1.00	1.00	1.00			1.30	
EX1B	1.00				1.30		
EX2B	1.00						1.30

4.4 Serviceability limit state results

The induced vertical deflections of the several members must never exceed the limiting values presented in Table 4-13 as a function of member's length, according to section 7.2.4 of the NORSOK Standard N-001 [11]. It should be noted that the mentioned lengths (L) correspond to the spans of the members except for the case of cantilevers where they represent twice their span [11].

Table 4-13 – Deflection requirements for the SLS checks [11]

Condition	Allowable deflection $\delta_{allowable}$
Deck beams	$L/200$
Deck beams supporting brittle finish or non-flexible partitions	$L/250$

Table 4-14 below summarizes the SLS checks for the multiple load combinations, as defined above. The unity check column represents the ratio of the maximum induced vertical deflection to the allowable one, thus the requirement is satisfied when its value is below 1.0.

Table 4-14 – SLS results from SACS

Member	Span [m]	Load combination	Joint of max deflection	$\delta_{allowable}$ [cm]	δ_{max} [cm]	Unity check
0001-0002-0003	9.50	SLS3	0003	4.75	0.27	0.06
0004-0005-0006	9.50	SLS2	0006	4.75	0.16	0.03
0009-0010	1.95	SLS2	0010	0.98	0.08	0.08
0010-0011	7.55	SLS2	0011	3.78	1.62	0.43
0002-0010-0005	9.90	SLS2	0010	4.95	0.08	0.02
0003-0011-0006	9.90	SLS2	0011	4.95	1.62	0.33
0012-0003	4.43	SLS2	0012	2.22	0.69	0.31
0003-0007	17.34	SLS3	0003	8.67	0.27	0.03
0006-0008	17.34	SLS2	0006	8.67	0.16	0.02

It is apparent that all member deflections are smaller than the allowable ones, thus all the serviceability requirements are satisfied. This is illustrated in the unity check values of the previous table, which are much smaller than 1.0 for every member.

4.5   Ultimate limit state results

Checking the bridge landing structure against the ultimate limit state was performed according to the NORSOK N-004 provisions [4]. The strength checks were thus performed by introducing a material (safety) factor of 1.15, whereas the analyses were conducted for the multiple load combinations as listed in Table 4-15, through SACS. The following table demonstrates the most critical per member strength check for the multiple ULS load combinations.

Table 4-15 – ULS results from SACS

Member	Section type	Load combination	Critical condition	Max Unity check
0003-0007	Tubular	OP2A	Axial tension	0.11
0006-0008	Tubular	OP1A	Axial tension	0.07
0001-0002	Plate girder	EX2B	Bending and axial tension	0.21
0002-0003	Plate girder	EX2B	Bending and axial tension	0.18
0004-0005	Plate girder	EX1B	Bending and axial tension	0.23
0005-0006	Plate girder	EX1B	Bending and axial tension	0.20
0002-0010	Plate girder	EX1B	Bending and axial tension	0.13
0010-0005	Plate girder	EX2B	Bending and axial tension	0.13
0003-0013	HEA	OP2A	Bending and axial tension	0.44
0011-0014	HEA	OP1A	Bending and axial compression	0.57
0012-0003	HEA	EX1A	Shear	≈ 0
0013-0011	HEA	OP2A	Bending and axial tension	0.54
0014-0006	HEA	OP1A	Bending and axial compression	0.47
0009-0010	HEA	EX1B	Bending and axial tension	0.15
0010-0011	HEA	EX1B	Bending and axial tension	0.20

The results demonstrate that the ultimate limit state requirements are satisfied for all the members of the structure and for all the defined load combinations. The unity check results indicate that material utilisation is low for this configuration, since the maximum unity check equals 0.57 (far below 1.0). However, whether the structure is adequate or not cannot yet be concluded, since the FLS checks remain to be performed.

4.6 Fillet welds strength checks

4.6.1 Requirements

All the connections between the different members of the bridge landing are welded ones, of either fillet or butt weld type. Fillet welds themselves need also to be checked concerning their strength for the ultimate limit state combinations. They need to be examined with reference to their throat plane, thus the applied stresses have to be defined with correspondence to that plane. Figure 4-2 demonstrates what the throat plane of a fillet weld is and the corresponding applied stresses.
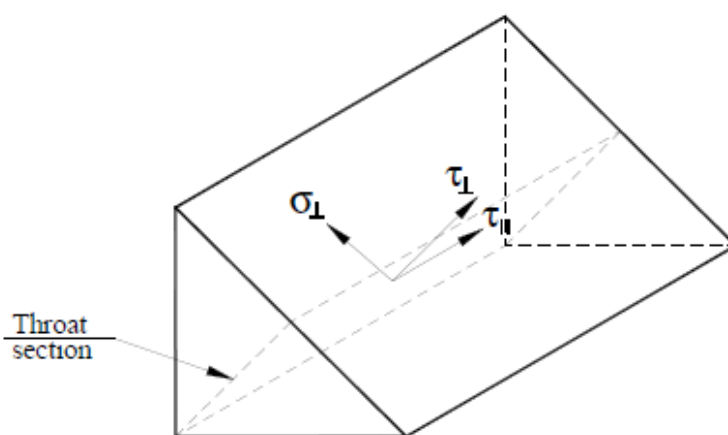
Figure 4-2 – Resultant stresses at the throat plane of a fillet weld [2]

According to part C607 of section 9 of DNV-OS-C101 [2], the criterion requires both of the following conditions to be fulfilled:

$$\sqrt{\sigma_{\perp d}^2 + 3 \cdot \left(\tau_{||d}^2 + \tau_{\perp d}^2\right)} \leq \frac{f_u}{\beta_w \cdot \gamma_{Mw}}$$

and $\qquad \sigma_{\perp d} \leq \frac{f_u}{\gamma_{Mw}}$

where: $\sigma_{\perp d}$ is the normal to the throat plane design stress

$\tau_{||}$ is the design shear stress in the throat plane that acts parallel to the longitudinal axis of the weld

$\tau_{\perp d}$ is the design shear stress in the throat plane that acts perpendicular to the longitudinal axis of the weld

f_u is the ultimate tensile strength of the weakest welded part. Since the grade of steel used is S355, its value is 510 MPa

β_w is a correlation factor, dependent on the steel grade. For S355 steel used, its value is 0.9

γ_{Mw} is the material factor used for welded connections. For the ULS check, its value is 1.3

4.6.2 Results

The results of these conditions are illustrated in the following table. These concern the most conservative load combination for each fillet weld examined. The member locations refer to the ones illustrated in the Figure C. 1, in Appendix C. In Appendix F, the way of defining the stresses with reference to the throat plane of the fillet welds is explained in detail.

Table 4-16 – Fillet welds resistance criterion

member location	$\tau_{\|d}$ (MPa)	$\tau_{\perp d}$ (MPa)	$\sigma_{\perp d}$ (MPa)	$\dfrac{\sqrt{\sigma_{\perp d}^2 + 3 \cdot (\tau_{\|d}^2 + \tau_{\perp d}^2)}}{\frac{f_u}{\beta_w \cdot \gamma_{Mw}}}$	$\dfrac{\sigma_{\perp}d}{\frac{f_u}{\gamma_{Mw}}}$
1	52.92	0	1.32	0.21	0.00
2	38.57	0	0	0.15	0.00
5	38.57	0	0	0.15	0.00
6	28.94	0.39	1.04	0.12	0.00
7	0.95	0.16	84.06	0.19	0.21
10	0.88	0.45	84.95	0.19	0.22
22	-1.46	0.30	212.91	0.49	0.54

Consequently, this criterion is satisfied for all the fillet welded connections of the bridge landing. It should be noted that details regarding those fillet welds (dimensions and detail drawings of the member connections) can be found in section 5.4.

5 Fatigue design of the bridge landing

In order to perform the analysis of the bridge landing against fatigue, a simplified case of the problem is first considered, allowing to examine the fatigue state in a quick way. This is done through simplifications in:

- the way of defining the generated friction load
- the amount of applied load cycles to be considered
- the value of friction coefficient to be used

This approach will be referred from now on as the "base case" and will set the basis for any further comparison and derived recommendations.

5.1   The base case approach

The base case consists of a quick and simplified method for analysing the bridge landing against fatigue. The main assumptions of this approach are the following ones:

- Wind loads are omitted. This is assumed because the cause of fatigue damage is the long term action of the generated friction load due to the platform deformations. These deformations are mainly caused by the wave loads that are continuously acting on the platforms during the entire service life. Wind speed has fluctuations with time, which in some cases (gusts) can be significant. However, when examining a structure's long term performance (i.e. during its service life), fluctuations of wind speed are negligible and the resultant loads can be considered to be constant, thus they are considered as static loads.
- The live loads acting on the bridge are not taken into account when defining the generated friction. This is considered because fatigue concerns a long-time state and live loads are temporary ones, present only for a short duration. Hence, they can be neglected when examining the fatigue state and only dead loads are taken into account, which results in a smaller generated friction load.
- All waves are considered at the longitudinal direction of the bridge, resulting in a friction load acting at that direction. This is assumed in order to perform a simple and quick fatigue assessment. It is a conservative assumption since the generated friction depends on the direction of the induced from the waves displacements
- All waves are considered to have the same period of 5 s, an average period as derived based on the service life of the structure and the number of waves to be encountered during that period. This was again assumed in order to conclude in a quick fatigue analysis. However, it is a valid assumption since the period that is considered was derived from the scatter information regarding the several wave periods and its probabilities of occurrence. The procedure followed to derive it is explained in Appendix B.
- The coefficient of friction is assumed to be constant and equal to 0.4. This is a value assumed without having any information for the type of bearing that is used. It is a high

value for cases where bearing pads with very low coefficient of friction may be used. This results in a high friction force, thus it is a conservative assumption

Since fatigue damage is the result of applied stress alterations, only varying loads are of concern. Based on the above assumptions made, the only varying load for the base case is the friction load that is generated at the two bearing pad locations. Given that the coefficient of friction is assumed to be constant and only permanent loads are considered to act on the bridge, the magnitude of the friction load is constant as well. What is varying is its direction, since this depends on the relative motion between the bridge and the bridge landing. For the base case, in a full wave cycle, this stress range is considered to be twice the amount of the resultant stresses due to the friction load applied. Such an assumption is conservative since it is possible that not all the waves result in the same level of friction load. If this is the case, then several stress ranges associated with different number of applied cycles are defined. The sensitivity of the incoming wave to the generated friction is investigated in section 6.2.

A static analysis will be performed considering the bridge landing with only the friction load applied at the two bearing pad locations. Its magnitude is derived from the coefficient of friction and the vertical reaction force at these locations. The vertical reaction forces are obtained considering only the permanent loads acting on the bridge, which is vertically supported at 4 points, 2 at each bridge landing.

Consequently, the two friction forces applied at the bearing locations of the landing have a magnitude of 75.3 kN, as can be found in Table 5-1 below, assuming that the vertical loads that act on the bridge are equally distributed to the 2 landings.

Table 5-1 – Derivation of the applied friction load

Load description	relation	magnitude [kN]
total permanent load on bridge	= bridge structural weight + appurtenances weight + equipment weight	752.9
vertical load per landing	= 752.9 / 2	376.5
vertical load per bearing pad	= 376.45 / 2	188.2
friction force per bearing pad	= 0.4 * 188.23	75.3

Regarding the incoming waves, these are only considered through their wave period, defining the amount of stress cycles that are applied during the service life of the structure, based on the following equation:

$$n = \frac{service\ life}{wave\ period} = \frac{25\ years}{5\ s} = 157680000\ cycles\ applied$$

The following block diagram illustrates the base case approach by indicating its most important points.

Drawings → Set up structural model geometry

Loadings

Derive friction load from vertical reaction forces at → Add load to analysis model

Run analysis model

Obtain member stresses | Calculate local section stresses

$stress\ range = 2 \cdot stress$

Select SCF → Fatigue analysis

Select S/N class →
Apply safety factor DFF → $stress\ range < (fatigue\ limit) \cdot DFF^{\,-0.33}$? —YES→ Construction OK

NO

Define applied number of cycles (wave period taken 5 sec) → Calculate fatigue damage (D)

Apply DFF → $Damage \cdot (DFF) < 1$? —NO→

YES

Service life of → $fatig\ life = \dfrac{serv\ life}{D}$

Construction OK

5.2   The critical locations to be checked

In the following Figure 5-1, the structural model of the bridge landing platform as defined in SACS, is depicted. All the joints that have been generated are shown in the figure for further reference from now on.
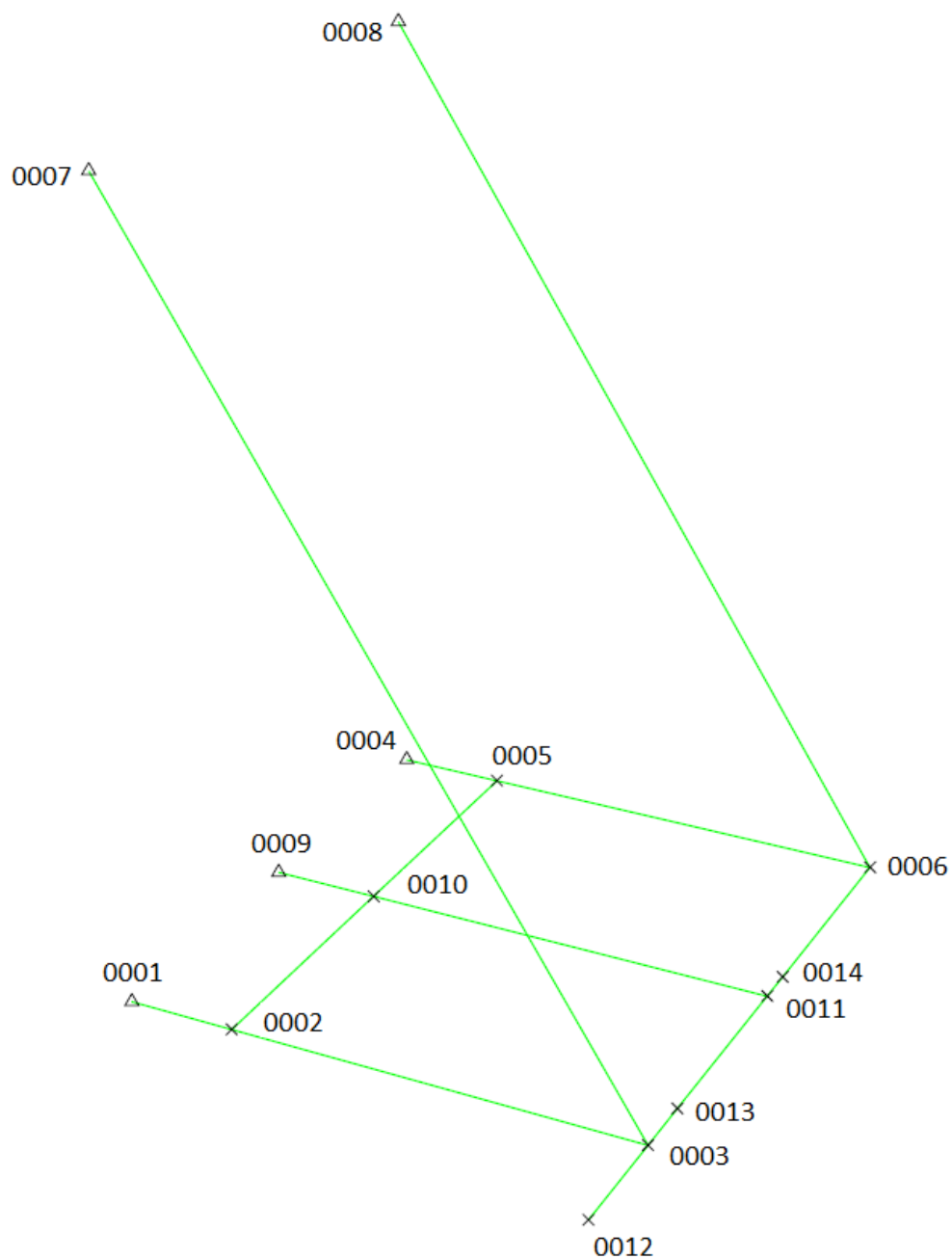
Figure 5-1 – SACS structural model of the bridge landing

In the Table 5-2 below, the different member sections together with their geometrical properties are listed.

Table 5-2 – Member section properties

Member	Section type	h [cm]	b [cm]	t_w [cm]	t_f [cm]	D [cm]	t [cm]	A [cm²]	I_y [cm⁴]	I_z [cm⁴]
0001-0003	plate girder	100	60	2	3	-	-	548	985517	108063
0004-0006	plate girder	100	80	2	3	-	-	668	1267878	256064
0009-0010	HE500A	49	30	1.2	2.3	-	-	197.53	86971	10370
0010-0011	HE400A	39	30	1.1	1.9	-	-	158.97	45070	8564
0012-0003	HE700A	69	30	1.45	2.7	-	-	260.47	215301	12180
0003-0006	HE700A	69	30	1.45	2.7	-	-	260.47	215301	12180
0002-0005	plate girder	100	30	2	3	-	-	368	561974	13563
0003-0007	tubular	-	-	-	-	45.7	1	140.43	35091	35091
0006-0008	tubular	-	-	-	-	45.7	1	140.43	35091	35091

All member ends were considered as possible locations of crack initiation due to fatigue. Hence, the applied stresses and the resultant stress ranges were determined at each of these locations, which are illustrated in Figures C-1 and C-2 in Appendix C. From the magnitude of stress that was applied at each location, the corresponding stress range was defined from doubling it, due to the alteration of friction's direction in a full wave cycle. Table C. 1 lists the applied stress ranges at the several locations examined.

Based on the resultant stress ranges, not all of these positions were worthwhile to be examined against fatigue, due to the low amount of applied stress. Therefore, only a number of them were exposed to an amount of stress range capable to result in a fatigue failure.

Figure 5-2 below highlights the most fatigue-prone locations of the bridge landing platform, facing the highest stress ranges. These are the locations that were finally examined against fatigue.
Results of the applied stresses and the resultant stress ranges for all the member ends locations can be found in Table C. 1 in Appendix C.
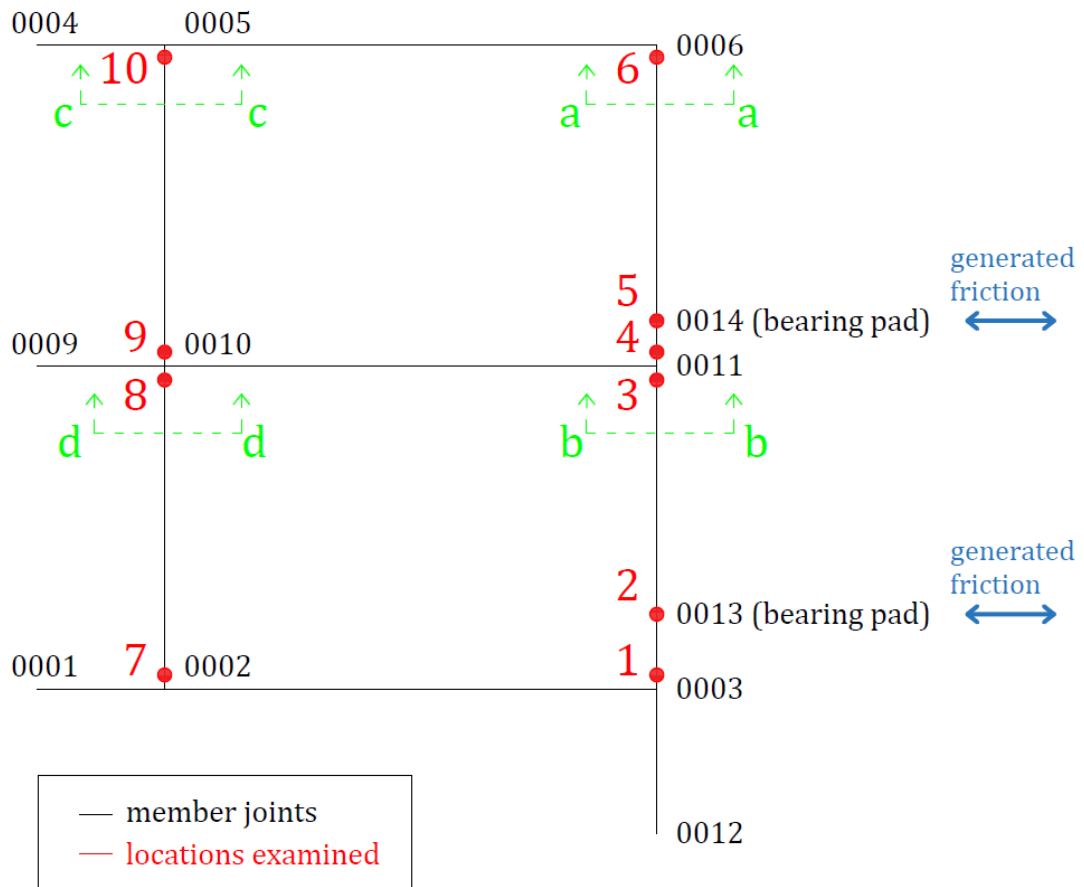
Figure 5-2 – Member locations to be examined

All these locations belong to members with either a HEA or a plate girder cross section. After determining the forces and moments applied at the member locations defined in the previous figure, the local stresses need to be examined at the different positions inside the section of interest. For that purpose, the HEA and plate girder sections are examined in multiple locations, which are illustrated in Figure 5-3 below.
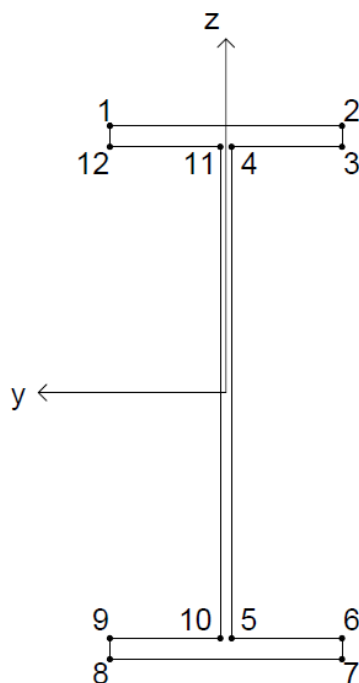
Figure 5-3 – Locations to be examined against fatigue

5.3 The applied nominal stresses and the derived hot spot stress ranges

Having defined the structural model, the applied friction load and the locations to be examined, everything has been set in order to proceed with defining the stresses at these locations. First, a static analysis was performed in SACS, with only the friction loads applied, at the bearing positions (joints 0013 and 0014 according to the model). The resultant member end forces and moments were obtained for the multiple member locations to be checked (Figure 5-2). These forces and moments refer to the center of gravity (CoG) of the corresponding cross section and the nominal stresses were finally calculated for the multiple section locations (Figure 5-3), based on the section's geometrical properties (A, I_y, I_z) according to the formula:

$$\sigma_{tot,i} = \frac{F_X}{A} \pm \frac{M_y \cdot z_i}{I_y} \pm \frac{M_z \cdot y_i}{I_z}$$

where: i denotes the critical section location considered (Figure 5-3)

and $\pm$ sign depends on the direction of moments and the location of the detail examined

After having defined the nominal stresses at the different critical locations, the hot spot ones need to be derived. These are calculated by considering any geometric, material or load discontinuity present at these locations. Such discontinuities are incorporated through the stress concentration factor (SCF) that is applied in the nominal stresses in order to amplify them, if needed. Here, all SCFs for the member locations examined were considered as 1,0 except for the ones at the tubular member locations.

Finally, the hot spot stress ranges (HSSR), for a full wave cycle, are defined by doubling the values of the corresponding hot spot stresses at the multiple locations examined. This was done due to the consideration that, in a full wave cycle, the magnitude of friction remains the same, but its direction changes. This results in a stress range that is double the generated stress. This is illustrated in the following figure.
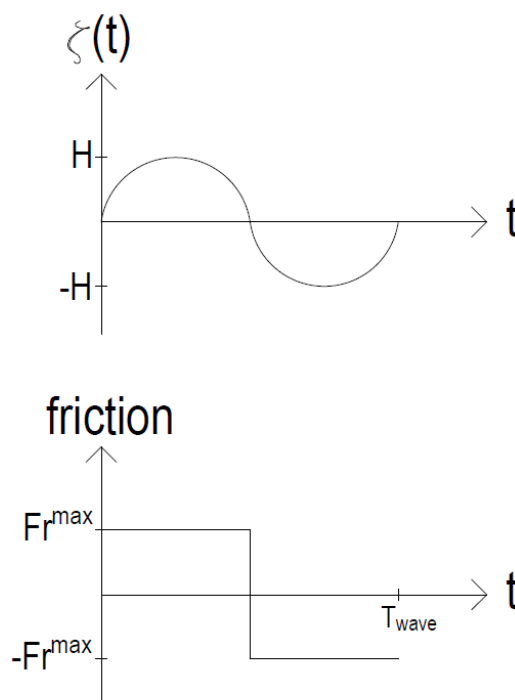
Figure 5-4 – Friction with time considered for the base case

5.4   Classification of the multiple structural details

This section presents the classification of the different local details in order to define their resistance against fatigue. Fatigue resistance is specified as the number of cycles that have to be applied to cause failure due to a certain amount of stress range. The classification of the member local details is performed according to the DNVGL RP-C203 provisions [1]. The exact classification and explanation of the chosen category is presented in the following paragraphs, for the critical member locations that are to be examined (with reference to Figure 5-2 for their labelling).

5.4.1   Member locations 1 and 6 (Connection of HE700A with plate girder)

These locations concern the continuous member (0003-0006) with cross section HE700A, which is connected to plates of 20 mm thickness, at its end joints 0003 and 0006. Its flanges are welded through double-fillet welds of 14 mm leg length, whereas the web through double fillet welds of 8 mm leg length, as shown in the Figure 5-5 below.
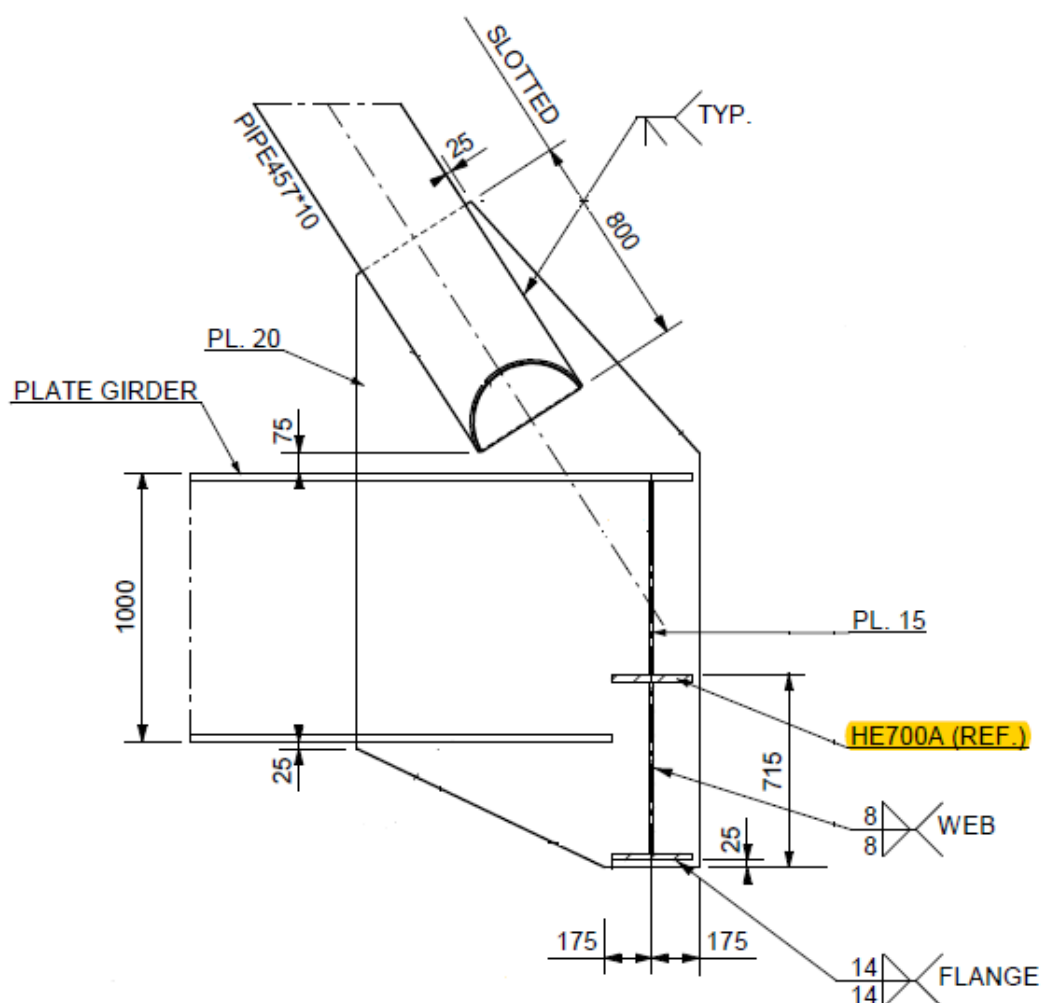
Figure 5-5 – Details 1 and 6 (section a-a from the top view in Figure 5-2)

The section local details of these locations are classified based on Table A-8 regarding "welded joint with load carrying welds" of the DNVGL RP-C203 code [1]. Since the connections are performed using fillet welds, construction detail 2 from that table is used, which requires the fatigue assessment of the root and the toe cracking failure modes exclusively.

Regarding the evaluation of weld root cracking, this is considered by assessing the fatigue damage of the fillet weld itself. For such an analysis, the reference plane is the throat of the weld and the resultant stresses are derived relevant to that plane. These applied stresses are then combined to derive the applied stress range, according to the formula below [37]. An explanation of the resultant stresses at the throat plane can be found in Figure 4-2 of section 4.6.1. The detail category adopted for the examination of the root cracking is category W3, as described in situation 2 of table A.8 of Appendix A in DNVGL RP-C203 [1].

$$\Delta \sigma_W = \sqrt{\Delta \sigma_\perp^2 + \Delta \tau_\perp^2 + 0.2 \cdot \Delta \tau_{||}^2}$$

where: $\Delta \sigma_\perp$ the normal to the throat plane stress range

$\Delta \tau_\perp$ the shear stress range at the plane of the throat, normal to the longitudinal axis of the weld

$\Delta \tau_{||}$ the shear stress range at the plane of the throat, parallel to the longitudinal axis of the weld

Regarding toe cracking, this consists of examining the stress range in the member section at that location (HE700A), considering the detail category to be the G one, as indicated in the code. Figure 5-6 demonstrates the DNV specifications for these kind of details.
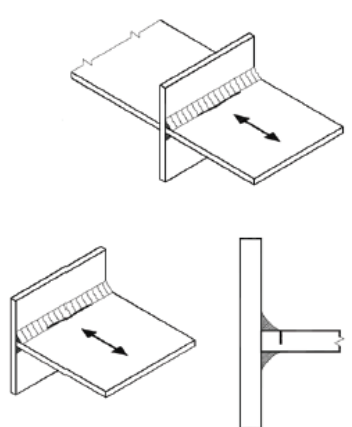
W3	2.		2.Partial penetration tee-butt joint or fillet welded joint and effective full penetration in tee-butt joint. See also [2.8].	2.:

2.:
— Two fatigue assessments are required. Firstly, root cracking is evaluated taking Category W3 for σ_w. σ_w is defined in section [2.3.5]. Secondly, toe cracking is evaluated by determining the stress range in the load-carrying plates and use Category G.
— If the requirement in section [2.8] that toe cracking is the most likely failure mode is fulfilled and the edge distance ≥ 10mm, Category F1 may be used for partial penetration welds and F3 for fillet welds.

Figure 5-6 – Classification of locations 1 and 6 according to DNVGL RP-C203 [1]

5.4.2   Member locations 2 and 5 (Bearing pad locations)

These are the locations where the two bearing pads are positioned, at the joints 0013 and 0014. The bearings are welded at the top flange of member (0003-0006) of HE700A cross section, as illustrated in Figure 5-7 below. Welding is performed through single-fillet welds of 10 mm leg length. The bearing is welded all around and the welding is performed at the field.
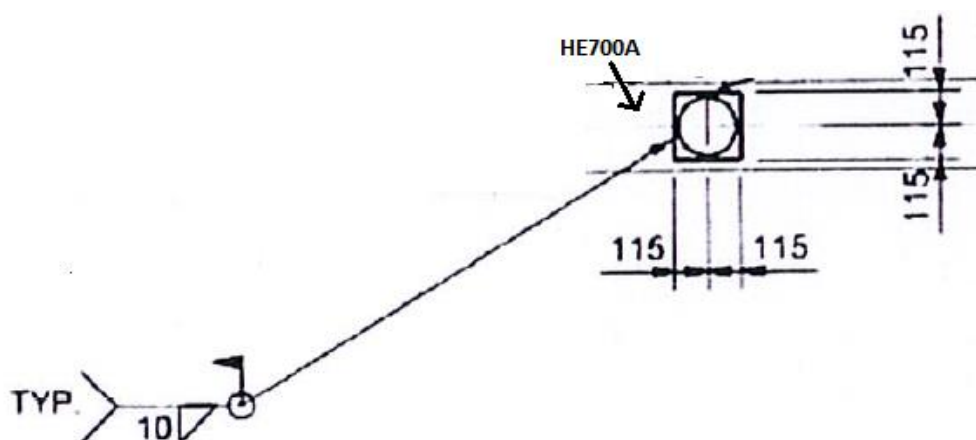
Figure 5-7 – Top view of details 2 and 5

The only attachment at these locations is the bearing pad, which is welded at the top flange of the wide flange section. Therefore, the section local details that are positioned at the outer fiber of the top flange, at the location of the bearing pad welding points, are classified based on Table A-7 for "welded attachments on the surface or the edge of a stressed member", according to construction detail 2 from that table. Since the edge distance is 35mm >10mm and the bearing welded length is l=230mm (120<l<=300mm), detail category F1 is used. Figure 5-8 depicts the applicable DNV provisions for these kind of details.

		given for:
E	$l \leq 50$ mm	— Edge distance ≥ 10mm
F	$50 < l \leq 120$ mm	— For edge distance < 10 mm the detail category shall be downgraded with one S-N-curve
F1	$120 < l \leq 300$ mm	
F3	$l > 300$ mm	

Figure 5-8 – Classification of locations 2 and 5 according to DNVGL RP-C203 [1]

Regarding the remaining local details of these locations, they are classified based on Table A-1 for "non-welded sections". Since the member has a rolled section (HE700A), construction detail 2 from that table is used and the detail category B1 is selected.

It should be noted that according to the DNV provisions [1], even though the connection is performed through fillet welds, there is no need for examining the weld root cracking failure mode exclusively for this type of detail. This is due to the consideration of a limiting value for the edge distance of the weld that is taken into account when classifying the detail.

5.4.3   Member locations 3 and 4 (Connection of HE400A to HE700A)

These consist of locations of the continuous member (0003-0006) with cross section HE700A, at joint 0011 where the member (0010-0011) of cross section HE400A is attached to it. The top flange of member (0010-0011) is welded at the facing edge of the top flange of member (0003-0006), through single-sided butt weld. The web and the bottom flange of member (0010-0011) are welded at the facing edge of the web of member (0003-0006) through double fillet weld of 4 and 7 mm throat size respectively. Figure 5-9 illustrates a top view of the crossing members and a detail drawing of the tee joint.
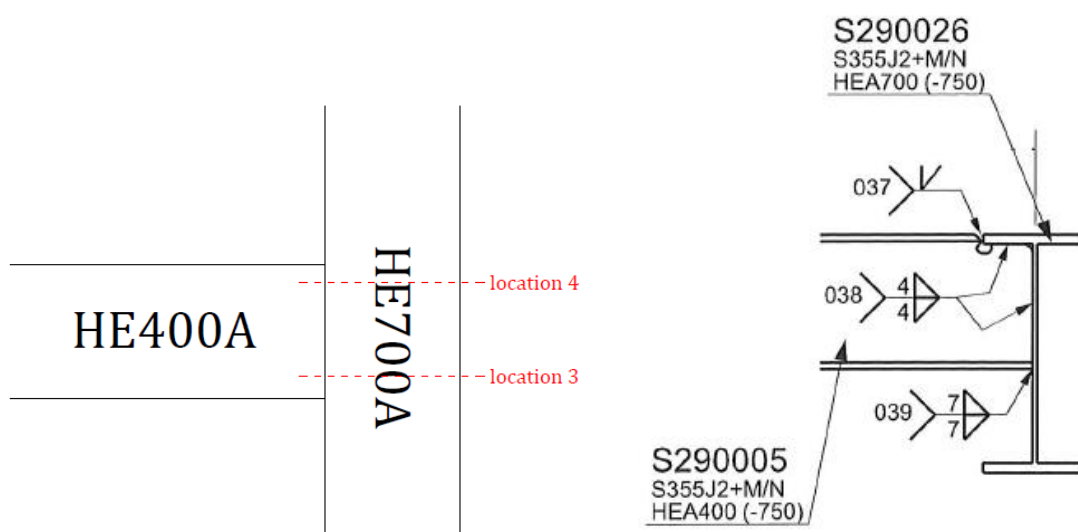
Figure 5-9 – Top view of crossing joint 0011 (left) and the corresponding section b-b from the top view in Figure 5-2 (right)

Therefore, the local section details that are positioned at the corresponding edge of the top flange and web are classified based on Table A-7 for "welded attachments on the surface or the edge of a stressed member" of the DNV code, according to construction detail 6 from that table. Since the welded flange width is l=300mm (150<l<=300mm), detail category W1 is selected. Figure 5-10 illustrates the DNV specifications for these kind of connection details.

Figure 5-10 – Classification of locations 3, 4, 7 and 10 according to DNVGL RP-C203 [1]

Regarding the remaining local details of these locations, these are classified based on Table A-1 for "non-welded sections". Since the member has a rolled section (HE700A), construction detail 2 from that table is used and the detail category B1 is selected.

5.4.4 Member locations 7 and 10

These are the locations where the continuous member (0002-0005) with a plate girder cross section is attached to the members (0001-0003) and (0004-0006) of plate girder cross section, at its end joints 0002 and 0005. The flanges of member (0002-0005) are welded at the edge of the flanges of members (0001-0003) and (0004-0006) through double (or single)-sided butt welds. The web of members (0001-0003) and (0004-0006) is welded at the facing web of member (0002-0005) through double fillet welds. Figure 5-11 illustrates this detail configuration.
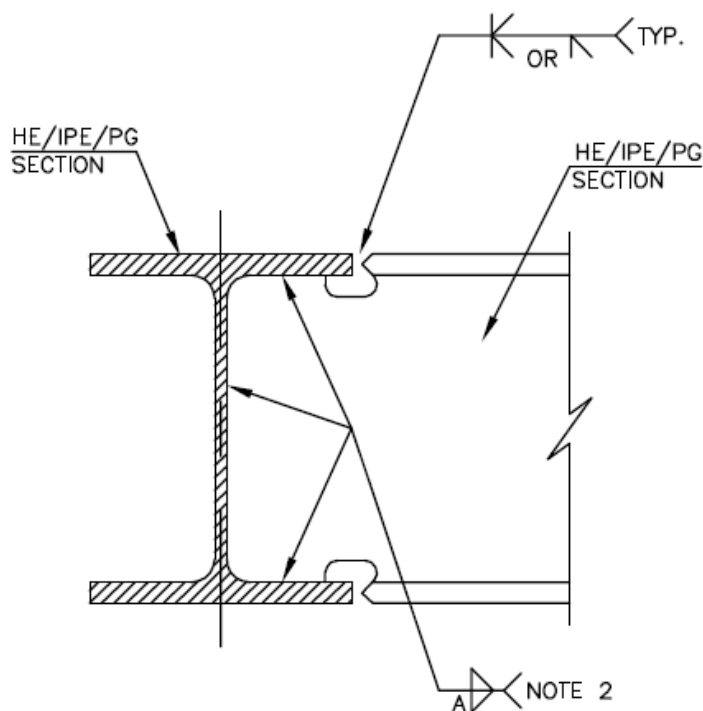
Figure 5-11 – Details 7 and 10 (section c-c)

All local section details are classified based on Table A-7 for "welded attachments on the surface or the edge of a stressed member" of the DNV code, according to construction detail 6 from that table. Since L=600mm (L>300mm), detail category W2 is selected. Figure 5-10 illustrates the DNV specifications for these kind of connection details as well.

5.4.5 Member locations 8 and 9

These consist of locations of the continuous member (0002-0005) with plate girder cross section type, at joint 0010 where the members (0009-0010) and (0010-0011) of HEA cross section types are attached to it. Welds are performed at both faces of the bottom part of the web and the bottom flange of member (0002-0005). Figure 5-12 illustrates a top view of the crossing members and a detail drawing of the tee joint.
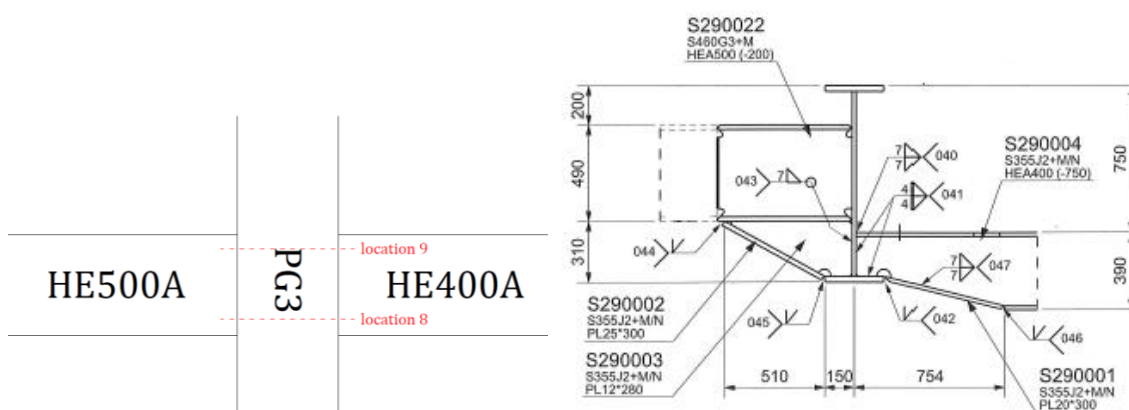
Figure 5-12 – Top view of cruciform joint 0010 (left) and the corresponding section d-d (right)

Therefore, the local section details that are positioned at the bottom flange and the relevant part of the web are classified based on Table A-7 for "welded attachments on the surface or the edge of a stressed member" of the DNV code, according to construction detail 7 from that table. Since the welded flange width is L=300mm (150<L<=300mm), detail category W1 is selected. Figure 5-13 depicts the applicable DNV specifications for these kind of connection details.
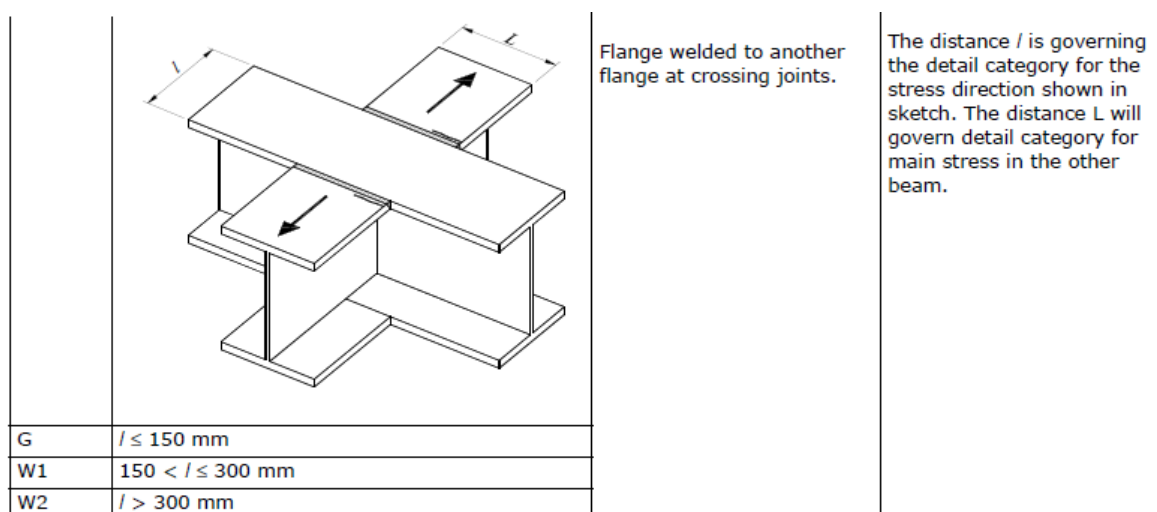
Figure 5-13 – Classification of locations 8 and 9 according to DNVGL RP-C203 [1]

Regarding the remaining local details of these locations (top flange and top web part), these are classified based on Table A-1 for "non-welded sections". Since the member has a built-up section with machine gas cut material (plate girder), construction detail 3 from that table is used and the detail category B2 is selected.

5.5 Fatigue assessment of the multiple critical locations

After having classified the details that will be examined against fatigue, the applicable SCFs could be determined and the corresponding S-N curves were selected. Thus, the resultant damage at these locations can be derived, based on the applied stress ranges. The damage value will finally indicate whether the certain detail is adequate or not and determine its fatigue life.

5.5.1 Procedure

The procedure that has to be followed in order to define the accumulated damage at each location consists of the following steps:

1) The nominal stress range at that location is calculated
2) The hot spot stress range (HSSR) is derived by applying the appropriate stress concentration factor (SCF)
3) According to the classification of the detail and the applied HSSR, the fatigue stress limit at 10^7 cycles and the number of cycles (N) that the detail can resist for that HSSR are defined, according to the applicable S-N curve of the detail category. The fatigue limit is defined based on the S-N curve that is used, reduced by a design fatigue factor (DFF$^{-0.33}$) depending on the location of the detail. The number of cycles until failure (N) is derived from the following equation:

$$\log N = \log \bar{a} - m \cdot \log\left(\Delta\sigma \cdot \left(\frac{t}{t_{ref}}\right)^k\right)$$

   where: $\log \bar{a}$, m, k are characteristics of the S-N curve used
   $\Delta\sigma$ is the HSSR considered
   t_{ref} is a reference thickness depending on the type of connection
   t is the thickness through which the crack is expected to grow ($t \geq t_{ref}$)

4) If the applied HSSR is lower than the fatigue limit, then no fatigue analysis is required
5) If the applied HSSR is higher than the fatigue limit, then the cumulative fatigue damage ratio (D) for the service life of the structure is determined, according to the following formula (Palmgren-Miner rule): $D = \sum_{i=1}^{k} \frac{n_i}{N_i}$, where k is the number of stress ranges considered, n_i is the number of cycles applied for the ith stress range considered and N is the number of cycles until failure for the ith stress range considered.
6) If D < 1 then the examined detail can resist the accumulated fatigue damage, otherwise failure due to fatigue will occur
7) The fatigue life of a detail is defined as: $fatigue\ life = \frac{service\ life}{D}$

5.5.2 Acceptance criteria

The results of this procedure, for the multiple member locations examined, are summarized in the following table, in which: structure's service life = 25 years, $n_i = 157680000$ cycles applied and DFF = 1, for all the member locations examined. A value of 1.0 was chosen for the design fatigue factor, considering all the locations of the bridge landing as locations of the external structure that are accessible for regular inspection and repair in dry and clean conditions, according to DNV-OS-C101 provisions [2].

Therefore, each of the following conditions results in satisfying the FLS for the certain detail of the bridge landing, given that the applied safety factor (DFF) equals 1.0:

➢ $\Delta\sigma < fatigue\ limit$
➢ $D < 1.0$

5.5.3 Results

Table 5-3 below demonstrates the results obtained from the fatigue analysis at the most prone locations.

Table 5-3 – Fatigue assessment of the most prone local section details of all critical member locations

member location	section detail	$\Delta\sigma_{nom}$ (MPa)	SCF (-)	$\Delta\sigma_{hot\ spot}$ (MPa)	S-N curve	fatigue limit (MPa)	N (cycles)	damage D (-)	fatigue life (years)
1	7	92.37	1.0	92.37	G (toe cracking)	29.24	$2.99 \cdot 10^5$	526.60	0.05
2	1	59.42	1.0	59.42	F1	36.84	$2.25 \cdot 10^6$	70.08	0.36
3	1	66.59	1.0	66.59	W1	26.32	$5.83 \cdot 10^5$	270.38	0.09
4	1	69.49	1.0	69.49	W1	26.32	$5.13 \cdot 10^5$	307.34	0.08
5	1	37.44	1.0	37.44	F1	36.84	$1.1 \cdot 10^7$	14.28	1.75
6	2	36.13	1.0	36.13	G (toe cracking)	29.24	$5 \cdot 10^6$	31.52	0.79
7	7	0.99	1.0	0.99	W2	23.39			
8	8	0.94	1.0	0.94	W1	26.32			
9	7	3.32	1.0	3.32	W1	26.32			
10	1, 8	4.72	1.0	4.72	W2	23.39			

It should be noted that in member locations 7, 8, 9 and 10 performing a detailed fatigue analysis was omitted, since the applied hot spot stress range is below the fatigue limit [1], as can be seen from the results in Table 5-3.

Regarding the examination of weld root fatigue cracking at the locations of the fillet welds, as noted in the previous section 5.4.1, such a check first requires defining the applied stresses with reference to the throat plane of the fillet weld. The procedure followed in order to calculate these stresses is demonstrated clearly in Appendix F. The resultant stress range is derived by combining all the different stresses applied at the throat plane, through the following formula:

$$\Delta \sigma_W = \sqrt{\Delta \sigma_\perp^2 + \Delta \tau_\perp^2 + 0.2 \cdot \Delta \tau_{||}^2}$$

Table 5-4 illustrates the weld root crack checks of the fillet welds at the critical locations 1 and 6.

Table 5-4 – Check against weld root fatigue cracking at the locations where fillet welds are used

member location	weld location examined	$\tau_{||}$ (MPa)	$\tau_\perp$ (MPa)	$\sigma_\perp$ (MPa)	$\Delta \sigma_w$ (MPa)	S-N curve	fatigue limit (MPa)	N (cycles)	damage D	fatigue life (years)
1	flange	5.04	0.14	62.47	125.03	W3	21.05	$4.78 \cdot 10^4$	3302	0.01
	web	0.01	0.14	3.30	6.61	W3	21.05			
6	top flange	0.65	0.15	24.35	48.71	W3	21.05	$8.07 \cdot 10^5$	195.29	0.13
	web	0.01	0.15	1.36	2.73	W3	21.05			

Based on the above results, it is apparent that the flange welds are not adequate against the fatigue requirements. The resultant stress ranges are higher than the stress fatigue limit and the accumulated damage is much above the limiting value of 1. On the other hand, regarding the welds of the web, the fatigue requirements are satisfied in both these locations.

6 Examination of sensitivity parameters

sensitivity parameters examined

coefficient of friction

- define the coefficients to be examined
- derive the corresponding friction loads
- perform analysis in SACS for the new friction loads
- perform fatigue analysis for the new friction loads

- define the limiting friction coefficient value
- select a value
- define new friction load
- run analysis in SACS
- derive stress ranges
- stress ranges < fatigue limit ?

  YES → decrease friction coefficient

  NO → value = limiting one satisfying the FLS criteria

direction of incoming waves

- model the situation with both platforms in SACS
- choose the wave characteristics (H, T) to be used
- calculate the damage for that wave period following the base
- split directional spectrum into sectors according to scatter data
- run SACS model for each incoming wave direction
- derive relative displacements with time for the bridge ends
- derive the magnitude of friction that is induced per wave direction
- derive stress ranges for the applied friction at the landing
- calculate the induced damage per wave direction
- define the total damage at the most prone locations

compare results to determine the impact

After examining the structure against the serviceability, ultimate and fatigue limit states it was found that, although the SLS and ULS checks were satisfied, the fatigue requirements were not fulfilled. Therefore, it seems meaningful to perform a sensitivity study on the main parameters that affect the fatigue limit state, before continuing with strengthening the structure. Such a sensitivity analysis will serve as a review of the base case approach and the results will indicate its level of conservatism.

The method that was followed regarding the FLS, as was described in chapter 5, is based on a simplified approach where a unidirectional wave is considered. From its characteristics, the number of applied cycles were derived and the analysis against fatigue was performed by applying the generated friction load. The main assumptions that were made concern the wave characteristics and the friction coefficient that were considered, both affecting the induced fatigue damage. The former through the number of applied cycles and the latter through the magnitude of friction.

6.1   Coefficient of friction of the bearing pad

6.1.1   Approach

The generated friction load is, in its most simplistic way, defined based on two parameters, the coefficient of friction and the vertical load that is applied at the locations of the bearing pads. The vertical load at that location depends on the structural system of the bridge landing and the loads that are applied to it. On the other hand, the friction coefficient depends on the tribological properties of the in-contact surfaces in which friction is generated. Its value is either considered based on experience or adopted from the properties of the bearing to be used. It mainly depends on the:

- roughness of the surfaces that are in contact
- material used for these surfaces
- existence of lubricant in between

A list with typical values of friction coefficients for the most common material combinations can be found on Table E. 1 of Appendix E.

In the analyses that were performed so far, both in the ULS and the FLS for the base case, the friction coefficient was considered to be equal to 0.4. Such a value is a big one, considering that spherical bearing pads with a PTFE sliding surface may be used for this case, resulting in much lower coefficients (see Table E. 1 in Appendix E). Therefore, it seems worthwhile to examine the effect that such a change has on the generated friction and consequently on the accumulated damage for the multiple locations.

For that purpose, three different friction coefficient values were examined to investigate their effect in the resultant accumulated damage. Their effect will be defined based on the comparison with the results obtained from the value of 0.4 that was used in the base case. The two values to be examined were chosen to be 25% and 50% less than the initial one of 0.4. The third one was defined according to the characteristics of the sliding bearing pads that were used in this situation,

thus as defined from the corresponding commercial brochure [12]. More specifically, only the highest value from the ones listed was considered, in order to use this information in the most conservative way. In Figure 6-1, the (according to the supplier) proposed friction coefficient values that should be used, are shown. Table 6-1 below lists the different friction coefficient values that were examined for this sensitivity study and the resultant friction. This was defined considering the same vertical loads as done in the base case (Table 5-1 in section 5.1), accounting only for the dead loads of the bridge.

Table 6-1 – The different friction coefficient values examined

coefficient of friction	description	difference with the coefficient of 0.4	generated friction load (kN)
0.3	lowering the value of 0.4 considered in the base case	-25 %	56.47
0.2	lowering the value of 0.4 considered in the base case	-50 %	37.65
0.04	the highest value from the commercial brochure for bearing pads	-90 %	7.53
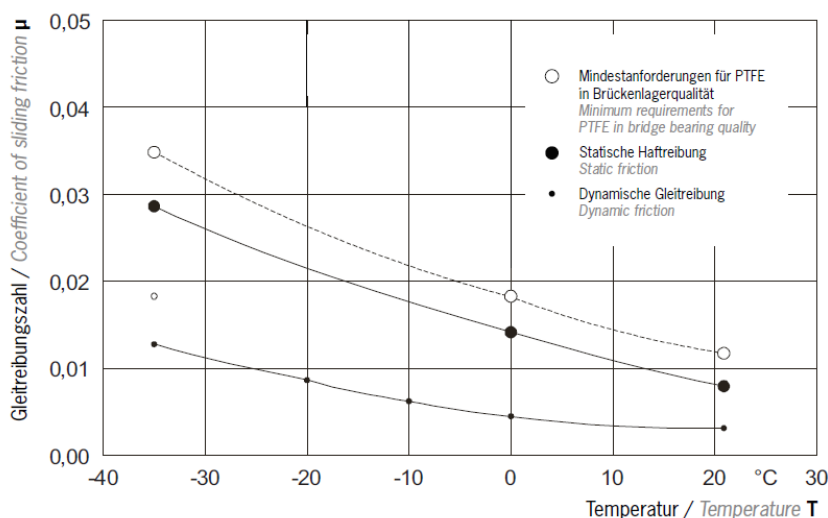
Figure 6-1 – Coefficient of friction values for sliding bearing pads [12]

The new friction loads were derived for the different coefficients that were tested. After performing the corresponding structural analyses for these friction loads, using SACS, the resultant stress ranges and the accumulated damage for the member locations, as highlighted in section 5.2, were calculated for the different cases. It should be noted that the structural analyses were conducted in the same manner as it was done for the base case, considering only the friction load to be applied at the bearing locations and assuming that one complete friction load cycle corresponds to one wave period.

6.1.2 Results

Table 6-2 below contains the results from the analyses performed to examine the effect of the friction coefficient on the fatigue life of the structure. As expected, the amount of the applied stress ranges decreased for the several locations, resulting in less fatigue damage and an associated longer fatigue life (the smaller the value of the friction coefficient the smaller the accumulated damage induced). What is important, though, is not the decrease of the damage as a general conclusion, but its amount in conjunction with the change in the friction coefficient. The results presented concern only the details that were found incapable of resisting the induced damage defined in the base case (member locations 1 to 6 with reference to Table 5-3).

Table 6-2 – Resultant damage for the different friction coefficients examined

case examined	member location	$\Delta\sigma$ (MPa)	fatigue limit (MPa)	damage D (-)	fatigue life (years)	damage difference with base case ($\mu = 0.4$)
friction coefficient $\mu = 0.3$	1	69.28	29.24	222.19	0.11	-57.81 %
	2	44.56	36.84	29.57	0.85	-57.81 %
	3	49.94	26.32	114.08	0.22	-57.81 %
	4	52.12	26.32	129.68	0.19	-57.81 %
	5	26.58	36.84	3.39	7.37	-76.26 %
	6	27.10	29.24	11.87	2.11	-62.33 %
friction coefficient $\mu = 0.2$	1	46.19	29.24	65.85	0.38	-87.50 %
	2	29.71	36.84	5.92	4.22	-91.55 %
	3	33.30	26.32	33.81	0.74	-87.50 %
	4	34.75	26.32	38.43	0.65	-87.50 %
	5	17.72	36.84	0.45	55.97	-96.87 %
	6	18.07	29.24	1.56	15.98	-95.04 %
friction coefficient $\mu = 0.04$	1	9.24	29.24	0.05	>>25	-100 %
	2	5.94	36.84	≈ 0	>>25	-100 %
	3	6.66	26.32	0.02	>>25	-100 %
	4	6.95	26.32	0.02	>>25	-100 %
	5	3.54	36.84	≈ 0	>>25	-100 %
	6	3.61	29.24	≈ 0	>>25	-100 %

6.1.3 Conclusion

As can be seen from the obtained results, there is a significant reduction in the accumulated damage, for using smaller friction coefficients. This reduction is much greater than the reduction of the coefficient's one, since the relation between coefficient of friction and the damage induced is not linear. Friction coefficient is linear related to friction ($Fr = \mu \cdot V$) and thus to the resultant

stresses and stress ranges at the several members, given that stress ranges were defined by doubling the induced stress. However, the fatigue damage is determined by the number of applied cycles (n) and the amount of cycles that result in failure of the detail (N). The amount of resistant cycles (N) depends on the applied stress range through the S-N curve equation, which is in logarithmic scale as was presented in section 2.1.2.

Regarding the results, although the resultant damage for these 6 most prone locations was reduced in all the cases examined, the fatigue requirement is yet not satisfied for all of them. Specifically:

- For the case of a coefficient of friction with a value of 0.3, locations 1 to 4 remain inadequate, whereas in locations 5 and 6 the fatigue limit requirement is fulfilled and they can be considered sufficient against fatigue[1] [1].

- In the case of $\mu = 0.2$, locations 1, 3 and 4 still remain insufficient. On the other hand, in locations 2, 5 and 6, although the resultant damage is larger than the limit value of 1, the applied stress ranges are smaller than the fatigue limit for these details and therefore they can be considered to be sufficient against fatigue[1] [1]

- For the last case, in which a much smaller value of friction coefficient is considered ($\mu = 0.04$), all the resultant stress ranges are smaller than the corresponding fatigue limit, hence the details are capable to resist the fatigue damage induced[1] [1]. This is also obvious from the values of the resultant damages for that case, which are much lower than the limiting value of 1

6.1.4   Limiting friction coefficient

The value of the limiting friction coefficient value that results in just fulfilling the fatigue requirement was also defined during this study. Multiple values were checked, in an effort to conclude in a stress range that is just below the fatigue limit, at the most critical member location (connection of the HE700A member (0003-0006) with a plate at its end). It was found that the required friction coefficient is 0.12. Table 6-3 presents the results.

Table 6-3 – Fatigue assessment for the case of the limiting friction coefficient

case examined	member location	$\Delta\sigma$ (MPa)	fatigue limit (MPa)
friction coefficient $\mu = 0.12$	1	27.72	29.24
	2	17.83	36.84
	3	19.98	26.32
	4	20.85	26.32
	5	10.63	36.84
	6	10.84	29.24

---

[1] Given that all the different applied stress ranges are below the fatigue limit. Here, the stress range level induced from the friction load is the only one applied, thus its value is the one to determine whether a detailed fatigue analysis can be omitted or not.

6.2 Directionality of incoming wave

The incoming wave affects the platform deformations and consequently the ones of the corresponding bridge landing. The wave parameters that influence this are:

- the wave height
- the wave period
- the direction of the wave

Since in this thesis the focus is on the generated friction load at the bridge's sliding direction, it seems worthwhile to examine the impact that the direction of the incoming wave has on the generated friction.

For that reason, the whole directional spectrum was split into 16 directional sectors (per 22.5°). The number of sectors to be used was determined from the scatter information that was used. It was decided to split the spectrum into the same number of sectors, thus being in accordance with the metocean data report concerning the probabilities of occurrence of the multiple combinations of wave height and period for each directional sector (Figure D. 2 of Appendix D).

As was previously mentioned, friction is a force that is generated at the interface of two surfaces that are in contact and is generated by their relative motion. In this case, the in-contact surfaces are the bearing pads of the bridge landing and the bridge end support points, whereas their relative movement is caused by the incoming wave. Before describing the way through which wave directionality was examined, the fundamental properties of friction are presented in order to explain the way that these were treated in this sensitivity study.

6.2.1   The fundamentals of friction

Friction is a phenomenon which is encountered when two surfaces that are in contact start moving relative to each other. The generated force is called friction and tends to resist the induced motion. It is applied at both these surfaces and is a very complex phenomenon, whose characteristics depend on the tribological properties of the surfaces.

Friction can exhibit two states during the whole phenomenon. Initially, while relative movement begins, static friction is generated. This is experienced while the surfaces tend to move due to an applied force, but movement has not yet started, because of static friction. It opposes the pulling force that would otherwise cause the object to move. This type of friction is associated with the static friction coefficient and during this phase the two surfaces are sticking to each other. The magnitude of static friction is equal to the pulling force until a certain limit, the maximum static friction, which is defined as the product of static friction coefficient with the vertical applied force.

When the pulling force exceeds that limit then the two surfaces start to move relative to each other. This is the kinetic phase, during which friction is still present, but in a different manner. This signifies its slipping state and the generated friction is called kinetic or dynamic. Its magnitude is constant and is determined as the product of the friction coefficient with the vertical applied force. Nevertheless, it is not equal to the maximum static friction due to the lower friction coefficient at that phase, which is known as the kinetic friction coefficient. This is approximately 75% of the static one. The direction of kinetic friction is such that it opposes the relative velocity that is generated. Figure 6-2 illustrates the two states of friction.
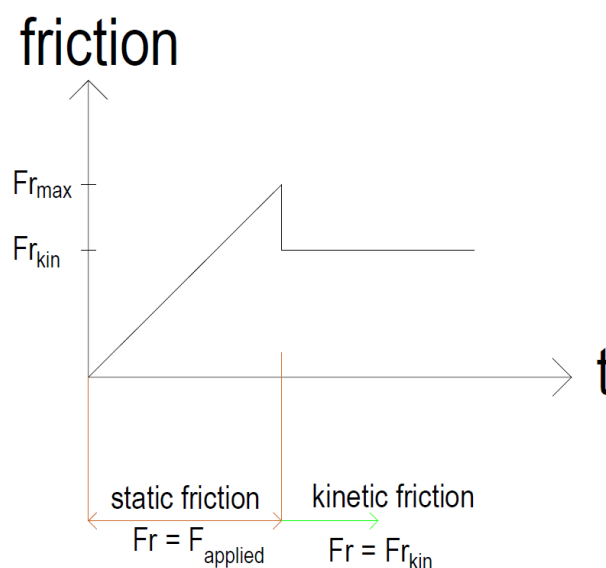
Figure 6-2 – The actual behaviour of friction

Based on these remarks and given that the thesis aims to provide a simple, yet not a simplistic, method to deal with the fatigue damage that is caused by the generated friction, the theory described here was applied through the examination of the effect of wave directionality. The way that it was introduced in the study is explained in sections 6.2.2, 6.2.4 and 6.2.5.

While closing this subsection containing the basic theory concerning friction, it should be mentioned that chapter 8 provides more insight regarding the different friction theories. At that section, a numerical approach is presented, in an effort to model the phenomenon more accurately.

6.2.2   Model

In order to examine whether the directionality of the incoming wave affects the resultant behaviour of the bridge landing against the induced fatigue, the structure's response in the different wave directions should be investigated. In order to study this effect, the same wave was applied for the several approaching directions considered. For that reason two identical platforms were used to model the situation, with a clearance of 25 m between their two bridge landings.

The analyses were performed using SACS with the only applied load being the introduced wave. The obtained results were focused on the displacements with time of the locations of the bearing pads at the two bridge landings. These results were finally used to derive the relative displacement between the bridge landing where the sliding ends of the bridge were located and those bridge end points. In order to do so, the bridge was assumed to be rigidly connected to the platform where its pin ends were located, thus the displacements of the bridge sliding ends were considered to be the same as the deflections of the bridge landing of its pinned ends. A top view of the whole model is depicted in the following figure, in which the two bridge landings are marked with green colour.
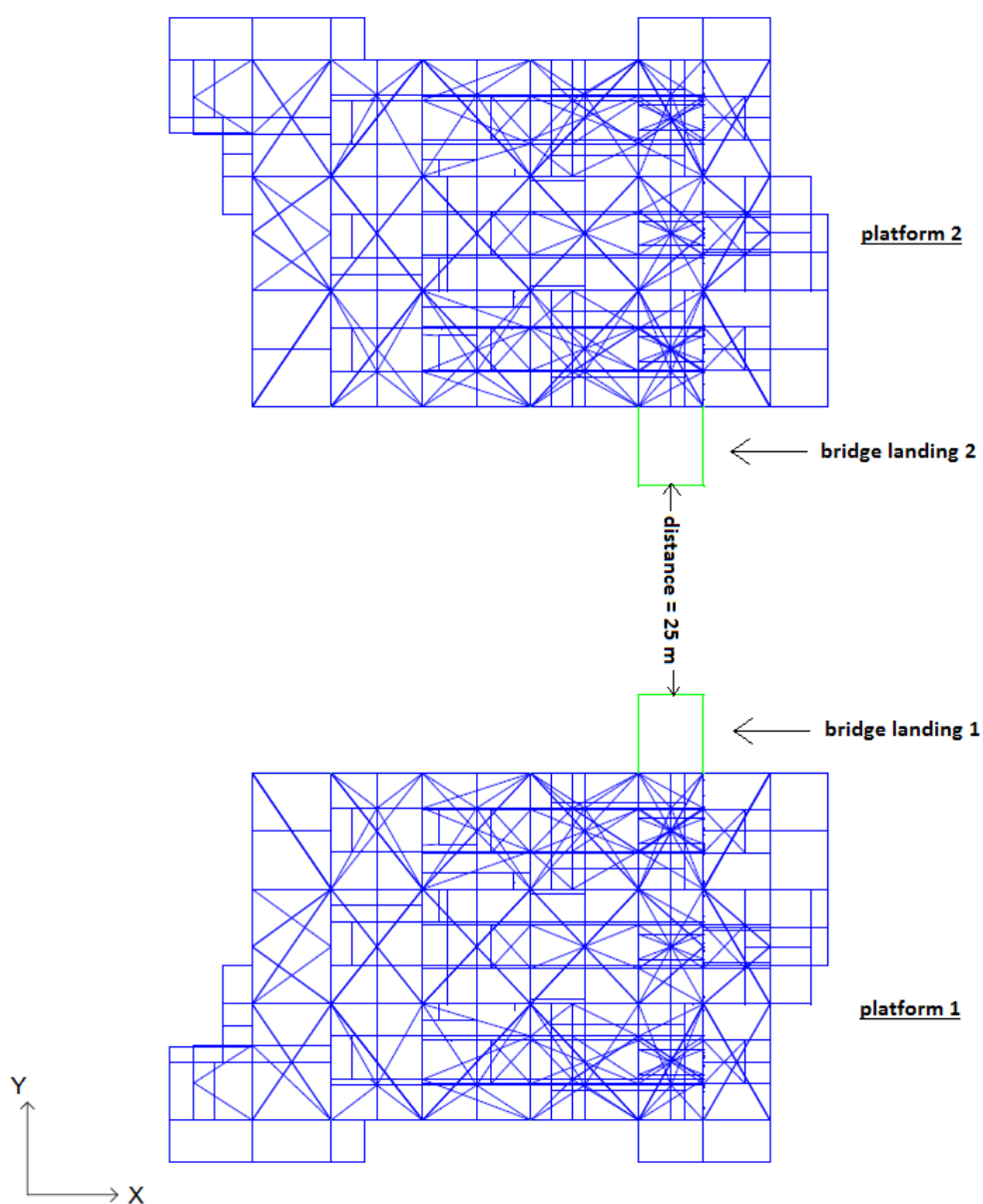
Figure 6-3 – Top view of the model with both platforms

6.2.3 Wave selection

The wave characteristics to be used for the analysis should be representative for the purpose of its use. Thus, the so called "centre of the fatigue damage" wave characteristics [13],[14] were selected, as an effective way to derive a single representative seastate to be used for a fatigue analysis purpose, using the scatter information for the structure's location.

The centre of fatigue damage is a particular seastate and is defined according to the particular fatigue damages caused from each seastate of the corresponding scatter. It is characterized by a wave height and period, such that:

- 50% of the damage is caused from seastates with a lower significant wave height and 50% from those with a higher one
- 50% of the damage occurs from the seastates with a smaller mean zero crossing period and 50% from those with a larger one

Thus, it is a seastate that results to the mean fatigue damage between the individual damages induced from each particular seastate exclusively.

The procedure for defining these characteristics is described below, according to the ISO 19902 provisions [14], as these are described in its corresponding section A.16.7.2.3.2. The scatter diagram that was used and the directional distribution of significant wave height can be found in Figure D. 1 and Figure D. 2 of Appendix D.

The procedure to define the centre of the fatigue damage contains several steps:

1) use the scatter with probabilities of occurrence of the different combinations of significant wave height and peak period [H_s, T_p]
2) derive the corresponding mean zero crossing period for the average T_p of each block, according to: $T_z = 0.778 \cdot T_p$
3) for each H_s block, use the corresponding average value
4) calculate the relative damage for each [T_z, H_s] combination, as: $(probability\ of\ occurrence) \cdot {H_s}^m / T_z$, where m is the inverse slope of the S-N curve. The

   value of m=3 was used in all cases, as it is the most common slope value of the first branch of the bilinear S-N curves where most of the damage is usually accumulated
5) for each T_z value, the summation of relative damages for all the relevant H_s values was calculated
6) the normalized corresponding values were defined, by dividing the above sum values with the total summation of relative damages for all T_z
7) the cumulative values were defined from the normalized ones, going from the smallest to the biggest T_z values
8) the characteristic wave period (T_c) that corresponds to the 50% of cumulative damage was derived, by applying linear interpolation among the cumulative values calculated previously

9) the wave period to be used as the centre of fatigue damage is $T_{ref} = \frac{T_c}{0.81}$

10) for each H_s, the summation of relative damages for all the relevant T_z values were similarly calculated

11) the normalized corresponding values were defined by dividing the above sum values with the total summation of the relative damages for all H_s

12) the cumulative values were defined from the normalized ones, going from the smallest to the biggest H_s values

13) the characteristic wave period (H_c) that corresponds to the 50% of cumulative damage was determined from the cumulative values calculated in step 12, using linear interpolation

14) the wave period to be used as the centre of fatigue damage, is then: $H_{ref} = 1.86 \cdot H_c$

After following the above described approach, the wave to be used in the sensitivity study of wave directionality has the following characteristics: period $T_{ref} = 7.93\,s$ and height $H_{ref} = 5.99\,m$, representing the centre of fatigue damage for the metocean data of the concerning location.

Consequently, the accumulated damage due to this wave characteristics following the base case assumptions (section 5.1) was calculated, for the 6 critical locations that have been defined. This was done in order to set the basis of comparison with the results to be obtained from the sensitivity study of wave directionality that follows. What has changed concerning the base case assumptions is the wave period considered, affecting the number of applied cycles. The new results are presented in the following table.

Table 6-4 – Damage considering the base case approach for the centre of fatigue damage wave period

member location	section detail	$\Delta\sigma$ (MPa)	fatigue limit (MPa)	damage D (-)
1	7	92.37	29.24	332.24
2	1	77.44	36.84	97.89
3	1	66.59	26.32	170.59
4	1	69.49	26.32	193.91
5	1	46.12	36.84	20.67
6	2	36.13	29.24	19.89

6.2.4 Examining the effect of wave directionality

It is, therefore, apparent that friction is actually a force that does not have a constant magnitude as usually is considered. Its magnitude depends on the applied "pulling force", which in this case is the axial force that is generated at the relevant end of the bridge. As long as this force does not exceed the limit of the maximum static friction, the magnitude of friction equals that force's one (their directions are opposite). After reaching that value, sliding starts and the friction force obtains a constant lower value, the kinetic friction. The question that arises is how to incorporate this behaviour in the obtained results for the relative displacements with time, in a clear and proper way.

Taking into account the main properties of friction as these were described previously, the way to link the directionality of the incoming wave with the resultant damage is by linking the generated load due to the deformations of the two bridge landings with the maximum static friction limit. Through this, the magnitude of the generated friction can be represented in a more realistic way, considering its different states (static/kinetic friction).

The approach that was followed is based on the axial load that is generated on the bridge as a result of the relative displacement that is applied to it. This relative displacement was obtained from the analysis performed for the two platforms per wave direction considered and was derived as a function of time for one wave period. Hence, at each time step, the axial load that is generated on the bridge was determined, according to the formula: $F_{applied} = \frac{EA}{L_{bridge}} \cdot y_{rel}$, where A is the cross section of each bridge's side, L_{bridge} is the length of the bridge and y_{rel} the relative displacement at the sliding direction of the bridge, considering the whole bridge as a rigid body.

Then, two situations were considered according to the (each time) results. The procedure that was followed is the following:

a) First, the limit value for the relative displacement that corresponds to the maximum static friction was defined, from the equality: $F_{applied} = Fr_{max}$

b) For the situations where $y_{rel}^{max}(i) < y_{rel}^{limit}$, the friction force to be considered should have a lower magnitude than the max static friction considered in the base case. This should then be $Fr = \frac{EA}{L_{bridge}} \cdot y_{rel}^{max}(i)$, where $y_{rel}^{max}(i)$ is the largest relative displacement induced from the certain wave direction examined

c) For the situations where $y_{rel}^{max}(i) > y_{rel}^{limit}$, the friction force to be considered should have the magnitude of the maximum static friction, since it cannot become larger than that

This resulted in obtaining different stress ranges per wave direction considered, thus in different number of load cycles until failure (N) and accumulated damage (D). Figure 6-4 below demonstrates the different situations that define the magnitude of the friction load that should be applied.
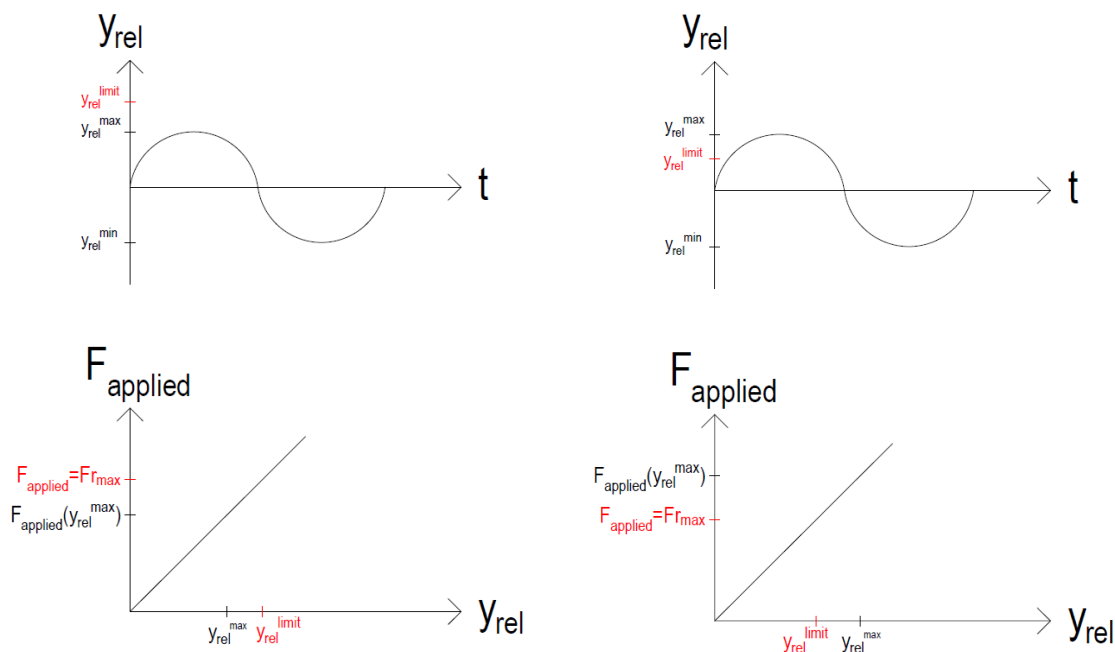
Figure 6-4 – Comparison of the maximum induced relative displacement with the one corresponding to the maximum static friction

The bridge comprises of two legs, each of which consists of two (top/bottom) tubular members with the following section: outer diameter D=323.9 mm and thickness t=8 mm. These characteristics, in accordance with the elastic modulus of 210 GPa, determine the limiting value for the relative displacement that results in the maximum static friction. This is $y_{rel}^{limit} = 0.056\ cm$. Apparently, this sets a very low limit for the exceedance of the sticking phase and the transition to the slipping one.

Having defined the limiting value for the relative displacements and the induced relative displacement with time plots from the analyses performed for the different wave directions, the magnitude of friction that should be considered at each situation was able to be determined. Figure 6-5 depicts how wave direction is defined with respect to the platforms' global axis system, while Table 6-5 below illustrates the results for the several directions examined.
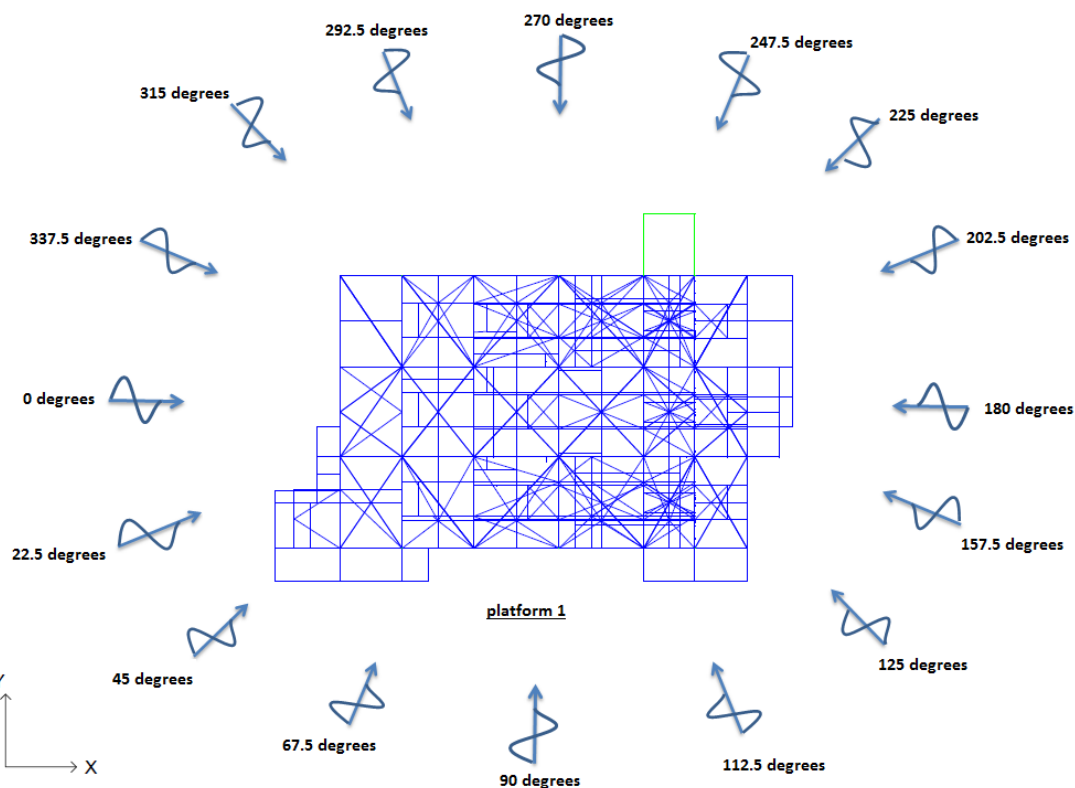
Figure 6-5 – Wave incoming directions

Table 6-5 – Generated friction per wave direction considered

Wave direction (degrees)	Probability of occurrence (%)	Largest relative displacement applied (cm)	Generated friction (kN)
0	6.34	0.005	7.20
22.5	3.31	0.292	75.29
45	2.76	0.513	75.29
67.5	4.17	0.362	75.29
90	5.60	0.235	75.29
112.5	2.89	0.351	75.29
135	1.54	0.516	75.29
157.5	1.14	0.293	75.29
180	1.18	0.006	7.47
202.5	1.77	0.293	75.29
225	3.96	0.516	75.29
247.5	11.51	0.351	75.29
270	11.88	0.236	75.29
292.5	10.67	0.362	75.29
315	12.64	0.513	75.29
337.5	18.65	0.292	75.29

According to the above obtained results, it is obvious that only in the cases where the wave approaches the platforms from the directions perpendicular to the bridge (0 and 180 degrees) the state is sticking, and the friction is smaller than the maximum static limit. In all the other cases, that limit is exceeded due to the relative displacement that is applied and the generated friction is considered to have its maximum static value.

Therefore, the resultant stress ranges are different than the initially considered ones only at these two cases. The following table shows the resultant damage for the 6 critical member locations, by summing up the damage occurring per wave direction and incorporating the probability of occurrence of each of these directions. The difference with the results obtained without treating the wave directionality effect (damage from Table 6-4) is also presented.

Table 6-6 – Induced damage from considering the wave directionality and its impact on the initial results

member location	section detail	damage (-)	difference (%)
1	7	307.26	-7.52
2	1	90.53	-7.52
3	1	157.76	-7.52
4	1	179.93	-7.52
5	1	19.12	-7.52
6	2	18.39	-7.52

The above results indicate a reduction in the accumulated fatigue damage of around 7.5% for all the details, due to the very small induced relative displacements at the sliding direction in the situations of an approaching wave direction perpendicular to the longitudinal direction of the bridge (sliding direction), which seems rational. However, this reduction is not that high to result in a sufficient damage, thus those details remain still inadequate against fatigue.

6.2.5   Validation of the new approach

In an effort to validate the method of considering the effect of wave directionality, it was decided to link the transverse load that is generated at the outer beam of the bridge landing due to the induced relative displacements (member 0003-0013-0011-0014-0005 of HE700A section) with the maximum static friction limit. The way of handling it is the following:

a) The force that is required to deform the relevant joints (0013, 0014) of the HE700A beam at the level of the maximum induced relative displacement (from the time plots of the platform deformations due to the applied wave) is defined

b) This force is compared with the maximum static friction

c) If this force is smaller than the maximum static friction load, then this implies that all the induced deformation can be captured as transverse deformation of the

HE700A member. This means that, in this case, there is always sticking between the bridge and the bridge landing's bearing pads. Therefore, friction is static and its magnitude is equal to the transverse force on the HE700A member

d) If this force is larger than the maximum static friction load, slipping occurs. Hence, the magnitude of friction is considered to be equal to the maximum static friction value

By following this approach, it was again concluded that slipping occurs in all the cases, except from the situations in which the wave approaches the platforms perpendicularly to the bridge (cases of 0 and 180 degrees). Only in these two cases the generated friction hasn't reached the maximum static limit. Consequently, the accumulated damage was the same as from the previous approach, resulting again in a reduction of 7.52% for all the critical member locations.

Therefore, the two ways of approaching the directionality effect are in agreement and it can be validated that the only wave directions that can be excluded are the perpendicular to the bridge ones. In all the other situations, the resultant damage is the same as the one obtained from the base case approach.

7 Weld improvements and strengthening of the structure

```
                        ┌─────────────────────────────────────┐
                        │ Improve structure's fatigue behaviour │
                        └─────────────────────────────────────┘
```

Column 1:
- weld improvements
- examine improvement options at the 6 prone locations
- select improvement leading in the highest detail class
- apply the new S-N class characteristics
- perform the fatigue checks for the improved details
- conclude whether the new details are sufficient

Column 2:
- modify structure
- modify configuration by adding beams at the sliding direction
- define properties of new members
- add new members in SACS model
- run analysis and define stresses and stress ranges
- determine the new member locations to be examined
- perform the fatigue checks for all the member locations
- conclude whether the new structure is sufficient

Column 3:
- strengthen front member's section
- option 1: weld a plate at the top flange
- option 2: weld a plate along section's height
- select plate dimensions
- determine the characteristics of the strengthened section
- define the new section locations
- classify new details
- calculate the new stresses and stress ranges
- stress ranges < fatigue limit ?
  - NO → increase plate dimensions
  - YES → plate dimensions are sufficient

From the fatigue analysis that was performed and presented in chapter 5, it was concluded that the bridge landing is not able to resist the cyclic stresses that are induced from the generated friction, during its service life of 25 years. Since when dealing with a fatigue issue, the design mostly concerns the connection details, the problem is identified in specific locations of the structure. These locations, in this case, were highlighted from the analysis that was performed and were listed in Table 5-3 of section 5.5. Figure 7-1 illustrates the 6 most sensitive locations that have been defined from the fatigue assessment.
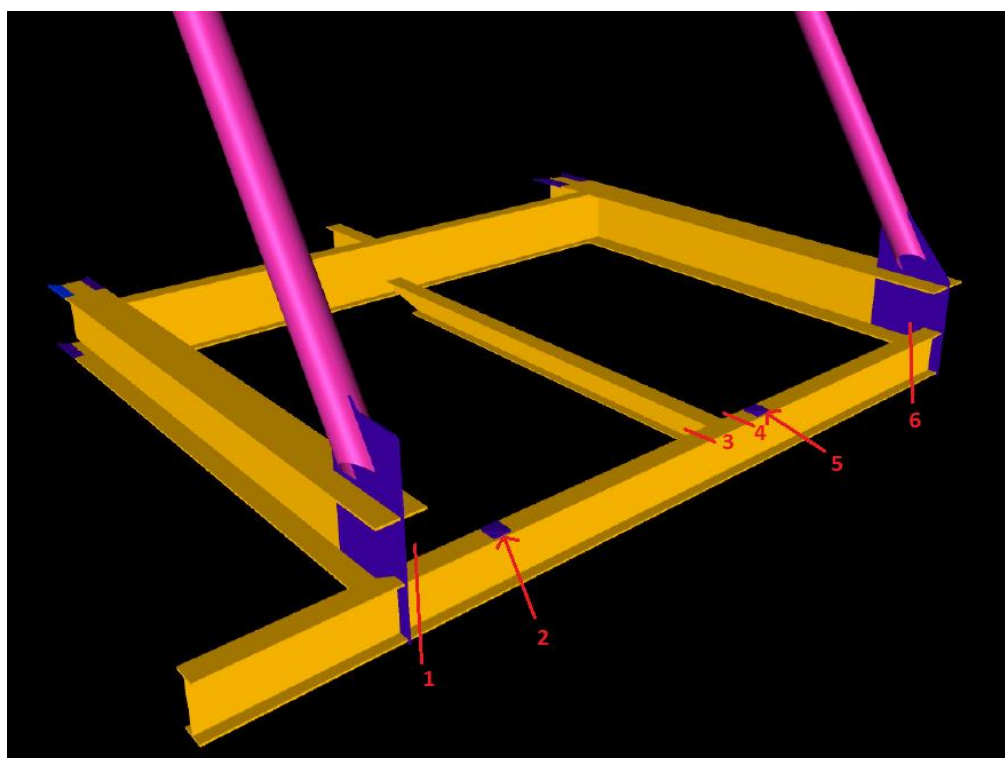
Figure 7-1 – The 6 fatigue-prone locations

Having these defined, the final step concerns the improvement of the structure in such a way that it will be fatigue-resistant. Without considering the results of the sensitivity studies that were performed in the previous chapter, the intention of this section is to strengthen the bridge landing according to the analysis that was performed for the base case (chapter 5).

The following options will be considered:
1) changing or improving the weld details in the sensitive locations that have been defined from the fatigue assessment
2) modifying the structure by adding beams perpendicular to HE700A, at the bearing pad locations
3) strengthening the section HE700A of beam (0003-0006), through welding a plate to its top flange
4) transforming the type of section HE700A of beam (0003-0006)

7.1   Improve or change the existing weld details at the prone locations

7.1.1   Approach description

This concerns the locations where the accumulated damage is above the limit of 1.0, thus it is about the locations described below:

- Connection of member HE700A with the plate girder PG1. Member (0003-0006) of section HE700A is welded to a plate of 20 mm which is slotted to the member (0001-0003): location 1
- Weld of the bearing pad at the top flange of the member (0003-0006) of HE700A: locations 2 and 5
- Connection of the HE400A member (0010-0011) to the HE700A member (0003-0006): locations 3 and 4
- Connection of member HE700A with the plate girder PG2. Member (0003-0006) of section HE700A is welded to a plate of 20mm that is slotted to the member (0004-0006): location 6

The actions to be made can be summarized in the following steps:

- Based on the classification of the examined detail, check what actions can be done in order to improve its class and select the best applicable one, taking into account the feasibility of the required actions
- Apply the new and improved S-N curve characteristics for that detail
- Calculate the new accumulated damage due to fatigue and reassess the details by comparing the stress range with their new fatigue limits

7.1.2   Locations 1 and 6 (end connection of HE700A with plate)

- Details classification so far

Both these locations represent the same kind of connection of a member welded to a plate. The classification of the detail was defined according to the situations 1 and 2 of Table A-8 of the DNVGL-RP-C203 provisions [1]. An illustration of the connections can be found on Figure C. 4 of Appendix C.

In these cases, the type of weld that was used to perform the connection plays a significant role to the classification of the detail and thus to its fatigue resistance. Since the connections were performed through fillet welds, two fatigue assessments were required, one by examining root cracking and the other concerning the toe cracking of the weld. The category that was applied was the W3 one for checking the weld root and the G one for examining its toe. Both these categories are among the weakest ones, whereas W3 is the worst possible category that can be achieved for such kind of connections and is the governing situation here.

- How can it be improved ?

The way that these connections can be improved is through changing the type of the weld. Fillet and partial penetration butt welds result in a poor fatigue behaviour of the detail, requiring examining weld root cracking in addition to a its toe failure.

On the other hand, performing the connection through full penetration butt welds is the only alternative that can enhance its fatigue behaviour. By using this kind of weld to these locations, the classification is performed according to situation 1 described in Table A-8 of the DNVGL-RP-C203. Not making any changes in the dimensions of the plate, the classification is defined from the following:

- plate thickness: $t = 20mm \leq 25mm$
- edge distance between the plate end and the weld: $175 - \frac{300}{2} = 25mm > 10mm$

These, in combination, conclude into the category E for that connection, which is the best possible to be achieved for such connection. Figure 7-2 below illustrates this detail categorization.

Figure 7-2 – Classification of improved locations 1 and 6 according to DNVGL RP-C203 [1]

- Results/Conclusions

The following Table 7-1 illustrates the changes in the fatigue assessment of locations 1 and 6, for the actions described. Both the initial and the improved situations are presented, in order for the changes in the results to be apparent.

Table 7-1 – Fatigue assessment for improved details at locations 1 and 6

member location	state	weld type	S-N curve	$\Delta\sigma_{applied}$ (MPa)	fatigue limit (MPa)	n (cycles)	N (cycles)	damage D (-)
1	initial	fillet weld	W3 (for root cracking)	125.03	21.05	$1.58 \cdot 10^8$	$4.78 \cdot 10^4$	3302
	improved	full penetration butt weld	E	92.37	46.78	$1.58 \cdot 10^8$	$1.24 \cdot 10^6$	127.19
6	initial	fillet weld	W3 (for root cracking)	48.71	21.05	$1.58 \cdot 10^8$	$8.07 \cdot 10^5$	195.29
	improved	full penetration butt weld	E	36.13	46.78			

The results presented in Table 7-1 indicate the amount of improvement in the fatigue assessment of the details for the locations presented. In this situation, the changes concern the type of S-N curve to be adopted, thus the fatigue limit and the resistant number of cycles (N) for the particular detail. These finally affect the induced damage and the fatigue life.

For location 1, the weld improvement that was suggested results in a much lower fatigue damage than the one defined for the initial case. Nevertheless, it is still above the limiting value of 1.0, thus that detail remains still incapable to resist fatigue for the service life of 25 years.

Regarding location 6, using a full penetration butt weld results in a fatigue limit that is larger than the applied stress range and thus the detail can be characterized to be sufficient against fatigue.

7.1.3   Locations 2 and 5 (bearing pad locations)

- Details classification so far

These locations refer to the attachment of the bearing pad on the top flange of the HE700A member (0003-0006). The classification of such a connection was defined according to the situation 2 of Table A-7 of DNVGL-RP-C203 [1]. A representation of the certain detail is available on Figure C. 5 of Appendix C.

In this case, the classification of the detail is determined from the weld length and the edge distance between the weld end and the base member (here the HE700A one). The category that was adopted was the F1 one, as described in section 5.4.2. Moreover, since it is fillet weld, weld root cracking should also be checked by using the W3 category.

- How can it be improved ?

The only way that the class of such connections can be improved is through decreasing the length of the welds, as depicted in Figure 7-3. However, this is not possible to be done, since the length of the welds is determined by the dimensions of the bearing pad (it is welded along its whole sides) which are specified from the provider of the bearing pads. In addition, reducing the weld length would increase the applied stresses in the fillet welds as a result of reducing their dimensions. This may jeopardize the strength adequacy of the weld itself, hence in case there is the possibility of doing so, attention shall be paid in the strength requirement of the fillet welds.

E	$l \leq 50$ mm
F	$50 < l \leq 120$ mm
F1	$120 < l \leq 300$ mm
F3	$l > 300$ mm
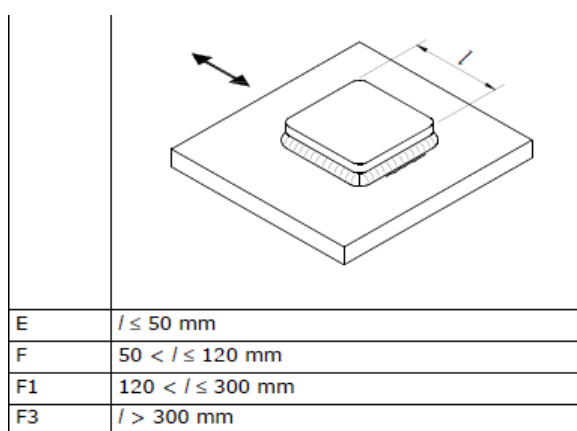
Figure 7-3 – Classification of locations 2 and 5 depending on weld length, according to DNVGL RP-C203 [1]

- Results/Conclusions

Since this connection depends on the dimensions of the bearing pad, there is not enough space left to make changes into these. Therefore, its detail categorization can't be improved.

7.1.4   Locations 3 and 4 (connection of HE400A to HE700A)

- Details classification so far

These locations refer to the attachment of one member to another transversely. The detail classification was defined according to the situation 6 of Table A-7 of DNVGL-RP-C203 [1]. A depiction of these locations can be found on Figure C. 6 of Appendix C.

The exact detail category for such a situation, is determined from the relevant dimension of the transversely attached member, which in this case is the HE400A one. Since the flange width of this member is 300 mm, category W1 was adopted.

- How can it be improved ?

There are two ways through which the detail can be improved. The first one concerns changing the dimension of the transverse member (HE400A). This is something that affects the whole structure and does not represent a very convenient choice that could be made directly. Moreover, based on the current classification (W1), the only available improvement is to enhance its behaviour by one category (G). However, this requires the relevant dimension of the attached member to be $\leq 150\ mm$, which requires a very small -not realistic- cross section (i.e. HE140A).

The other way of improving the detail is through handling the weld itself. Grounding the ends of the weld will result in a much better behaviour by means of fatigue, since the transition becomes smoother. According to the code provisions, this is described in the situation 5 of Table A-7, where the weld ends are grounded to a certain radius by grinding.

The classification of the detail is then defined from the following:
- r: weld grounding radius, which is achieved by grinding
- W: the continuous member's width

Since the continuous member is the HE700A one, $W = 300mm$. In order to achieve the best possible category, it is required that: $\frac{r}{W} \geq \frac{1}{3}$ and $r \geq 150mm$. Thus, with a grounding radius of $r = 150mm$, the highest classification can be obtained, which is the E curve. Figure 7-4 below illustrates this categorization.

	5.	5. Gusset plate with a radius welded to the edge of a plate or beam flange.	5. The specified radius to be achieved by grinding.
E	$\frac{1}{3} \leq \frac{r}{W}, r \geq 150mm$		
F	$\frac{1}{6} \leq \frac{r}{W} < \frac{1}{3}$		
F1	$\frac{1}{10} \leq \frac{r}{W} < \frac{1}{6}$		
F3	$\frac{1}{16} \leq \frac{r}{W} < \frac{1}{10}$		
G	$\frac{1}{25} \leq \frac{r}{W} < \frac{1}{16}$		

Figure 7-4 – Classification of improved locations 3 and 4 according to DNVGL RP-C203 [1]

- Results/Conclusions

The following table illustrates the changes in the fatigue assessment of locations 3 and 4, for the improvements described. Both the initial and the new situation are presented, in order for the changes in the results to be apparent.

Table 7-2 – Fatigue assessment for improved details at locations 3 and 4

member location	state	weld radius (through grinding)	S-N curve	$\Delta\sigma_{applied}$ (MPa)	fatigue limit (MPa)	n (cycles)	N (cycles)	damage D (-)
3	initial	no radius	W1	66.59	26.32	$1.58 \cdot 10^8$	$5.83 \cdot 10^5$	270.38
	improved	$r = 150mm$	E	66.59	46.78	$1.58 \cdot 10^8$	$3.31 \cdot 10^6$	47.64
4	initial	no radius	W1	69.49	26.32	$1.58 \cdot 10^8$	$5.13 \cdot 10^5$	307.34
	improved	$r = 150mm$	E	69.49	46.78	$1.58 \cdot 10^8$	$2.91 \cdot 10^6$	54.15

The results presented in Table 7-2 show the level of fatigue improvement for the details at the locations presented. Any changes affect the type of S-N curve to be applied, thus the fatigue limit and the resistant number of cycles (N) for the particular detail, which finally influence the induced damage and the fatigue life.

The improvements result in a much better fatigue behaviour, which is expressed through a significant reduction in the accumulated damage. Nonetheless, both of the details still remain incapable to be sufficient for the FLS. This is expressed by the value of the accumulated damage, which remains to be larger than the limiting value (1.0).

7.2   Modify the structure by adding beams at the bearing pad locations

The second way through which the fatigue behaviour of the bridge landing can be improved concerns its strengthening, through adding members, hence changing the layout. It is apparent that, in the critical locations 1 to 6 where the FLS requirement is not satisfied, there is a large resultant applied stress (thus a high stress range). This high applied total stress is determined by the high stresses caused by the out-of-plane moment that is induced from the generated friction at the bearing pad locations. Hence, strengthening the structure should be done in such a way that this moment at these locations is decreased drastically.

7.2.1   The strengthened structure

The following option is investigated: to add two beams in the horizontal plane of the bridge landing, such that they reduce the applied bending moment at the critical locations of the front beam (0003-0006). These were added at the direction of sliding, in the locations of the bearing pads. As a start, they were modelled to be identical to the member (0010-0011), having the same section (HE400A) and connection details as this. The figure below illustrates the top view of the strengthened bridge landing, where the two added beams are highlighted. The joint names are also shown in the figure.
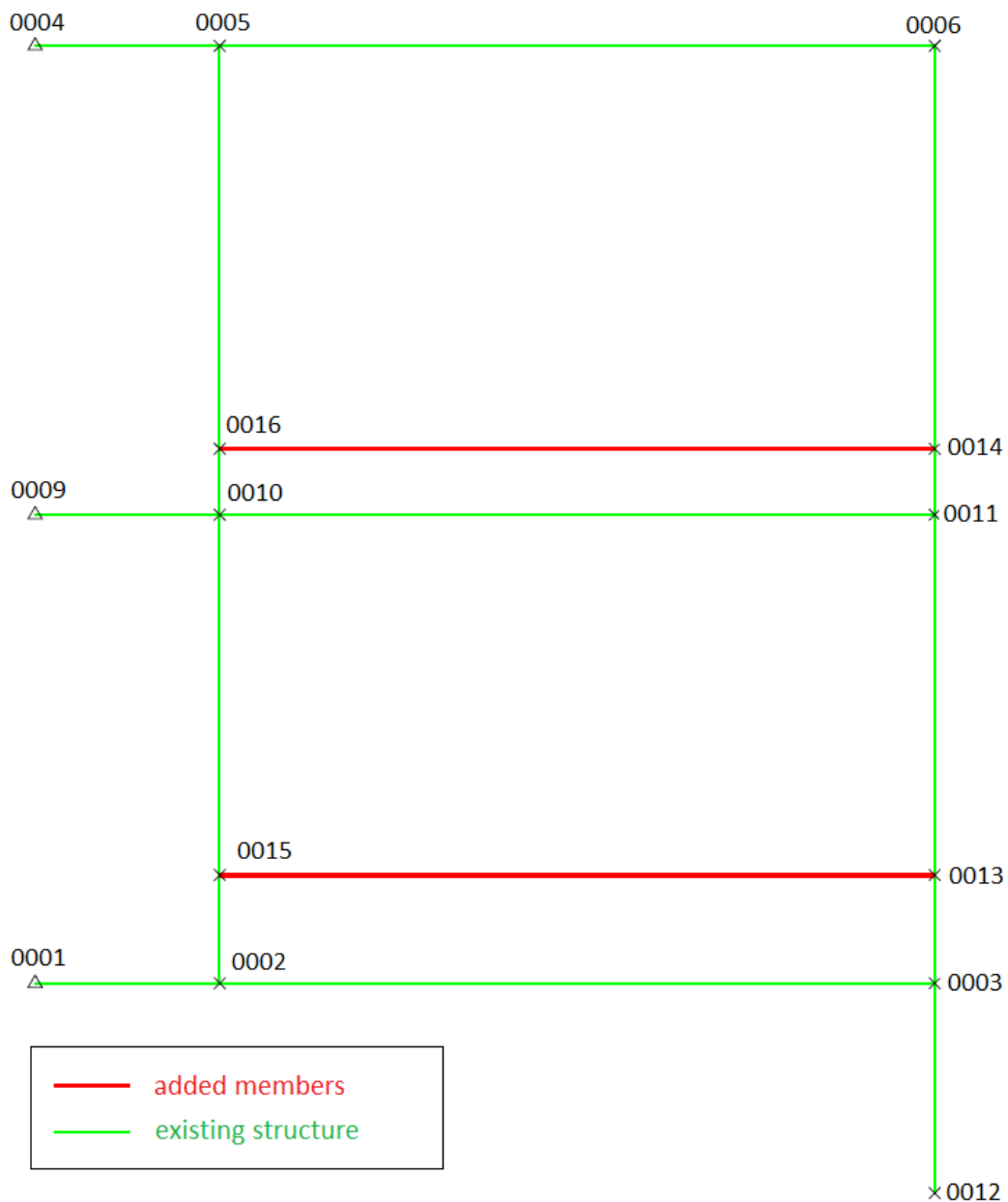
Figure 7-5 – Top view of the strengthened bridge landing

A new fatigue assessment was performed for the strengthened structure, following the same approach that was defined for the base case. A new analysis was first performed, in SACS, in order to define the new applied stresses at the multiple locations, due to the applied friction load. Apart from the changes in the applied stresses and member forces, additional critical member locations need to be checked in the updated structure . The locations that were examined for the fatigue assessment are depicted in Figure 7-6 below, in which the new ones are marked with green.
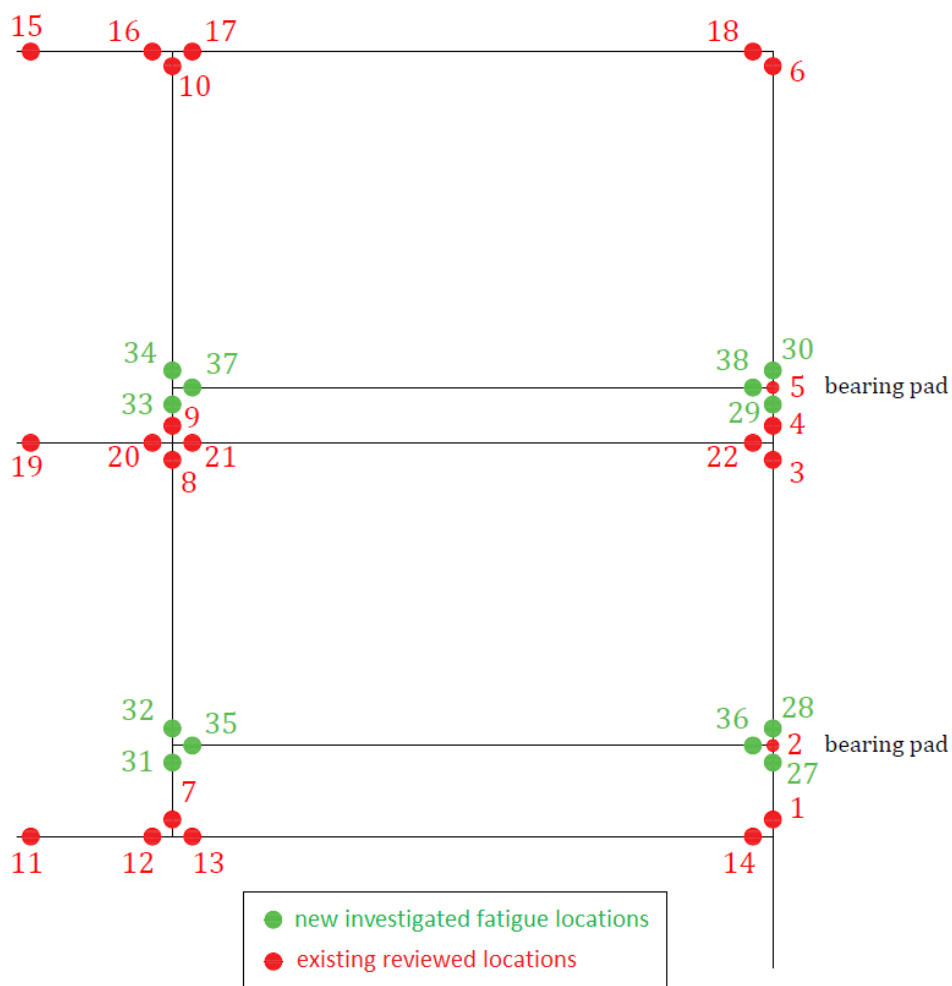
Figure 7-6 – Locations to be examined against fatigue

It should be noted that, since the added beams were assumed to have the properties of the middle beam (0010-0011), the new details were classified in the same way as the corresponding ones of the member (0010-0011). Thus, regarding their classification, the following correlations apply:

Table 7-3 – Classification of new details

existing locations	corresponding new locations	description of connection detail	S-N curve
3, 4	27, 28, 29, 30	location of a continuous member in a crossing joint with another member	W1
8, 9	31, 32, 33, 34	location of a continuous member in a crossing joint with another member	W1
21, 22	35, 36, 37, 38	split member connected transversely to a continuous one	W1

7.2.2 Results

Table 7-4 demonstrates the fatigue assessment for the strengthened bridge landing, for all the locations that the requirement was not satisfied. The initial prior to strengthening values of fatigue damage are also listed for reference.

Table 7-4 – Results for the problematic locations of the strengthened bridge landing

member location	σ_{Mz} (MPa)	$\Delta\sigma_{tot}$ (MPa)	S-N curve	fatigue limit (MPa)	N (resistant cycles)	damage D (-)	previous damage D (-)
2	21.24	42.23	F1	36.84	$6.27 \cdot 10^6$	25.15	155.15
3	-16.24	32.60	W1	26.32	$4.97 \cdot 10^6$	31.72	270.38
4	-16.86	33.82	W1	26.32	$4.45 \cdot 10^6$	35.43	307.34
7	32.72	66.02	W2	23.39	$3.88 \cdot 10^5$	406.68	≈ 0
8	-15.75	30.94	W1	26.32	$5.37 \cdot 10^6$	29.36	≈ 0
9	19.06	38.73	W1	26.32	$2.74 \cdot 10^6$	57.60	≈ 0
27	21.24	42.23	W1	26.32	$2.29 \cdot 10^6$	68.96	N/A
28	18.12	36.03	W1	26.32	$3.68 \cdot 10^6$	42.85	N/A
29	9.44	18.79	W1	26.32	$4.89 \cdot 10^7$	3.22	N/A
31	22.20	44.98	W1	26.32	$1.75 \cdot 10^6$	90.21	N/A
32	-19.09	37.63	W1	26.32	$2.98 \cdot 10^6$	52.83	N/A
33	11.28	23.17	W1	26.32	$1.51 \cdot 10^7$	10.48	N/A
34	-9.56	18.53	W1	26.32	$4.60 \cdot 10^7$	3.43	N/A

7.2.3 Conclusions

The obtained results demonstrate that the case changed in a lot of points. Although the front beam (0003-0006) was alleviated by the generated out-of-plane bending moment (M_z), there are still locations that are not adequate in that member. These are locations 2, 3 and 4 in which although the accumulated damage decreased a lot in comparison with the initial structure case, it remains larger than 1.0 and thus inadequate.

However, in addition to these three locations, 3 new ones appear to be insufficient. These are locations 7, 8 and 9, which initially were totally unaffected with having a negligible damage. These locations refer to the rear beam (0002-0005) and are found to be insufficient for the strengthened structure. The reason for that change is the transfer of the friction force through the added beams (different load path), which now generates large out-of-plane bending moment to the rear member.

Finally, there are also some new defined member locations that are inadequate for the FLS design. These are locations 27, 28, 29, 31, 32, 33 and 34 which were defined for the new structure. In all these locations, the accumulated damage is larger than 1.0, although in locations 29, 33 and 34 the fatigue limit requirement is satisfied and thus a detailed fatigue assessment can be neglected.

Consequently, the added beams helped in reducing the out-of-plane bending moment in the locations of the front beam, although some of them remain inadequate. However, the total amount of locations that are insufficient increased, because of the new sensitive locations appeared. Thus, it was decided to extend the added members until the support ends of the landing, through adding the members (0017-0015) and (0018-0016). This is presented in the following section.

7.2.4   New strengthened case

This situation comprises adding the members (0017-0015) and (0018-0016) to the analysis model, in order to reduce the out-of-plane bending moment generated at beams (0003-0006) and (0002-0005). The new members are placed until the supports of the bridge landing with their end joints (0017) and (0018) modelled as pinned points. The new members were considered to be identical to member (0009-0010), having the same section (HE500A) and connection details. Figure 7-7 shows a top view of the structure with the new members highlighted and the joint names depicted.
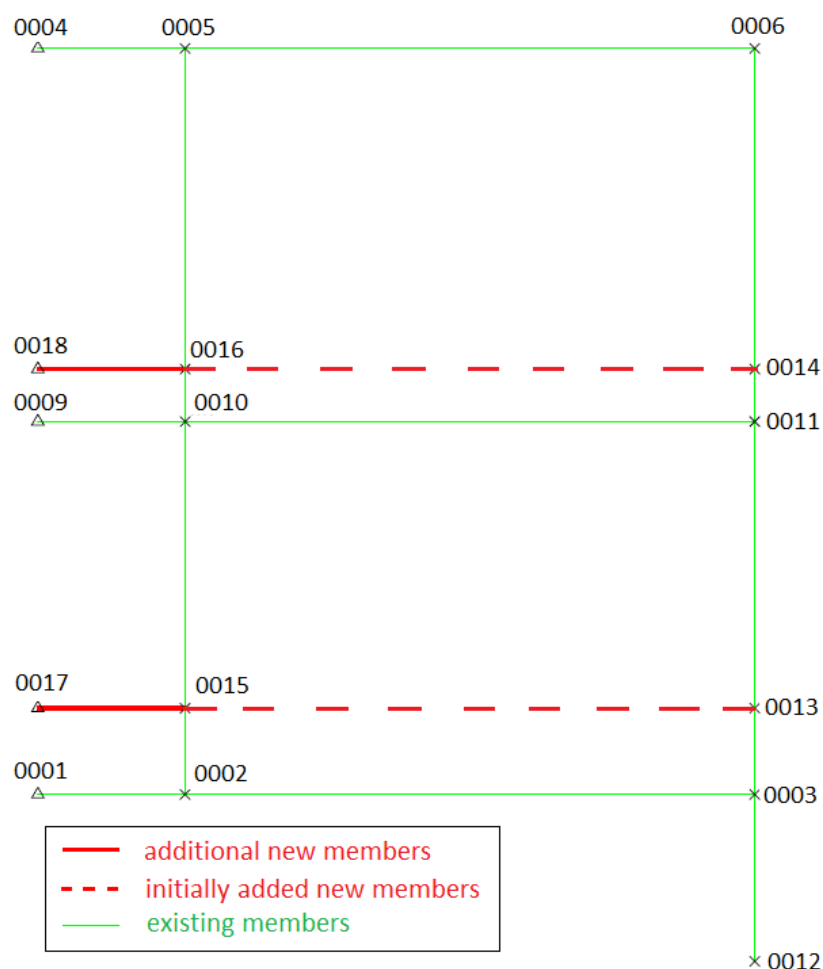
Figure 7-7 – Top view of the new strengthened case

The addition of the two members generated new member locations that can be critical for the fatigue assessment of the structure. Figure 7-8 demonstrates all the locations that were examined for this case, in which the new ones are marked with blue.
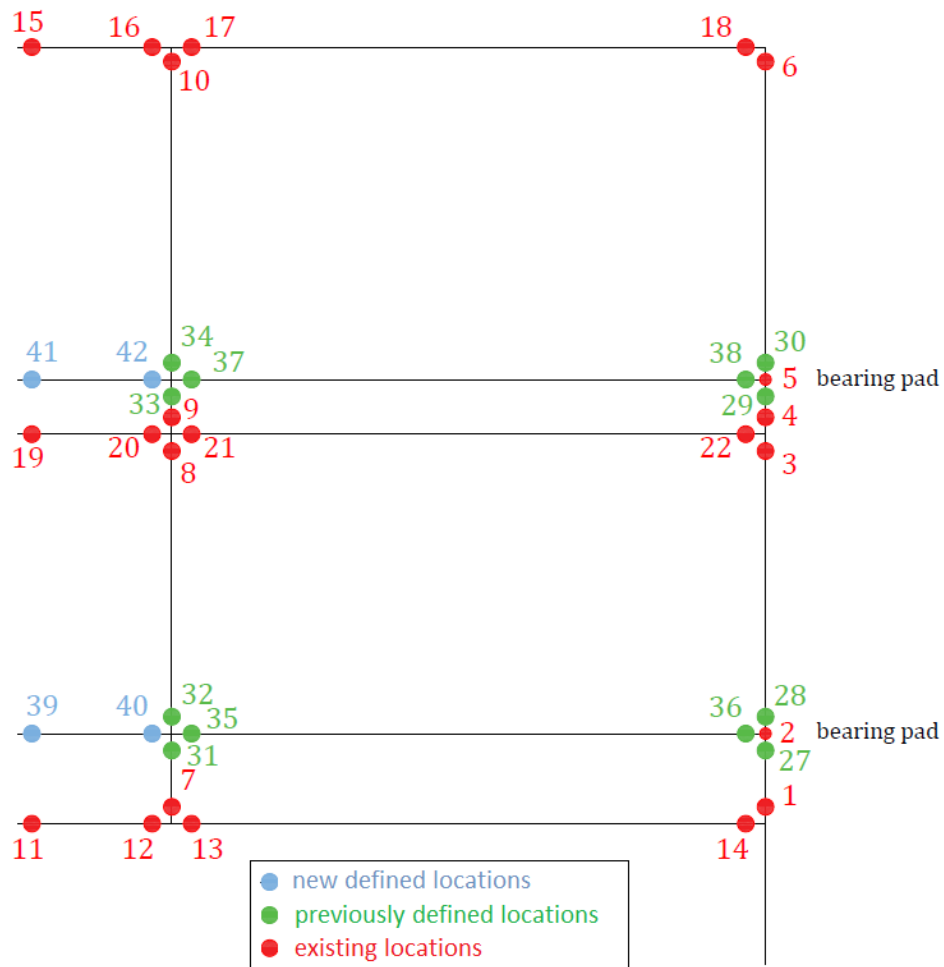
Figure 7-8 – Locations considered for the FLS of the new case

Since the added beams were assumed to have the properties of the middle member (0009-0010), the new details were classified in the same way as the corresponding ones of member (0009-0010). The new correlations are listed in Table 7-5.

Table 7-5 – Classification of new details

existing location	corresponding new locations	description of connection detail	S-N curve
19	39, 41	location of a member in a crossing joint with another member	W3
20	40, 42	location of a member in a crossing joint with another member	W3

1) Results

A new fatigue analysis was conducted, for the last defined structural model. Table 7-6 demonstrates details regarding the fatigue assessment that was performed for this case. Results for all the locations that were critical prior to the addition of the new members are presented. The damage defined in the previous strengthened situation is also listed for comparison.

Table 7-6 – FLS results for the new strengthened structure

member location	σ_{Mz} (MPa)	$\Delta\sigma_{tot}$ (MPa)	S-N curve	fatigue limit (MPa)	N (resistant cycles)	damage D (-)	previous damage D (-)
2	6.48	12.87	F1	36.84	$1.75 \cdot 10^9$	0.09	25.15
3	-6.44	12.96	W1	26.32	$3.14 \cdot 10^8$	0.50	31.72
4	-7.41	14.88	W1	26.32	$1.57 \cdot 10^8$	1.003	35.43
7	1.51	3.05	W2	23.39	$2.12 \cdot 10^{11}$	≈ 0	406.68
8	-0.92	1.81	W1	26.32	$5.24 \cdot 10^{12}$	≈ 0	29.36
9	1.51	3.06	W1	26.32	$3.76 \cdot 10^{11}$	≈ 0	57.60
27	6.48	12.87	W1	26.32	$3.24 \cdot 10^8$	0.49	68.96
28	5.89	11.71	W1	26.32	$5.21 \cdot 10^8$	0.30	42.85
29	5.18	10.31	W1	26.32	$9.83 \cdot 10^8$	0.16	3.22
31	1.46	2.96	W1	26.32	$4.42 \cdot 10^{11}$	≈ 0	90.21
32	-0.94	1.85	W1	26.32	$4.61 \cdot 10^{12}$	≈ 0	52.83
33	1.54	3.11	W1	26.32	$3.46 \cdot 10^{11}$	≈ 0	10.48
34	-0.78	1.54	W1	26.32	$1.18 \cdot 10^{13}$	≈ 0	3.43
39	0.00	6.57	W3	21.05	$3.38 \cdot 10^9$	0.05	N/A
40	-0.41	5.75	W3	21.05	$6.57 \cdot 10^9$	0.02	N/A
41	0.00	5.62	W3	21.05	$7.40 \cdot 10^9$	0.02	N/A
42	-0.34	4.94	W3	21.05	$1.41 \cdot 10^{10}$	0.01	N/A

2) Conclusions

As is demonstrated in the above Table 7-6, the fatigue analysis of the new strengthened bridge landing highlights only one location with accumulated damage larger than 1.0. This comprises location 4, where the accumulated is slightly above the limiting value of 1.0 for the entire service life of 25 years. However, the applied stress range at this location is below the fatigue limit, hence it can be regarded to be adequate against fatigue. In all the other locations, the requirement for the FLS is satisfied and the structure is considered to be fatigue-resistant.

7.3 Strengthen the front beam by welding a plate to its top flange

This improvement option concerns strengthening the front member by welding a plate to its top flange. By doing so, the stiffness of the HE700A section will be increased, thus reducing the applied stresses and the resultant stress ranges. Since the main cause for the high induced stresses is the out-of-plane bending moment M_z, welding a plate in the direction of the flange seems to be an effective way to face the large stress σ_{M_z}.

The way of examining this option can be summarized in the following steps:

- Select the plate dimensions and determine the properties of the strengthened section
- Define the new applied stresses and stress ranges
- Derive the critical locations of the new section and classify them concerning fatigue (corresponding S-N curve)
- Perform the fatigue assessment of the sensitive locations and define the required plate dimensions such that the fatigue requirement is satisfied
- Define the required length of the welded plate

7.3.1 New section characteristic

Regarding the plate dimensions, its thickness was selected to be the same as the HE700A top flange's one. This was decided in order to avoid any thickness changes inside the new section, thus not having to incorporate any stress concentration factors in these locations. Taking this for granted, the width of the plate should be determined from the fatigue requirement. Moreover, the plate is considered to be welded through full penetration butt welds, since it is the strongest option and is feasible due to the same thickness between the HEA-flange and the plate.

It should be noted that, for calculating the properties of the new section, only the top flange of the HE700A section was considered. This was done because the applied friction load acts at the top flange of the HE700A section. Thus, it was assumed that its top flange receives the whole load[2].

---

[2] This was considered instead of considering the whole section which would require including also a torsional moment with respect to its center of gravity, due to the eccentricity of the applied friction. Since HEA is an open type section, including a torsional moment in the stress calculations would not be beneficial. However, this is something that is considered in the 4th improvement option examined, in section 7.4.

- Center of gravity

The center of gravity (CoG) of the strengthened section is defined according to the following equations, with reference to Figure 7-9 below:

$$Y_{CoG} = \frac{\frac{b_{flange}}{2} \cdot A_{flange} + \left(b_{flange} + \frac{b_{plate}}{2}\right) \cdot A_{plate}}{A_{tot}}$$

$$Z_{CoG} = \frac{t_f}{2}$$

where: b_{flange} is the width of the HE700A top flange
         t_f is the thickness of the HE700A top flange
         $A_{flange} = b_{flange} \cdot t_f$ is the area of the HE700A top flange
         b_{plate} is the (unknown yet) width of the welded plate
         $A_{plate} = b_{plate} \cdot t_{plate}$ is the area of the welded plate
         $t_{plate} = t_f$ is the welded plate thickness
         $A_{tot} = A_{flange} + A_{plate}$ is the area of the strengthened section
         the origin of the system of axis used refers to the bottom left end of the considered section, as can be seen in the upcoming figure

Figure 7-9 illustrates the new cross section considered, with its CoG and the origin system of axes depicted.
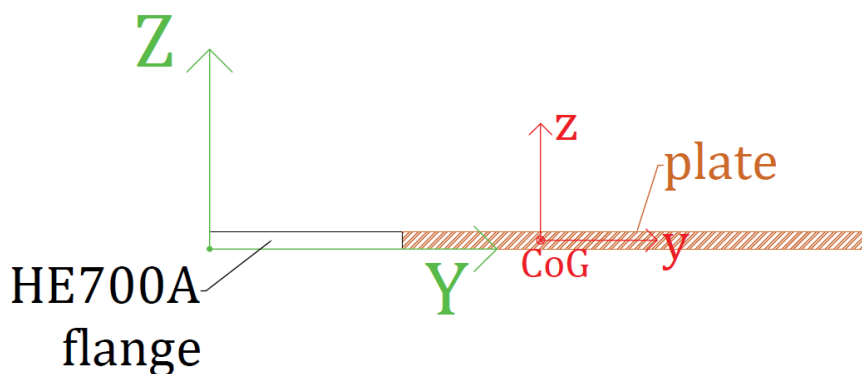
Figure 7-9 – Strengthened cross section

- Moments of inertia

The moments of inertia of the strengthened section are defined by using the parallel axes theorem, according to the following equations:

$$I_y = I_y^{flange} + I_y^{plate}$$

$$I_z = I_z^{flange} + A_{flange} \cdot \left(Y_{CoG} - \frac{b_{flange}}{2}\right)^2 + I_z^{plate} + A_{plate} \cdot \left\{\left(b_{flange} + \frac{b_{plate}}{2}\right) - Y_{CoG}\right\}^2$$

where: $I_y^{flange} = \frac{b_{flange} \cdot t_f^3}{12}$ is the moment of inertia of the flange over its y-centroid axis

$I_y^{plate} = \frac{b_{plate} \cdot t_f^3}{12}$ is the moment of inertia of the plate over its y-centroid axis

$I_z^{flange} = \frac{t_f \cdot b_{flange}^3}{12}$ is the moment of inertia of the flange over its z-centroid axis

$I_z^{plate} = \frac{t_f \cdot b_{plate}^3}{12}$ is the moment of inertia of the plate over its z-centroid axis

Y_{CoG} is the horizontal distance of the section's CoG from its bottom left end

7.3.2 Critical locations of strengthened section and classification

The new cross section considered consists of four critical locations, at its corner points. These comprise section locations 1, 2, 3, 12, 13 and 14. Locations 13 and 14 are the new defined ones, at the plate free corner. All section locations are demonstrated in Figure 7-9 below.

Figure 7-10 – Critical section locations of reinforced HE700A

The classification of the new locations 13 and 14 is the following, for the different member locations:

- Member locations 1 and 6 (end connection of HE700A with plate)

These locations concern the weld attachment of the front beam to an end plate. The whole section is welded through fillet welds to the end plate, hence for all the section locations the S-N curve that is considered is the G one for examining the weld toe cracking.

- Member locations 2 and 5 (bearing pad locations)

These are the locations where the bearing pads are attached at the top flange of the HE700A member. As was mentioned in the section 5.4.2, the critical section locations are the ones at the bearing ends, for which the S-N curve F1 is considered. The new section locations 13 and 14 are classified as all the remaining ones, thus adopting class B1.
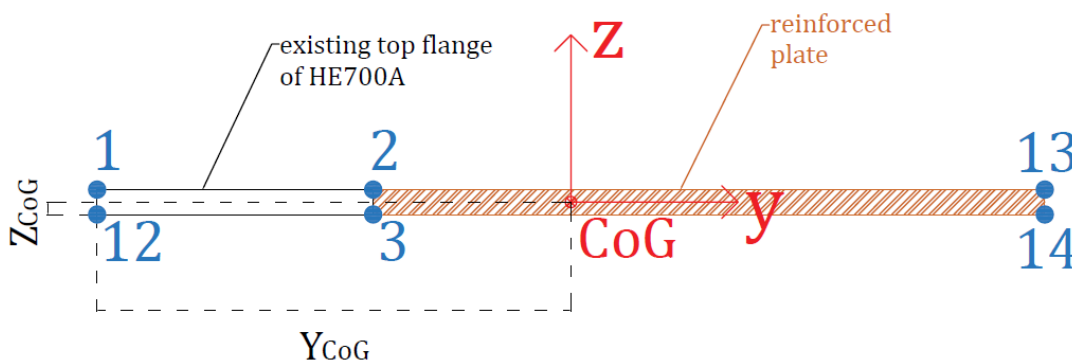
- Member locations 3 and 4 (connection of HE400A to HE700A)

Here, there is correspondence of the new section locations 13 and 14 with the previous 1 and 12 respectively, since the connection concerns the weld attachment of member HE400A transversely to the HE700A one, at its top flange. Therefore, the new locations 13 and 14 are classified to the S-N category W1.

7.3.3 Fatigue assessment and required plate width

The plate width that was required in order to have the fatigue requirement satisfied, at the multiple member locations, was defined such that it resulted in an applied stress range that is less than the fatigue limit of the detail at the certain member location. Thus, different plate widths were required for each of the 6 sensitive member locations. The whole procedure was a repetitive one, the results of which are presented in the following two tables. Table 7-7 lists the characteristics of the required plates and the resultant strengthened sections for the multiple member locations. Table 7-8 demonstrates the fatigue assessment for the strengthened sections at the 6 member locations, where it is apparent that the fatigue limit requirement is satisfied for every location.

Table 7-7 – Required plate dimensions and strengthened section properties

member location	welded plate		strengthened section		
	b_{plate} (cm)	t_{plate} (cm)	A_{tot} (cm^2)	I_y (cm^4)	I_z (cm^4)
1	73	2.7	278.1	168.95	245863.58
2	19	2.7	132.3	80.37	26471.03
3	50	2.7	216	131.22	115200
4	51	2.7	218.7	132.86	119574.23
5	14	2.7	118.8	72.17	19166.40
6	25	2.7	148.5	90.21	37434.38

Table 7-8 – Fatigue assessment for the strengthened sections

member location	most critical section location	S-N curve	$\Delta\sigma_{tot}$ (MPa)	fatigue limit (MPa)
1	14	G	28.71	29.24
2	bearing end	F1	35.99	36.84
3	14	W1	25.47	26.32
4	14	W1	25.73	26.32
5	bearing end	F1	35.17	36.84
6	13	G	28.49	29.24

7.3.4 Required length of the welded plates

Having defined the section dimensions of the plates that need to be welded at the multiple locations, what remains to be determined is their length. Apparently, strengthening the front beam (HE700A) in order to be adequate against fatigue may not be required for the whole length of the member, since the classification of the details along the front beam is not the same.

In order to determine the required length inside which the member needs to be strengthened, the unstrengthened section was examined. The location where it is adequate against the fatigue requirement indicates the end of the required plate. The fatigue assessment for the unstrengthened section was conducted for classifying it as a continuous member, thus adopting the "B1" S-N curve characteristics. Figure 7-11 depicts the required lengths of the defined welded plates along the length of the front beam.
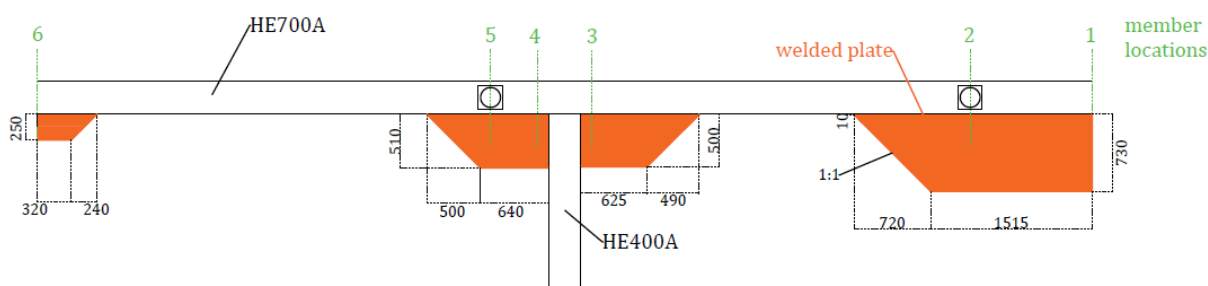

Figure 7-11 – Top view of the strengthened front beam

7.4   Strengthen the front beam by welding a vertical plate along its section height

The last improvement case that is investigated comprises reinforcing the HE700A wide flange section of the front beam by welding a vertical plate at its top and bottom flange edges. Welding a plate in such a way not only enhances the section's moments of inertia I_y and I_z, but it also transforms the type of the section. Specifically, from an open section that is sensitive to torsion, it now approaches a close form that has significantly larger resistant against torsion.

Thus, in contrast to the 3rd improvement option that was described in section 7.3, here the whole section is taken into account (not only its top flange part). This implies that the resultant torsional moment is considered when defining the applied stresses. The approach consists of several steps:

- Choose the plate dimensions and define the characteristics of the strengthened section
- Calculate the applied stresses and the resultant stress ranges
- Define the critical section locations to be examined against fatigue and classify them
- Perform fatigue analysis of the sensitive member locations and determine the plate that results in satisfying the fatigue requirement
- Calculate the length of the welded plate that is required

7.4.1   New section characteristics

Regarding the plate dimensions, its width had to be equal to the height of the HE700A section in order to be welded from the one flange to the other. On the other hand, its thickness should be defined by the fatigue assessment, such that it results in satisfactory results regarding fatigue.

- Center of gravity

The center of gravity (CoG) of the strengthened section is defined according to the following equations, with reference to Figure 7-12 below:

$$Y_{CoG} = \frac{\frac{t_{plate}}{2} \cdot A_{plate} + \left(t_{plate} + \frac{b_{HEA}}{2}\right) \cdot A_{HEA}}{A_{tot}}$$

$$Z_{CoG} = \frac{h_{HEA}}{2}$$

where: t_{plate} is the (unknown yet) welded plate thickness
        $b_{plate} = h_{HEA}$ is the width of the welded plate
        $A_{plate} = b_{plate} \cdot t_{plate}$ is the area of the welded plate
        b_{HEA} is the width of the HE700A flange
        h_{HEA} is the total height of the HE700A section
        A_{HEA} is the area of the HE700A section
        $A_{tot} = A_{HEA} + A_{plate}$ is the area of the strengthened section
        the origin of the system of axis used refers to the bottom left end of the whole section, as illustrated in the upcoming figure

Figure 7-12 illustrates the new cross section, with its CoG and the origin system of axes depicted.
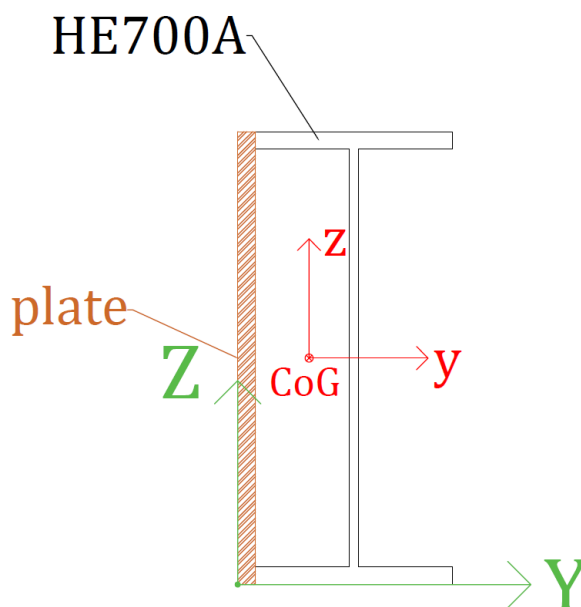
Figure 7-12 – Strengthened cross section

- Moments of inertia

The moments of inertia of the strengthened section are defined by using the parallel axes theorem, according to the following equations:

$$I_y = I_y^{HEA} + I_y^{plate}$$

$$I_z = I_z^{HEA} + A_{HEA} \cdot \left\{ \left(t_{plate} + \frac{b_{HEA}}{2} \right) - Y_{CoG} \right\}^2 + I_z^{plate} + A_{plate} \cdot \left(Y_{CoG} - \frac{t_{plate}}{2} \right)^2$$

$$I_t = I_t^{HEA} + A_{HEA} \cdot \left\{ \left(t_{plate} + \frac{b_{HEA}}{2} \right) - Y_{CoG} \right\}^2 + I_t^{plate} + A_{plate} \cdot \left(Y_{CoG} - \frac{t_{plate}}{2} \right)^2$$

where: I_y^{HEA} the moment of inertia of HE700A over its y-centroid axis

$I_y^{plate} = \frac{t_{plate} \cdot b_{plate}^3}{12}$ the moment of inertia of the plate over its y-centroid axis

I_z^{HEA} the moment of inertia of HE700A over its z-centroid axis

$I_z^{plate} = \frac{b_{plate} \cdot t_{plate}^3}{12}$ the moment of inertia of the plate over its z-centroid axis

I_t^{HEA} the torsional moment of inertia of HE700A over its centroid axis

$I_t^{plate} = \frac{b_{plate} \cdot t_{plate}}{12} \left(b_{plate}^2 + t_{plate}^2 \right)$ the torsional moment of inertia of the welded plate over its centroid axis

Y_{CoG} the horizontal distance of the section's CoG from its bottom left end

7.4.2 Applied stresses and resultant stress range

As already mentioned, the torsional moment is also considered for this type of section. This results in shear stresses applied at the multiple locations inside the section. The induced shear stress is defined according to the following formula:

$$\tau = \frac{M_t \cdot r}{I_t}$$

where: τ is the shear stress induced from the applied torsional moment
M_t is the applied torsional moment
r is the distance of the specific location from the section's CoG
I_t is the section's torsional moment of inertia over its centroid axis

The total applied stress is defined by combining the applied normal and shear stresses. This is achieved by applying the von Mises combination rule:

$$\sigma_{vM} = \sqrt{\sigma_{tot}^2 + 3 \cdot \tau_{yz}^2}$$

where: σ_{vM} is the von Mises resultant applied stress
$\sigma_{tot} = \sigma_{F_x} \pm \sigma_{M_y} \pm \sigma_{M_z}$ is the total applied normal stress
τ_{yz} is the applied shear stress that is induced from the applied torsional moment

Therefore, the applied stress range that is considered in this case is:

$$\Delta\sigma_{tot} = 2 \cdot \sigma_{vM}$$

7.4.3 Critical locations of strengthened section and classification

Strengthening of the HE700A section through welding a plate vertically generates two extra critical locations in the new section. These are located at the two outer corners of the welded plate, labelled as locations 13 and 14. The most critical section locations are located at the 4 corner points of the strengthened cross section and are depicted in the following figure.
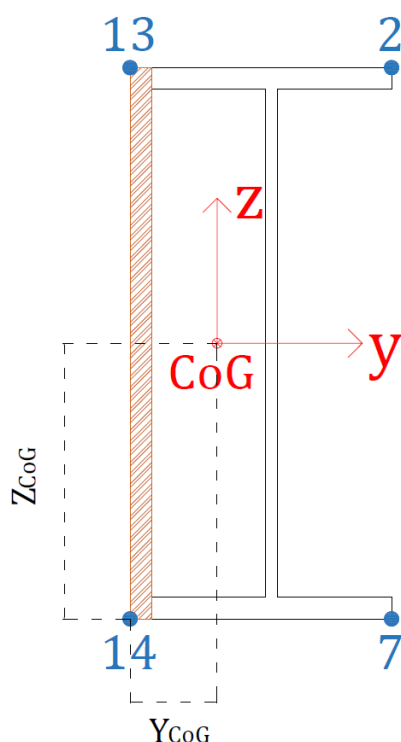
Figure 7-13 – Most critical section locations

The classification of the new defined section locations 13 and 14, for the different member locations, is:

- Member locations 1 and 6 (end connection of HE700A with plate)

These locations concern the weld attachment of the front beam to an end plate. The whole section is welded through fillet welds to the end plate, hence for all the section locations the S-N curve that is considered is the G one for examining the weld toe cracking.

- Member locations 2 and 5) (bearing pad locations)

These are the locations where the bearing pads are attached at the top flange of the HE700A member. As was mentioned in the section 5.4.2, the critical section locations are the ones at the bearing ends, for which the S-N curve F1 is considered. The new section locations 13 and 14 are classified as all the remaining ones, thus adopting class B1.

- Member locations 3 and 4 (connection of HE400A to HE700A)

Here, there is correspondence of the new section locations 13 and 14 with the previous 1 and 8 respectively (see Figure 5-3), since the connection concerns the weld attachment of member HE400A transversely to the HE700A one, at its top flange. Therefore, the new locations 13 and 14 are classified to the S-N category W1.

7.4.4   Fatigue assessment and required plate thickness

The plate thickness required in order to have the fatigue requirement satisfied, at the multiple member locations, was defined such that it resulted in an applied stress range that is less than the fatigue limit of the detail at the certain member location. As a result, different plate thicknesses are required for the several sensitive member locations.

The procedure of defining the optimal plate thickness was a repetitive one, the results of which are presented in the following two tables. Table 7-9 lists the characteristics of the required plates and the resultant strengthened sections for the multiple member locations. Table 7-10 demonstrates the fatigue assessment for the strengthened sections at the 6 member locations, where it is apparent that the fatigue limit requirement is satisfied for every location.

Table 7-9 – Required plate dimensions and strengthened section properties

member location	welded plate		strengthened section			
	b_{plate} (cm)	t_{plate} (cm)	A_{tot} (cm^2)	I_y (cm^4)	I_z (cm^4)	I_t (cm^4)
1	69	9.0	881.47	461683.03	86148.61	320864.09
2	69	4.0	536.47	324804.28	51275.55	149112.28
3	69	1.5	363.97	256364.91	30573.05	59970.40
4	69	4.0	536.47	324804.28	51275.55	149112.28
5	69	3.5	501.97	311116.41	47584.81	131733.66
6	69	1.0	329.47	242677.03	25291.34	41000.82

Table 7-10 – Fatigue assessment for the strengthened sections

member location	most critical section location	S-N curve	$\Delta\sigma_{tot}$ (MPa)	fatigue limit (MPa)
1	7	G	27.99	29.24
2	bearing end	F1	34.89	36.84
3	13	W1	23.76	26.32
4	13	W1	25.26	26.32
5	bearing end	F1	34.82	36.84
6	2	G	26.45	29.24

7.4.5   Required length of the welded plates

After the required plate section dimensions have been defined, the last thing to be defined is their length. Since the classification of the details for the multiple locations along the front beam changes, it is possible that strengthening the beam may not be required for its whole length.

In order to determine the required length inside which the member needs to be strengthened, the unstrengthened section was examined. The location where it is adequate against the fatigue requirement indicates the end of the required plate. The fatigue assessment for the unstrengthened section was conducted for classifying it as a continuous member, thus adopting the "B1" S-N curve characteristics.

The analysis indicated that the unstrengthened HE700A section is inadequate to satisfy the fatigue requirement in all the locations along the front beam. This is rational since the unstrengthened HEA section is an open type one with a very low torsional moment of inertia. This resulted in having very high resultant shear stresses and therefore high total stresses and stress ranges, in all the locations across the front beam. Thus, strengthening is required along its whole length.

In order to be practical, strengthening was performed according to the following:

- the largest required plate thickness inside the locations 1-3 is retained along the whole corresponding member's length
- the largest required plate thickness inside the locations 4-6 is retained for the whole corresponding member's length

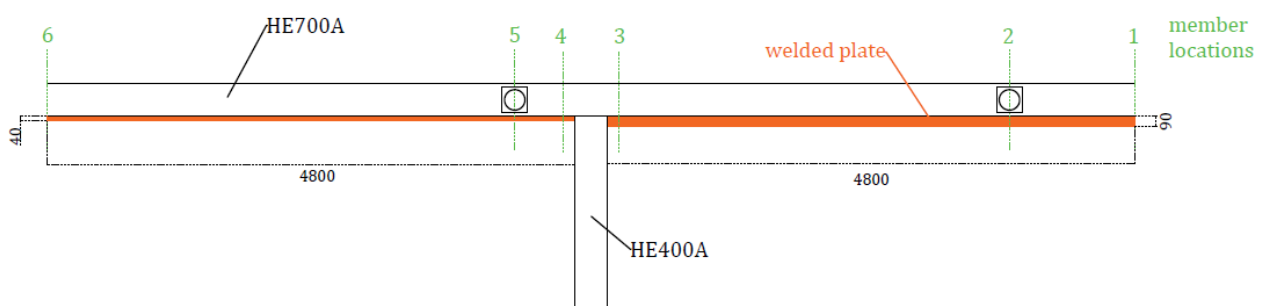Figure 7-14 depicts a top view of the strengthened front beam.

Figure 7-14 – Top view of the strengthened front beam

8 The actual behaviour of friction and the numerical approach

A significant parameter that influences the investigation of the topic as examined in this thesis, is friction. The way it is defined influences the resultant fatigue damage, something that was also shown in the examination of the sensitivity parameters. This chapter intends to clarify the most fundamental aspects around this phenomenon and provide guidance on how it can be modelled accurately through numerical simulations. The chapter ends with a description of a numerical model that was set in Matlab [30], in order to represent the situation that was examined in the present document in a more precise way.

8.1 Actual behaviour of friction

As already mentioned previously, in section 6.2.1, determining the friction force accurately is not that straightforward. The amount of investigation that has been spent on this topic and still continues, as well as the number of different models that have been generated by researchers globally in order to represent the phenomenon, indicate its complexity and the difficulty in modelling it accurately.

Friction can be encountered in multiple types like dry, fluid, lubricated, skin and internal. However, the specific thesis concerns only the dry type, which is the one that resists the relative motion of two solid surfaces that are in contact. This is a force having the purpose to oppose any relative motion between two solid surfaces that are in contact. It is produced by the asperities of the two in-contact surfaces and it is split into static and kinetic (or dynamic) friction. The first type is generated when the surfaces don't move relatively to each other and comprises the sticking phase of the phenomenon. The second type is encountered when there is movement between the surfaces [16].

The fundamental properties of friction were first understood by experiments from the 15th to the 18th century. This concerns work done by Leonardo da Vinci, Amontons and Coulomb, who set the five classical laws of friction [16], [17]:

1) Friction is proportional to the normal to the surface contact force. Their proportionality is expressed by the coefficient of friction, which is expressed by two values, the static and the kinetic one. The static friction coefficient applies to friction generated up to the start of sliding, whereas the kinetic one refers to the friction present during the sliding motion
2) Friction is independent of the apparent area of contact. This implies that friction does not depend on the roughness of the surfaces, which is not the case for real experiments. However, it is an accurate consideration in a macroscopic view
3) Kinetic friction is independent of the sliding velocity
4) Kinetic friction acts in the opposite direction of the relative velocity
5) The coefficient of static friction is larger than the kinetic one

It should be noted that the 3rd mentioned law was questioned by experiments conducted, indicating a variation in the magnitude of kinetic friction with the sliding velocity. As a result, several empirical formulas representing the dependence of the kinetic friction with the sliding velocity have been generated so far.

The motion that results from the friction characteristics and, more specifically, from its two different coefficients (static, kinetic) depending on the state, is the so called stick-slip motion. It is a nonlinear effect that is associated with friction, during which the two in-contact surfaces alternately switch between sticking and slipping. This motion makes it difficult to define a relationship between the kinetic friction and the sliding velocity, although it has been studied extensively through relevant experiments by several researchers [18], [19].

8.1.1   Static friction – sticking phase

Static is the state of friction generated at the interface of two bodies, tangentially to their contact surface, when these are not sliding relative to each other. This can occur either when both the surfaces are in rest or when they move equally (both in direction and magnitude), resulting in zero relative displacement. The magnitude of static friction is such that the net relative velocity, and hence, the net relative acceleration, of the two surfaces in contact is zero. Thus, static friction is equal in magnitude and opposite in direction to the "pulling" force that would otherwise induce motion to occur [20].

According to the Coulomb model of friction (see also section 8.2), there is a maximum limit in the magnitude that static friction can have. This equals $\mu_s \cdot N$, where N is the normal force between the two surfaces and μ_s is the coefficient of static friction, which depends on the nature of the surfaces. As long as the applied external force parallel to the plane of contact has lower magnitude than $\mu_s N$, there is no sliding and static friction is generated. When the external force exceeds that limit, slipping begins and static friction no longer applies. Therefore, it can be summarized that [20]:

- Static friction is a variable force that tries to keep the object stationary. It is equal in magnitude and opposite in direction to the net external force acting along the plane of contact that is causing a tendency for the surfaces to slip against each other. In other words, it acts to precisely cancel out the external force that would otherwise have caused slipping (relative motion)

- The magnitude of the static friction force increases until it reaches a limiting value. The maximum value of static friction that can be experienced through the surface of contact equals $\mu_s \cdot N$. When that value is surpassed, the objects will begin to slide

8.1.2   Kinetic friction – slipping phase

After the limit of maximum static friction is exceeded, the two surfaces start moving with respect to each other and kinetic, or dynamic, friction is applied. Its direction is such that it opposes the slipping against each other. Its magnitude is determined by the corresponding coefficient of kinetic friction, which again depends on the nature of the two surfaces in contact but has different value than the static one. The following can be summarized for that state of friction [20]:

- The direction of kinetic friction is opposite to that of the induced relative motion (velocity), hence it does not depend on the direction of the external forces

- The magnitude of kinetic friction is always equal to $\mu_k \cdot N$, where μ_k is the coefficient of kinetic friction

The kinetic friction coefficient is smaller than the static one, indicating that once two bodies start slipping against each other, it is easier to keep that motion instead of initiate movement from rest.

Figure 8-1 illustrates the different states of friction, as well as their relation with the applied force at the direction of sliding.
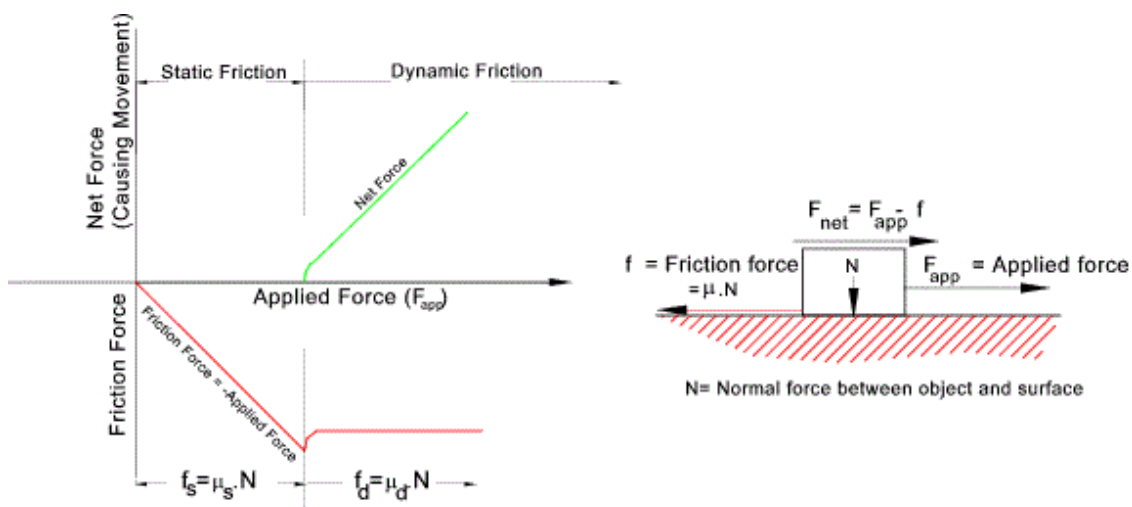
Figure 8-1 – Applied force and generated friction [21]

8.2   Friction models generated

Various types of models have been generated so far, in an effort to represent the friction behaviour accurately. These consist of the numerical representation of the evaluation of friction force and the model differences are upon either the event case for altering between its two states or the determination of its magnitude. Some of the most famous models are presented below:

- Coulomb friction model [22]: This is the simplest and most well-known model. Although it is a very simple representation of the frictional behaviour, it is widely used inside the engineering world. Its significance is proven from the fact that any other more developed model is based on this. Coulomb friction is a force of constant and independent of the sliding velocity magnitude. It acts in such a way that it opposes the motion.

  The biggest problem of the specific model is that it lacks representing smoothly the condition of zero-crossing velocity in which the friction state changes abruptly. The mathematical expression representing this model is the following:

  $$F(t) = \begin{cases} -F_c * sign(v_r), & v_r \neq 0 \\ F_{app}, & v_r = 0 \ and \ |F_{app}| < F_c \end{cases}$$

  where: $F(t)$ is the friction force

  v_r is the relative sliding velocity between the two surfaces

  $sign(v_r) = \begin{cases} +1, & when \ v_r > 0 \\ -1, & when \ v_r < 0 \end{cases}$

  F_{app} is the applied force at the direction of sliding

  $F_c = \mu \cdot F_N$ is the Coulomb friction force, defined through the friction coefficient μ and the normal force F_N

  When $|F_{app}| < F_C$, there is no sliding between the two surfaces (where $v_r = 0$) and the Coulomb friction force can take any value lower than F_C. On the other hand, when $v_r \neq 0$, the friction force can only become equal to $\pm F_C$, with the sign depending on the direction of the relative sliding velocity (opposing the direction of sliding).

- Viscous friction model [22]: The viscous friction element models the friction force as a force linearly proportional to the sliding velocity, defined by a viscous coefficient (of the lubricant) k_v. Its application is limited, since it can only be applied in cases where a lubricant is present. It is represented by the following simple formula:

  $$F(t) = k_v \cdot v_r$$

- Integrated Coulomb and viscous model [22]: An efficient combination of the two previous models is described by the following equation:

  $$F(t) = \begin{cases} \min(F_c; \ k_v \cdot v_r), & if \ v_r \geq 0 \\ \max(-F_c; \ k_v \cdot v_r), & if \ v_r < 0 \end{cases}$$

- <u>Stribeck friction model</u> [22]: The Stribeck curve is an advanced model of friction, representing it as a continuous function of sliding velocity. This is described by the following relation:

$$F(t) = \left(F_c + (F_s - F_c) * e^{-\left(\left|\frac{v_r}{v_s}\right|\right)^i} \right) \cdot sgn(v_r) + k_v * v_r$$

where: F_s is the static friction force

v_s is the Stribeck velocity

i is an exponent

Stribeck friction force has lower and upper limits. Specifically, the minimum value it can obtain is F_c, whereas the maximum one is F_s.

Figure 8-2 represents these 4 friction models, as a function of friction with the sliding velocity.

a)   Coulomb model   b)   viscous model

c)   integrated Coulomb model   d)   viscous and Stribeck friction model
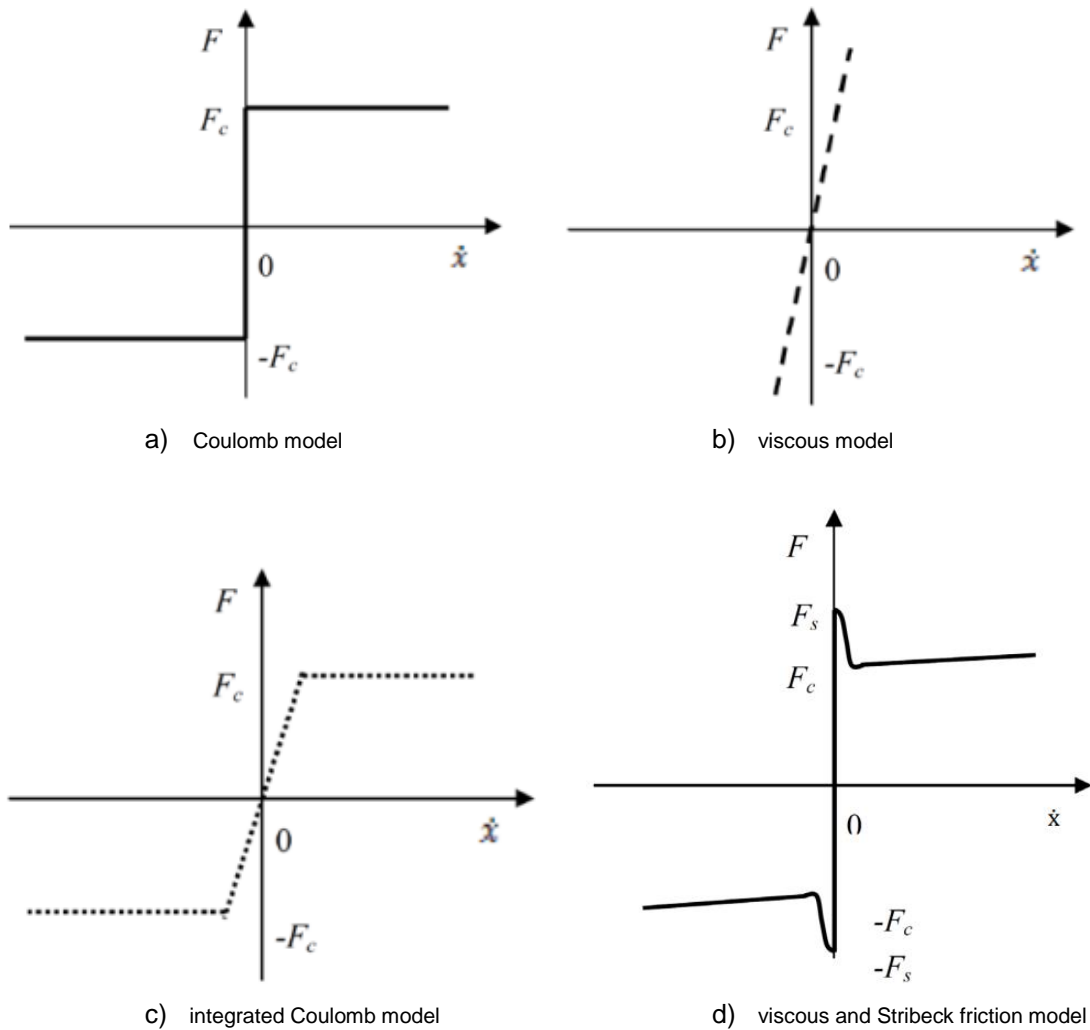
Figure 8-2 – Friction models [22]

- Model combining Coulomb, viscous, static friction and the Stribeck effect [23]: This model is defined by the following relation:

$$F(t) = \begin{cases} F(v_r), & if \ v_r \neq 0 \\ F_e, & if \ v_r = 0 \ and \ |F_e| < F_s \\ F_s * sgn(F_e), & if \ v_r = 0 \ and \ |F_e| \geq F_s \end{cases}$$

where: $F(v_r)$ is the function that captures the friction profile of the Stribeck curve

The model is illustrated in the following figure.
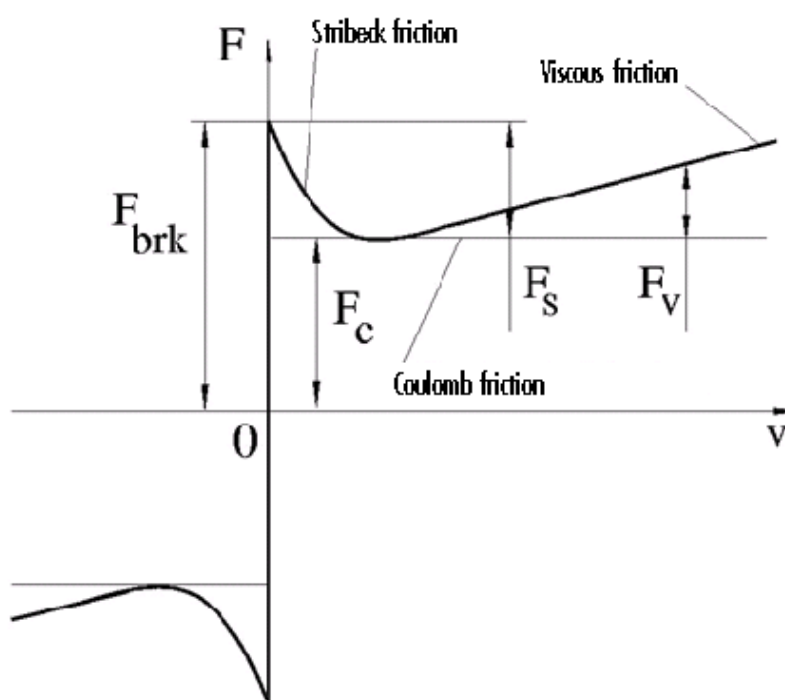
Figure 8-3 – Combination of Coulomb, viscous, static and the Stribeck friction model [24]

8.3   Purpose and description of the numerical method

In order to obtain accurately the fatigue load that is induced due to the generated friction in the sliding end of the bridge, it is important to model the characteristics of friction in an accurate way. This implies that the distinction between the static and the kinetic type of friction will be able to be incorporated in the model that is used for the analysis.

Since SACS software does not provide options to incorporate this, a numerical model had to be created in Matlab. This model was created with the intention to allow for a proper representation of the stick-slip behaviour that friction exhibits. Relevant work from other researchers can be found on [31] and [32], although they are based on modeling the behaviour of a concentrated mass and not a continuous system like the one attempted here.

Therefore, the bridge was modeled, in such a way that the final time variation of the friction load could be obtained and afterwards incorporated in the SACS software to finally get the stresses distribution at the critical positions of the bridge landing. For that purpose, the "Finite Difference Method" was used, in order to make the numerical modeling of the bridge possible, the whole procedure which is explained in detail in the following sections [34].

The whole idea is based on the numerical modeling of the bridge through the application of the one-dimensional (1-D) continuous equation of motion, considering only its axial displacement degree of freedom. The main input of the model is the imposed support excitations of the bridge's supports. These are the time-dependent horizontal displacements of the platform points where the bridge supports are located, due to the wave acting in the longitudinal direction of the bridge. These displacements were derived from the SACS model of the two platforms.

The appropriate type of 1-D continuous model to represent the situation described is a rod model, being able to represent the longitudinal motion of the bridge. The equation of motion of the rod is the following one mentioned:

$$\rho \cdot A(x) \cdot \frac{\partial^2 u(x,t)}{\partial t^2} = \frac{\partial}{\partial x}\left(EA(x)\frac{\partial u(x,t)}{\partial x}\right) + q_x(x,t) \cdot A(x) \quad (1)$$

where: ρ is the density of the type of material used

$A(x)$ is the cross section of the bridge at every section x

E is the Young's modulus of elasticity of the material used

$u(x,t)$ is the longitudinal deformation of the rod at any position x and time t

$q_x(x,t)$ is the axial distributed load acting on the rod model

This equation is simplified, after considering the characteristics of the specific problem situation. Specifically, the bridge is homogeneous, with constant cross section ($A(x) = A$) through its whole length, whereas is no axial distributed load considered in the rod model ($q_x(x,t) = 0$). Consequently, the above mentioned equation is simplified into the following one:

$$\rho \cdot A \cdot \ddot{u} - EA \cdot u'' = 0 \quad (2)$$

where: dot notation (·) represents the time derivatives

prime symbol (′) denotes the space derivatives

Therefore, the equation of motion consists of partial differential equations, since $u = u(x,t)$ depend on two variables, space (x) and time (t). In order to be able to be solved numerically, the differential equations have to turn into ordinary ones, something that can be achieved by applying the finite difference method. In order to do so, the model must be discretized in space. Then, the spatial derivatives can be approximated by incorporating the information of the adjacent discretized points,

for each location examined. The resultant equations are only time-dependent, hence ordinary differential ones and able to be solved numerically. The discretized bridge is illustrated in the following figure, where a number of (N+1) points (from n=0 to n=N) are applied in order to discretize the model in N segmented elements of length l_{seg} $\left(l_{seg} = \frac{L}{N}\right)$.
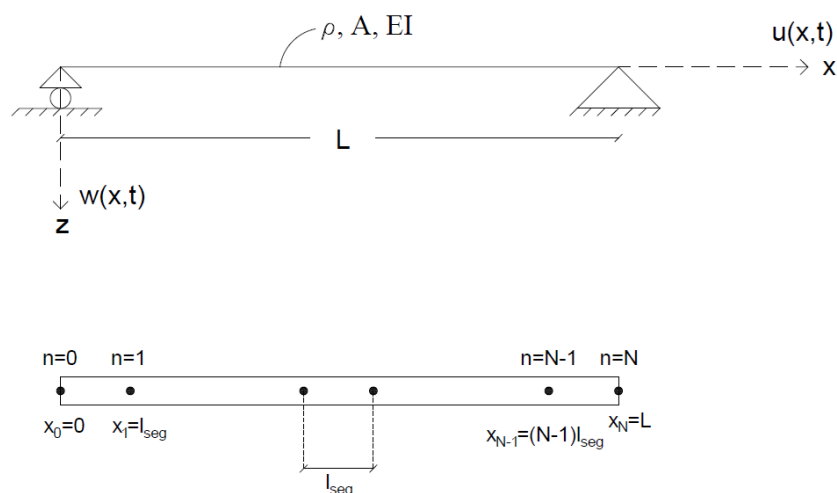
Figure 8-4 – Discretized numerical model representation

The discretized equation of motion for the rod model is the following one:

$$\rho \cdot A \cdot \ddot{u}_n + EI \cdot u_n'''' = 0 \quad (3)$$

where: $n = 0,1,2,\dots,N$ are the multiple discretized points

By applying the central finite difference, the spatial derivatives can be approximated and finally eliminated from the equation of motion. The coefficients applied to the approximated formula are defined based on the order of accuracy used and can be found from predefined tables on [15]. Thus, by approximating the 4th derivative with a 2nd order accuracy we obtain:

$$u_n'' = \frac{1}{l_{seg}^2}(u_{n-1} - 2u_n + u_{n+1}) + O\left(l_{seg}^2\right) \quad (4)$$

where: n: the index of the discretized point that is approximated

$O(l_{seg}^2)$: the truncated error generated due to the approximation accuracy used

Therefore, by inserting the expression for u_n'' into the equation of motion (3), the final ordinary differential equation of motion is derived:

$$\rho \cdot A \cdot \ddot{u}_n - \frac{EI}{l_{seg}^2}(u_{n-1} - 2u_n + u_{n+1}) = 0 \,, \forall n = 0,\dots,N \quad (5)$$

which contains a total number of (N+1) equations.

The final discretized equation of motion (5) implies that, in order to solve for every point n, information for the adjacent points (n-1) and (n+1) is required. As a result, this requirement generates, at some points, some input for locations that do not exist. To be more specific, when solving for point n=0 the displacements at point n=−1 is needed. This point falls outside of the model and is therefore a ghost point. The way to eliminate it is by applying the boundary conditions at the end location (n=0). Similarly, the same applies for the other end location (n=N) which requires the ghost point n=N+1,), thus 2 boundary conditions (BC) will be applied to eliminate them.

8.4 Boundary conditions and set of equations

Regarding the type of supports at the two bridge ends (points n=0 and n=N): In such a case, the left end (n=0) is sliding supported whereas the right one (n=N) is pinned. Nevertheless, the type of the (each time) friction state (sticking or slipping) will define the boundary condition of the left (typically sliding) end. This happens because: (a) when sticking, that end of the rod (n=0) is not moving relatively to the connecting landing, but is following its excitation, whereas (b) when slipping occurs, there is movement of that end (n=0) independently of the connecting landing's excitation. These imply that there is a difference in the consideration of the structural support system of the rod during each friction state: During sticking, both ends of the rod can be considered to be fixed with prescribed displacements applied at the two ends (= the excitations of the two landings). On the other hand, during slipping, the left end of the rod is considered to be sliding supported and does not follow the excitation of the connecting landing, which is now the case only for the right end (n=N).

The structural model and the BCs for the two states are the following ones described, in which:

- $u_{slid}(t)$ is the horizontal excitation of the left-end's (x=0) connecting landing
- $u_{pin}(t)$ is the horizontal excitation of the right-end's (x=L) connecting landing

8.4.1 Sticking state
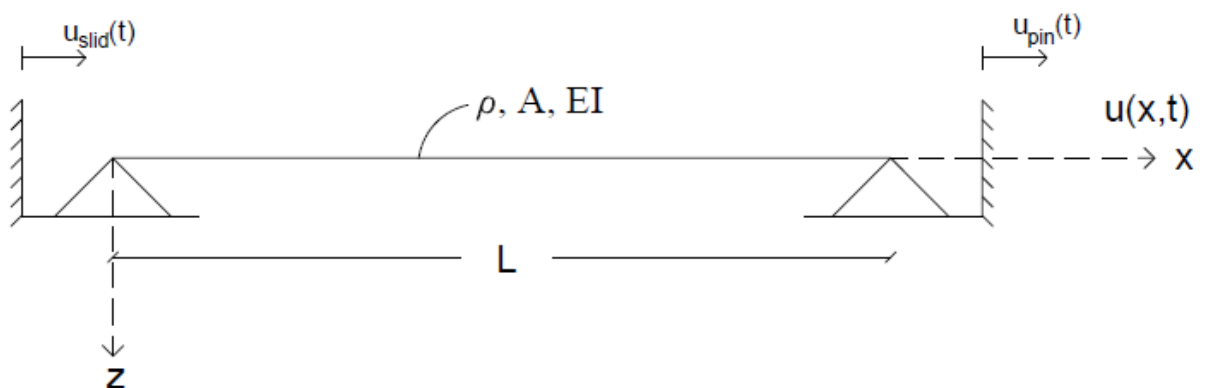The structural model is the following depicted one:

Figure 8-5 – The rod model considered for the sticking state

Boundary conditions:

1) $u(0, t) = u_{slid}(t)$, where $u_{slid}(t)$ is the horizontal excitation of the landing supporting the left end of the bridge, concluding in the expression for the relevant discretized point: $u_0 = u_{slid}(t)$

2) $u(L, t) = u_{pin}(t)$, where $u_{pin}(t)$ is the horizontal excitation of the landing supporting the right end of the bridge, concluding in the expression for the relevant discretized point: $u_N = u_{pin}(t)$

Consequently, after applying the boundary conditions and eliminating all ghost points generated, the resultant equations of motion for the discretized rod during sticking are the following ones:

- <u>for n=0</u>: $u_0 = u_{slid}$
- <u>for n=1</u>: $\rho \cdot A \cdot \ddot{u}_1 - \frac{EA}{l_{seg}^2}(-2u_1 + u_2) = \frac{EA \cdot u_{slid}}{l_{seg}^2}$
- <u>for n=2 to (N-2)</u>: $\rho \cdot A \cdot \ddot{u}_n - \frac{EA}{l_{seg}^2}(u_{n-1} - 2u_n + u_{n+1}) = 0$
- <u>for n=N-1</u>: $\rho \cdot A \cdot \ddot{u}_{N-1} - \frac{EA}{l_{seg}^2}(u_{N-2} - 2u_{N-1}) = \frac{EA \cdot u_{pin}}{l_{seg}^2}$
- <u>for n=N</u>: $u_N = u_{pin}$

These can be expressed in a matrix form:

$$\rho \cdot A \cdot \underline{\ddot{u}} - \frac{EA}{l_{seg}^2} \cdot \underline{\underline{K_{coef}}} \cdot \underline{u} = \underline{F}$$

which after multiplying both sides with l_{seg}, becomes:

$$\rho \cdot A \cdot l_{seg} \cdot \underline{\ddot{u}} - \frac{EA}{l_{seg}} \cdot \underline{\underline{K_{coef}}} \cdot \underline{u} = \underline{F} \cdot l_{seg} \rightarrow$$

$$\underline{\underline{M}} \cdot \underline{\ddot{u}} + \underline{\underline{K}} \cdot \underline{u} = \underline{F_{ext}}$$

where:
$$\underline{u} = [u_1 \quad u_2 \quad u_3 \quad ... \quad u_{N-2} \quad u_{N-1}]^T$$

$$\underline{\underline{K_{coef}}} = \begin{matrix} n=1 \\ 2 \\ . \\ . \\ . \\ N-2 \\ N-1 \end{matrix} \begin{bmatrix} -2 & 1 & 0 & 0 & 0 & 0 & 0 \\ 1 & -2 & 1 & 0 & 0 & 0 & 0 \\ 0 & 1 & -2 & 1 & 0 & 0 & 0 \\ 0 & 0 & ... & ... & ... & 0 & 0 \\ 0 & 0 & 0 & ... & ... & ... & 0 \\ 0 & 0 & 0 & 0 & 1 & -2 & 1 \\ 0 & 0 & 0 & 0 & 0 & 1 & -2 \end{bmatrix}$$

$$\underline{F_{ext}} = \left[\frac{EA \cdot u_{slid}}{l_{seg}} \quad 0 \quad 0 \quad ... \quad 0 \quad \frac{EA \cdot u_{pin}}{l_{seg}} \right]^T$$

Event case for altering the state:

While advancing in time to compute the displaced situation for the discretized points considered, there must be set an indicator for altering the state of sticking and continuing with the slipping state. The event case for altering the state while sticking is regarding the axial force generated at the left end (n=0). Since during the sticking state static friction is generated, altering of the state will be performed when that axial force exceeds the limit of maximum static friction ($Fr_{static}^{max} = \mu_{static} \cdot V_0$), where μ_{static} is the coefficient of static friction and V_0 the vertical force at that end (n=0). The axial force generated at the left end of the rod (n=0), which indicates where the state will change, is computed for every time instant based on the formula: $F_{(0,t)}^{axial} = EA \cdot u_0'$. Applying the Forward Finite Difference scheme to represent the first derivative u_0' , the equation for the axial force at the left end becomes: $F_{(0,t)}^{axial} = \frac{EA \cdot (u_1(t) - u_0(t))}{l_{seg}}$.

8.4.2   Slipping state

The structural model is the following depicted one:
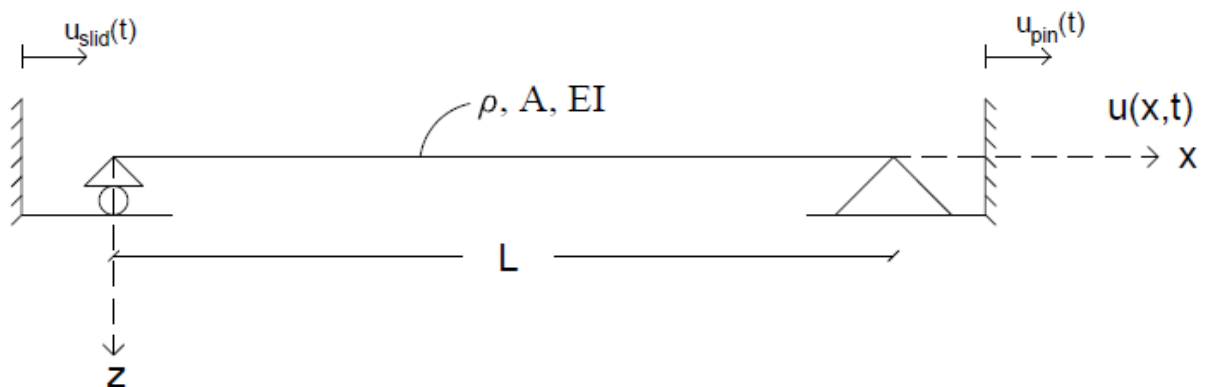
Figure 8-6 – The rod model considered for the slipping state

Boundary conditions:

1)   axial force equilibrium: $EA \cdot u'(0,t) = Fr(0,t)$, where $Fr(0,t)$ is the dynamic friction load generated during slipping. Substituting $u_0' = \frac{u_1 - u_{-1}}{2l_{seg}}$, this boundary condition eventually results in: $u_{-1} = u_1 - \frac{2l_{seg}}{EA} \cdot Fr_{(0,t)}$. The dynamic friction load is defined based on the following formula: $Fr(0,t) = \mu_{kin} \cdot V(0,t) \cdot \left\{\frac{-\dot{u}_{rel}}{|\dot{u}_{rel}|}\right\}$, in which μ_{kin} is the dynamic friction coefficient, $V(0,t)$ the vertical force at that point and $\left\{\frac{-\dot{u}_{rel}}{|\dot{u}_{rel}|}\right\}$ the indicator of its direction in such a way that it opposes the direction of the relative velocity at that point , with $\dot{u}_{rel}(t) = \dot{u}(0,t) - \dot{u}_{slid}(t)$ being the relative velocity between the sliding end of the rod model and the landing supporting the sliding end of the bridge

2) $u(L,t) = u_{pin}(t)$, where $u_{pin}(t)$ is the horizontal excitation of the landing supporting the right end of the bridge, concluding in the expression for the relevant discretized point: $u_N = u_{pin}(t)$

Consequently, after applying the boundary conditions and eliminating all the ghost points that are generated, the resultant equations of motion for the discretized rod during slipping are the following ones:

- <u>for n=0</u>: $\rho \cdot A \cdot \ddot{u}_0 - \frac{EA}{l_{seg}^2} \cdot (u_{-1} - 2u_0 + u_1) = 0 \overset{(u_{-1})}{\Longrightarrow}$

$$\rho \cdot A \cdot \ddot{u}_0 - \frac{EA}{l_{seg}^2} \cdot \left(u_1 - \frac{2l_{seg}}{EA} \cdot Fr_{(0,t)} - 2u_0 + u_1 \right) = 0 \rightarrow$$

$$\rho \cdot A \cdot \ddot{u}_0 - \frac{EA}{l_{seg}^2} \cdot \left(-2u_0 + 2u_1 - \frac{2l_{seg}}{EA} \cdot Fr_{(0,t)} \right) = 0 \rightarrow$$

$$\rho \cdot A \cdot \ddot{u}_0 - \frac{EA}{l_{seg}^2} \cdot (-2u_0 + 2u_1) = -\frac{2 \cdot Fr_{(0,t)}}{l_{seg}}$$

- <u>for n=1 to (N-2)</u>: $\rho \cdot A \cdot \ddot{u}_n - \frac{EA}{l_{seg}^2} \cdot (u_{n-1} - 2u_n + u_{n+1}) = 0$

- <u>for n=N-1</u>: $\rho \cdot A \cdot \ddot{u}_{N-1} - \frac{EA}{l_{seg}^2} \cdot (u_{N-2} - 2u_{N-1} + u_N) = 0 \overset{(u_N)}{\Longrightarrow}$

$$\rho \cdot A \cdot \ddot{u}_{N-1} - \frac{EA}{l_{seg}^2} \cdot (u_{N-2} - 2u_{N-1}) = \frac{EA \cdot u_{pin}}{l_{seg}^2}$$

- <u>for n=N</u>: $u_N = u_{pin}$

These can be expressed in a matrix form:

$$\rho \cdot A \cdot \underline{\ddot{u}} - \frac{EA}{l_{seg}^2} \cdot \underline{\underline{K_{coef}}} \cdot \underline{u} = \underline{F} \overset{\cdot l_{seg}}{\Longrightarrow}$$

$$\rho \cdot A \cdot l_{seg} \cdot \underline{\ddot{u}} - \frac{EA}{l_{seg}} \cdot \underline{\underline{K_{coef}}} \cdot \underline{u} = \underline{F} \cdot l_{seg} \rightarrow$$

$$\underline{\underline{M}} \cdot \underline{\ddot{u}} + \underline{\underline{K}} \cdot \underline{u} = \underline{F_{ext}}$$

where: $\underline{u} = [u_0 \quad u_1 \quad u_2 \quad \dots \quad u_{N-2} \quad u_{N-1}]^T$

$$\underline{\underline{K_{coef}}} = \begin{matrix} n=0 \\ 1 \\ . \\ . \\ . \\ N-2 \\ N-1 \end{matrix} \begin{bmatrix} -2 & 2 & 0 & 0 & 0 & 0 & 0 \\ 1 & -2 & 1 & 0 & 0 & 0 & 0 \\ 0 & 1 & -2 & 1 & 0 & 0 & 0 \\ 0 & 0 & \dots & \dots & \dots & 0 & 0 \\ 0 & 0 & 0 & \dots & \dots & \dots & 0 \\ 0 & 0 & 0 & 0 & 1 & -2 & 1 \\ 0 & 0 & 0 & 0 & 0 & 1 & -2 \end{bmatrix}$$

$$\underline{F_{ext}} = \begin{bmatrix} -2Fr_{(0,t)} & 0 & 0 & \dots & 0 & \dfrac{EA \cdot u_{pin}}{l_{seg}} \end{bmatrix}^T$$

Event case for altering the state:

As considered in the sticking state as well, there must be an event case for altering the state of slipping and continuing to the sticking case. Since during the slipping state dynamic friction is generated, the event case for altering the state is regarding the relative velocity generated between the left end of the rod (n=0) and the corresponding landing, at every time instant. Specifically, as long as the relative velocity is non-zero slipping is the state, which alters to the sticking one the moment that the relative velocity becomes zero (when there is no relative movement between the concerning end point of the rod and the corresponding landing). During this state, dynamic friction is generated $\left(Fr_{dynamic} = \mu_{kinetic} \cdot V_0 \cdot \left\{ \frac{-\dot{u}_{rel}}{|\dot{u}_{rel}|} \right\} \right)$, where $\mu_{kinetic}$ is the coefficient of dynamic friction, V_0 the vertical force at that end (n=0) and $\dot{u}_{rel}(t_i) = \dot{u}_0(t_i) - \dot{u}_{sliding\ platform}(t_i)$ the relative velocity between the left end point of the discretized rod (n=0) and the corresponding landing at the time instant t_i. Apparently, dynamic friction is a constant-valued force, altering only direction wise (opposing the direction of relative velocity).

The idea and the working mechanism of the numerical model that was generated is illustrated in the block diagram that follows.

$$t_{initial} = 0$$
$$t_{simul} = T$$

- $IC =$ zero displacements/ velocities
- $mode = "stick"$

$$t_{initial} = [t_{initial}\ t_{simul}]$$

Legend:

IC : initial conditions of the discretized points of the model

$mode$: state of friction

q_i : state vector, containing all displacements and velocities of the discretized rod model

$u_0, \dot{u}_0$: displacement and velocity of the sliding end of the bridge

$u_{slid}, \dot{u}_{slid}$: displacement and velocity of the landing corresponding to the sliding end of the bridge

t_{out} : vector of all time instants considered while computing the certain state

$F_{(n=0)}^{axial}$: the axial force generated at the sliding end of the bridge

V_0 : the vertical force applied at the sliding end of the bridge

mode = "stick"

mode = "slip"

Stick branch:

- advance in time
- compute new state (q_i)
- $u_0 = u_{slid}, \dot{u}_0 = \dot{u}_{slid}$
- $Friction = F_{(n=0)}^{axial}$

$$F_{(n=0)}^{axial} > Fr_{static}^{max}$$

NO

YES

- $t_{initial} = t_{out}(last)$
- $IC = q_i(last)$
- $mode = "slip"$

Slip branch:

- advance in time
- compute new state (q_i)
- $\dot{u}_{rel} = \dot{u}_0 - \dot{u}_{slid}$
- $Friction = \mu_{dyn} \cdot V_0 \cdot \left\{ \frac{-\dot{u}_{rel}}{|\dot{u}_{rel}|} \right\}$

$$\dot{u}_{rel} = 0$$

NO

YES

- $t_{initial} = t_{out}(last)$
- $IC = q_i(last)$
- $mode = "stick"$

store t_{out} and q_i for every time instant considered

8.5 Obtained results and remarks

Now that the equations of motion have been generated, transformed into ordinary differential equations (ODE) and implemented in matrix form, what remains to be done is to use an ODE solver to advance the state of the model (displacements and velocities of every discretized point) at each time step and return the state of the system for all the time instants that are implemented. The state advances each time, while manipulating a function (ODE function) inside which all time-dependent parameters are also calculated. These consist of the relative velocity between the bridge sliding end and the connecting platform at every time instant, the axial forces generated and the resultant horizontal accelerations for every discretized point. The accelerations are computed simply using the equation of motion and solving for the acceleration parameter.

Having specified all the above mentioned requirements and after selecting an appropriate ODE solver from the provided from Matlab ones (i.e. ode45, ode23), the outcome is a matrix containing the displacements and velocities, for all the discretized points and for all the time instants specified.

Calling the Matlab ODE solver was extended by enabling the "event function" option. In that way, the state of the system alters while advancing on time, based on the relevant event case which specifies whether static or kinetic friction is present. The two event cases were described on the previous section for each state of friction exclusively.

The friction force, applied at the left end (point n=0), is computed for every time instant based on the certain event (sticking/slipping) and therefore the vector $\underline{F_{ext}}$ changes accordingly.

More specifically, regarding the generated friction force:

$$Fr_{(0,t)} = \begin{cases} stat\ frict = min\{\mu_{static} \cdot V_0; \ |F^{axial}_{(0,t)}|\} \cdot sign(F^{axial}_{(0,t)}), if\ sticking \\ dynamic\ frict = \mu_{kinetic} \cdot V_0 \cdot \left\{\dfrac{-\dot{u}_{rel}}{|\dot{u}_{rel}|}\right\}, if\ slipping \end{cases}$$

where: V_o: vertical load acting at the bearing (vertical reaction at bridge end)

$F^{axial}_{(0,t)} = \dfrac{EA \cdot (u_1(t) - u_0(t))}{l_{seg}}$:   the axial load generated at the sliding end

$\left\{\dfrac{-\dot{u}_{rel}}{|\dot{u}_{rel}|}\right\}$:   an indicator to show that the generated kinetic friction's direction is

opposite to the corresponding relative velocity

As a start, in order to test the model, the input excitations of the two supports were both considered to be of sinusoidal type, with a small amplitude of 1 cm. The sinusoidal type was selected in order to have a smooth transition as time advances and make computations easier and thus faster. The derived friction load with time is depicted in the following figure, together with the relative velocity with time plot. Although the problem was solved for a simulation duration of 8 s, only a first part of the results is presented in the following figure, in order to avoid any confusion.
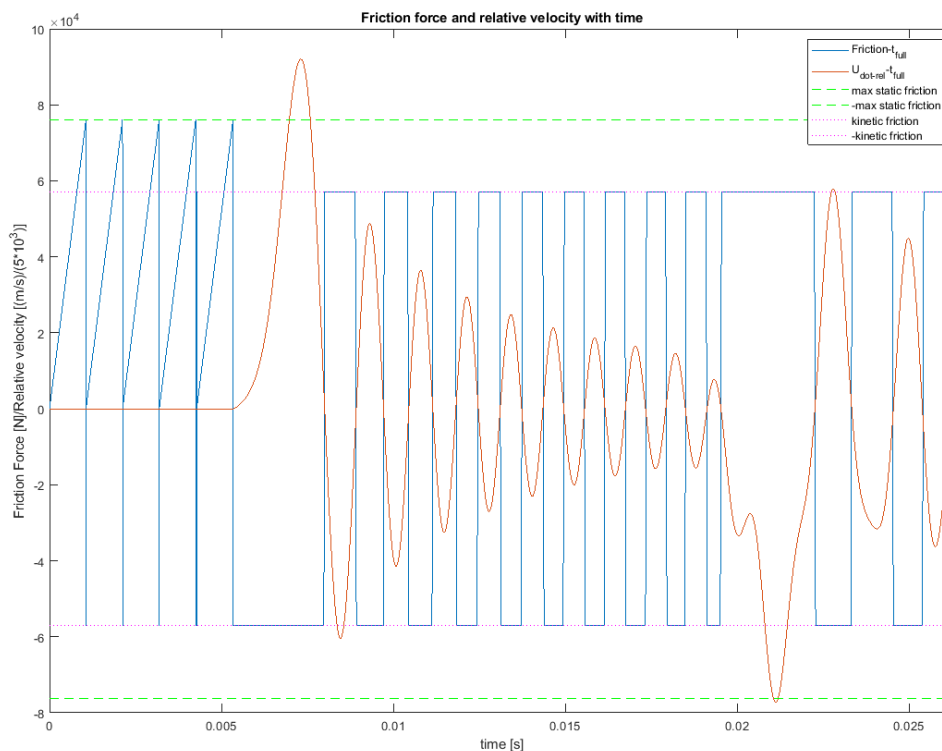
Figure 8-7 – Friction force and relative velocity with time

It is obvious that the obtained results show some inconsistency. While advancing on time, the solver requires extremely small time intervals ($\leq 10^{-4}s$), even when using less accurate solvers. This is an indication that the problem is not well defined or that it is very complicated to be solved in an efficient way.

Besides that, it should be noted that the event cases for altering the state of friction are fulfilled very rapidly. This is something that can be justified for the event case that has to be fulfilled when sticking is the state. During this state, the event case in order to change to slipping has to do with the exceedance of the maximum static friction, which is something that can be fulfilled very quickly due to the very large value of the stiffness factor (EA) in comparison with the maximum static friction load. This condition needs a very small amount of imposed displacement in order to be fulfilled and thus can be justified.

What cannot be explained is the fulfillment of the condition while slipping is the state. In such a situation, the event condition that needs to be fulfilled in order to alter the state to sticking, contains the relative velocity between the landing (due to its imposed excitation) and the first discretized point of the bridge (n=0). It seems that there are times when this condition is fulfilled much more rapidly than the one concerning the sticking state. To be more specific, there are time intervals where the relative velocity changes its sign in infinitesimally small time intervals ($< 10^{-4}s$), as can be seen in the following figure, which is an extended zoom of the previous one presented.
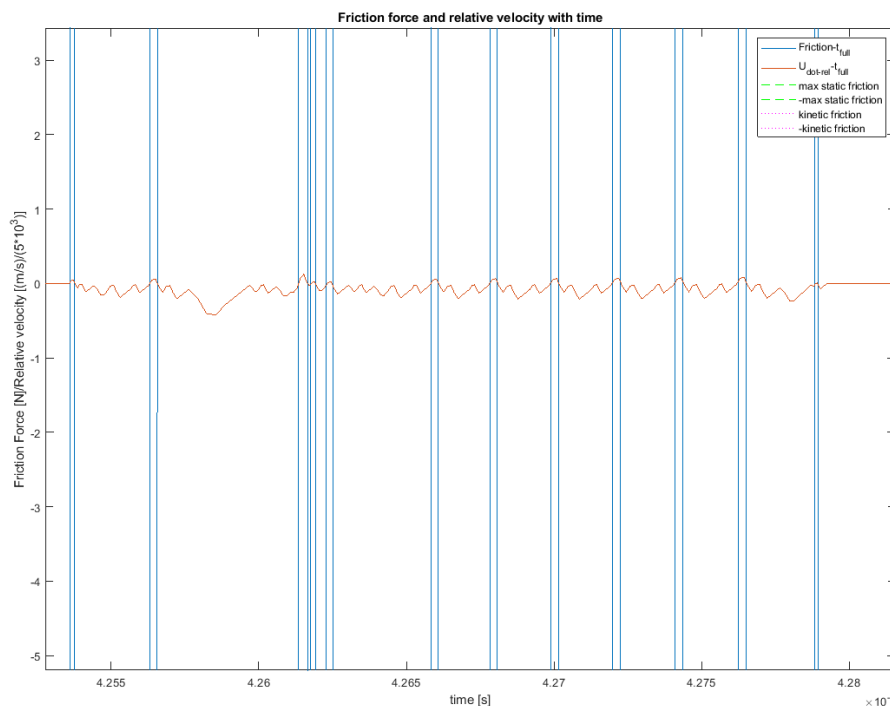
Figure 8-8 – Extended zoom-in of the results of Figure 8-7, at the region of 0.00425-0.00428 s

Such a behavior can't be reality. It cannot be realistic to have changes of the relative velocity between such small time intervals. The slipping state should not last that short, it is not rational and is a something that is in conjunction with the very small time intervals that the solver requires in order to advance in time.

While trying to clarify the unexpected results, some possible ones are the followings:

- The problem is very complicated in the way that has been defined
- There may be inconsistency in the way of writing the Matlab script
- The change of distance between the landing and the discretized points of the bridge has not been taken into account. More specifically, the first discretized point of the bridge (n=0) is always considered to be the only point of contact with the landing, but after slipping occurs there is relative movement between the bridge which has not been taken into account in this numerical model. The relative movement results in a change of the position of the bridge discretized points with respect to the landing and this results in imposed excitations at different discretized points each time that a slipping state occurs.

9 Conclusions and recommendations

This thesis was generated with the aim to:

- highlight the governing limit state when designing a bridge landing, through evaluating the structural performance of a specific configuration
- review and evaluate a simplified methodology that was followed to perform the fatigue analysis of the bridge landing
- conclude into the required (if any) improvements or reinforcements that will make the structure to be adequate against the corresponding limit states

The abovementioned questions can now be answered and relevant conclusions can be derived for each of them. These are presented in the following.

9.1 Important aspects in the design of a bridge landing

Examining the structure against the different limit states (SLS, ULS and FLS) was the starting point of the thesis, in order to indicate the governing one for such a design. It was derived that, although the criteria for the serviceability and ultimate limit states were satisfied, the structure was inadequate against the fatigue requirements.

The base case approach that was followed in order to perform the fatigue analysis in a simple and quick way signified the necessity of performing a fatigue assessment into such a type of structure, something that is not always the case for bridge landings.

9.2 Reviewing the base case method of fatigue analysis

The base case approach, as described in chapter 5, was a method to quickly assess the fatigue behaviour of the bridge landing through considering certain simplifications regarding the wave characteristics, the friction coefficient and the behaviour of the friction load. Following this method as a start, the critical locations where the fatigue requirement is not satisfied became apparent. These consist of positions in the front beam of the structure, specifically in the connection points with the transverse members of the structure and in the locations of the bearing pads.

The sensitivity analysis that was conducted in order to evaluate the level of the method's conservatism concerned the two main parameters, the wave directionality and the coefficient of friction. The actual behaviour of friction was also considered when examining the wave directionality parameter. The following conclusions can be derived:

9.2.1 Wave directionality

Considering all waves coming from the same direction (direction of sliding), as was assumed in the base case, is a conservative assumption. It is conservative to do so, because in such a case the largest magnitude of friction is generated, due to the direction of the induced displacements at the connected platforms. This was explained in detail in section 6.2, where some main characteristics of the friction mechanism (static-kinetic state) were also taken into account. The followings can be concluded:

- The waves with a direction perpendicular to the bridge can be entirely excluded from the analysis. This is justified because such waves result in very small relative displacements between the two ends of the bridge, which result in a generated friction much below the maximum static one. This load, in the fatigue assessment, results in a stress range lower than the fatigue limit and thus it can be neglected. For the specific case examined, excluding the perpendicular waves resulted in a 7.5 % reduction in the accumulated damage. Although it is not a negligible reduction, it was not enough to turn the structure fatigue-resistant. Moreover, taking into account the amount of work needed in order to justify exclusion of these waves from the fatigue analysis, it can be concluded that it is not worthy to do so, thus proceeding with the base case assumption is preferable. The difference in results is very small, whereas the amount of added work is significant.

- In any other wave direction considered, the generated friction overcomes the maximum static limit and the bridge is sliding. This limit was also found to be exceeded very rapidly inside a single wave cycle, indicating that the bridge is mainly sliding and the kinetic type of friction is generated. This implies that the friction load can be defined by using the kinetic friction coefficient, resulting in lower values.

- The sensitivity of the wave directionality is a strongly site-dependent study. In order to derive conclusions for its impact on the analysis, a number of parameters play a significant role which depend on the specific details of the case. These are the wave scatter information of the location, as well as the direction of the bridge with respect to the incoming waves. To be more specific, the orientation of the bridge will indicate which waves can be excluded from the analysis (those coming perpendicular to the bridge), which in combination with the specific scatter information may result in a small or, perhaps in some cases, a big reduction in the amount of applied load cycles.

- Finally, the length of the bridge may also be an important parameter in the analysis. This influences the amount of relative displacement that is induced between the two platforms, through the resultant phase difference, which may define the state of the generated friction and the magnitude of the friction load

9.2.2   Coefficient of friction

The value of the coefficient of friction to be considered is another important aspect of the analysis. In the base case approach, a typical value of 0.4 was taken into account for the analysis. The sensitivity study highlighted the following:

- Reducing the friction coefficient value results in a much larger percentage decrease in the accumulated damage. The required friction coefficient limiting value that results in satisfying the fatigue requirements is 0.12.

- A very low value of friction coefficient can be achieved through the application of sliding bearing pads with a PTFE sliding surface. Taking into account the manufacturer provisions for such a commercially available bearing pad indicates a maximum friction coefficient value of 0.04. This value is also in correspondence with the ones suggested from the different available sources found, also indicating a value of 0.04 for this case. Performing a fatigue analysis for the case considered and with such a friction coefficient results in an adequate structure by means of fatigue. The analysis pointed out a 100 % reduction in the accumulated damage, in comparison to the results obtained from the base case (where the friction coefficient used was 0.4). This highlights the big impact of the friction coefficient in the induced fatigue damage.

- Uncertainties may arise in the consideration of such a low friction coefficient value for the entire life of the structure. Dirt and corrosion may impact the friction coefficient, since the impact of those parameters was not mentioned by the manufacturer. This is a point where attention should be paid before incorporating such a low value for a fatigue analysis concerning a period of 25 years.

9.3   Examination of several improvement options

Four options were examined in order to improve the fatigue behaviour of the bridge landing. Any comparison was made with reference to the results obtained from the base case approach. It was found that not all the options were able to make the structure resistant against fatigue. Specifically:

9.3.1   Weld improvements

The possibility of improving the existing welds was examined in such a way that the best possible improvement by means of detail classification was achieved. The following can be concluded:

- Improving the existing welds was not able to be done for all the fatigue sensitive locations. Specifically, the locations where the bearing pads are attached cannot obtain a higher classification. The only way to improve them, according to the DNV provisions [1], was through decreasing the weld length. This implies reducing the dimensions of the bearing pad, which is something that is specified by the manufacturer and cannot be changed.

Moreover, decreasing the weld dimensions would result in higher applied stresses in the weld itself, thus setting in risk its strength integrity.

- Regarding the remaining locations, weld improvement was possible and it was found that the detail characteristics could be enhanced significantly. The corresponding S-N curve could appoint a 5 to 7 times better class, which resulted in better characteristics and thus much lower accumulated damages. Nevertheless, none of the locations became adequate and the fatigue requirements remained unfulfilled.

9.3.2 Modifying the structure by adding new beams

This comprises an option of modifying the existing structure through adding some extra members. It was found that the addition of members, starting at the bearing locations, was an effective option to reduce the accumulated damage and result into an adequate configuration which is not prone to fatigue.

Through this way of modification, the large induced out-of-plane bending moment (mainly at the bearing pad locations) was eliminated due to the presence of the new beams. The generated friction was delivered from the new beams, thus alleviating the front beam (HE700A) where all the critical locations were defined.

It should be noted that the added members were considered having the same properties (cross section, connection details) as the existing corresponding members at the same direction. This is a point that should be optimized if that improvement option is selected.

9.3.3 Strengthening the cross section of the front beam

This was done in two different ways. The first one comprises welding a horizontal plate at the top flange of the front beam, whereas the second consists of welding a vertical plate such as it connects the two flanges of the front beam's HEA section. Both these options resulted in making the bridge landing fatigue-resistant.

Regarding the first option, different plate widths and lengths were defined for the several critical locations of the front beam. On the other hand, the second option resulted in two required plates, one along the whole first half of the member and another one along the remaining other half of the member.

Comparing the two options by means of the amount of material that is required, welding a plate horizontally, as an extension of the section's top flange results in much less required material than welding a plate vertically. Specifically, the former requires 49823.5 cm^3 of steel, whereas the latter 430560 cm^3 (8.6 times more steel).

On the other hand, the first option is more complicated by means of welding, since welding is required in multiple locations, whereas the second option is simpler in that sense since there are no start-stop points and the plates are welded along the whole front member's length. This is another important point that should be considered in the comparison of the two options.

9.4   Recommendations regarding improving the base case approach

Following the base case approach, some simplifications regarding the friction and wave characteristics were considered. The sensitivity analysis highlighted the level of significance of those parameters in the design, hence enabling to derive certain recommendations for improving the approach:

- Regarding the wave characteristics: Excluding the amount of waves that have a direction perpendicular to the bridge is a way of improving the base case approach. Although the approach does not become very complicated, the required work is incomparable to the amount of improvement that is achieved in the fatigue assessment. Therefore, for the specific case that was examined, such an implementation is not recommended and the base case approach is concluded to be an adequate method for that case. However, the impact on the results may be significant in another situation, depending on the metocean data of the certain location.

- Regarding the coefficient of friction: Incorporating a better representative value for the case of using sliding bearing pads with a PTFE surface is recommended, since it concerns significantly lower friction coefficient values. Such low values are suggested by both the commercial brochure and the literature findings. However, adoption of these values being unaffected with time is an issue that should be further investigated and relevant experiments should be conducted in order to examine its dependence on dirt and corrosion effects.

- Regarding the stick-slip behaviour of friction: It may be useful to incorporate the real behaviour of friction through a numerical model. This would result into having multiple stress ranges inside a wave cycle with several lower (than the one considered in the base case) stress ranges. This will induce less accumulated damage in the structure and a comparison of its results with the base case's ones should indicate whether it is worthwhile including such characteristics in the analysis.

9.5   The recommended approach to be followed

Based on the investigation that was conducted, the approach that should be followed when designing a bridge landing structure can now be indicated. This is summarized in the following:

1) If there is the possibility, orient the bridge in such a way that the majority of the waves (according to the metocean data) approaches the bridge perpendicularly
2) Base the design of the bridge landing and its configuration on satisfying its fatigue limit state (critical state) due to the generated friction
3) Use bearing pads with a low friction coefficient (preferably < 0.2). The required friction coefficient that results in satisfying the fatigue requirements can be defined by following the approach described in section 6.1.4
4) Perform fatigue analysis of the bridge landing according to the base case approach
    o Calculate the generated friction load, based on the friction coefficient to be used and the vertical load at the bearing pad location resulting from the permanent loads of the bridge
    o Perform a static analysis with the friction load applied at the bearing pad locations and derive the applied member stresses
    o Double the applied stresses to derive the resultant stress ranges in a full wave cycle
    o Calculate the average wave period to be used, based on the metocean data of the concerning location, according to the procedure described in Appendix B.
    o Derive the number of applied stress cycles, as: $n = \frac{service\ life}{average\ wave\ period}$
    o Classify the critical connection details and obtain the characteristics of the applicable S-N curve
    o Check for every critical connection detail:
        ▪ if $applied\ stress\ range < fatigue\ limit$, then the detail is sufficient
        ▪ if $applied\ stress\ range > fatigue\ limit$, then calculate the accumulated damage: $D = \frac{n}{N}$
        ▪ if $D < 1$, then the detail is sufficient
        ▪ if $D > 1$, then the detail is insufficient
            • if the calculated damage is not much above the limit (1.0), it is advised to check whether excluding the waves coming perpendicular to the bridge results in satisfactory results
            • if the requirements are still not satisfied, improvements have to be performed in order to satisfy them
    o If the fatigue requirements are satisfied for every detail, then the bridge landing design is adequate
5) Perform the SLS and ULS design checks for the configuration defined
6) Examine all the weld connections against their strength requirements

9.6 Further study proposals

During the present study, some new investigation points were indicated, which were not initially considered. Due to time limitations and lack of data, these were not able to be examined here, thus they are pointed out for further investigation. They consist of the following:

- The effect of time in the coefficient of friction value that us used is something that seems worthwhile to be studied and considered properly. This comprises considering the effect of accumulated dirt and corrosion in the friction coefficient that is adopted. Since offshore is a harsh environment and structures are considered to have a long service life, these effects can be significant.

- In the sensitivity study, the impact of the considered wave characteristics was examined through studying the effect of the incoming wave's direction with respect to the direction of the bridge. Although this indicated the option of excluding certain directions when calculating the amount of applied waves (thus the number of applied load cycles) to be considered in the base case, the effect of wave height was not taken into account. It should be meaningful to investigate its effect on the resultant friction load, in the same way that the directionality effect was examined. Then, the limiting wave height value, for which friction exceeds its static state and the bridge starts sliding, could be identified and thus based on this value certain number of waves should be excluded from the analysis (similarly to the directionality parameter).

- Another interesting point that may be useful to be examined concerns again the sensitivity analysis regarding the wave directionality. In this analysis, the whole spectrum was split into 16 directional sectors, as described in section 6.2. The choice of using 16 sectors was determined by the metocean information that was available for this case. The option of using less number of sectors, thus wider ones including more waves, may also affect the impact of this sensitivity study. Although for this particular case its effect may not be adequate in order to set the structure fatigue-resistant, it may be interesting to investigate its effect on the results. Specifically, if the conditions for the waves coming perpendicular to the bridge continue to be valid, decreasing the sectors' width would result into excluding more waves from the analysis, thus alleviating even more the structure against fatigue.

References

[1] Det Norske Veritas, *Fatigue Design of Offshore Steel Structures*, Recommended Practice DNV-RP-C203, 2016

[2] Det Norske Veritas, *Design of Offshore Steel Structures, General (LRFD Method)*, Recommended Practice DNV-OS-C101, 2011

[3] Bentley Systems. (2016). SACS Offshore Structural Analysis and Design Software (Version 10.2.0.1) [Microsoft Windows]

[4] NORSOK Standard N-004, *Design of steel structures*. October 2004

[5] Zaaijer, M.B. *Strength and Fatigue*. Introduction to Wind Energy presentation. Delft University of Technology, 2014

[6] EN 1993-1-9, Eurocode 3: *Design of Steel Structures - Part 1.9: Fatigue*, CEN, 2004

[7] Hobbacher A.F. *Recommendations for fatigue design of welded joints and components*, 2008. Doc. IIW-1823-07 (ex-doc. XIII-2151r4-07/XV-1254r4-07)

[8] Butt welding (2018). Retrieved from https://en.wikipedia.org/wiki/Butt_welding

[9] Fillet weld (2018). Retrieved from https://en.wikipedia.org/wiki/Fillet_weld

[10] Friction and Friction Coefficients. (2018). Retrieved from https://www.engineeringtoolbox.com/friction-coefficients-d_778.html

[11] NORSOK Standard N-001, *Structural design*. February 2004

[12] IBG Monforts Gleitlagertechnik GmbH & Co. KG. *PTFE Sliding Supports Product Overview*

[13] Vugts, J.H. *Handbook of Bottom Founded Offshore Structures, Part 2 - Fixed steel structures*. Eburon, Delft, 2016. ISBN 978-94-6301-013-9

[14] International Organization for Standardization. ISO 19902, *Petroleum and natural gas industries - Fixed steel offshore structures*. 1st edition December 2007; Clause A.16.7.2.3.2

[15] Finite difference coefficient (2019). Retrieved from https://en.wikipedia.org/wiki/Finite_difference_coefficient

[16] F. P. Bowden and D. Tabor (1954). *Friction and Lubrication.* Oxford University Press

[17] Moore, D. (1975). *Principles and applications of tribology*. Oxford, New York, Pergamon Press

[18] Bowden, F., & Leben, L. (1939). *The nature of sliding and the analysis of friction*. Proc. Of the royal society Of London A

[19] Elmer, F. (1997). Nonlinear dynamics of dry friction. *Journal Of Physics A: Mathematical And General*, *30*(17), 6057-6063. doi: 10.1088/0305-4470/30/17/015

[20] Gross D., Hauger W., Schröder J., Wall W.A., Rajapakse N. (2009) *Static and Kinetic Friction*. Engineering Mechanics 1. Springer, Berlin, Heidelberg

[21] Beardmore, R. (2019). Coefficients Of Friction. Retrieved from http://www.roymech.co.uk/Useful_Tables/Tribology/co_of_frict.htm

[22] Liu, Y., Li, J., Zhang, Z., Hu, X., & Zhang, W. (2015). *Experimental comparison of five friction models on the same test-bed of the micro stick-slip motion system*. Copernicus Publications

[23] Chen, G. (2014). *Handbook of friction-vibration interactions*. Amsterdam: Elsevier, Woodhead Publishing

[24] Friction in contact between moving bodies - MATLAB- MathWorks Benelux. (2019). Retrieved from https://nl.mathworks.com/help/physmod/simscape/ref/translationalfriction.html

[25] Friction and Friction Coefficients. (2019). Retrieved from https://www.engineeringtoolbox.com/friction-coefficients-d_778.html

[26] Schijve, J. (2014). *Fatigue of structures and materials*. [Place of publication not identified]: Springer

[27] International Organization for Standardization. ISO 19902, *Petroleum and natural gas industries - Fixed steel offshore structures*. 1st edition December 2007; Clause 16.15.3

[28] EN 1993-1-1, Eurocode 3: *Design of Steel Structures - Part 1.1: General rules and rules for buildings*, CEN, 2004

[29] American Petroleum Institute (API). *Petroleum and natural gas industries - Recommended Practice for Planning, Designing and Constructing Fixed Offshore Platforms—Working Stress Design*. API RP 2A-WSD, 21st edition. December 2000; Clause 2.3.2

[30] *MathWorks. (2018). MATLAB (Version R2018a)*

[31] Leine, R. I., Campen, van, D. H., Kraker, de, A., Steen, van den, L. (1998). *Stick-slip vibrations induced by alternate friction models.* Nonlinear dynamics, 16(1), 41-54. DOI: 10.1023/A:1008289604683

[32] Vrande, van de, B. L., Campen, van, D. H., Kraker, de, A. (1999). *An approximate analysis of dry-friction-induced stick-slip vibrations by a smoothing procedure.* Nonlinear dynamics, 19(2), 157-169. DOI: 10.1023/A:1008306327781

[33] Berger, E. (2002). Friction modeling for dynamic system simulation. *Applied Mechanics Reviews*, *55*(6), 535. doi: 10.1115/1.1501080

[34] Keijdener, C., & Laguna, A. *Finite Difference*. Introduction to Computational Dynamics of Offshore Structures, Lecture. Delft University of Technology (2018).

[35] Det Norske Veritas, *Fatigue Design of Offshore Steel Structures*, Recommended Practice DNV-RP-C203; Figure 2-8

[36] *American Welding Society. (2012). Standard Symbols for Welding, Brazing, and Nondestructive Examination*

[37] Det Norske Veritas, *Fatigue Design of Offshore Steel Structures*, Recommended Practice DNV-RP-C203; Clause 2.3.5

APPENDICES

Appendix A   Acting loads on the bridge landing

In section 4.2, the different loads that act on the bridge landing were described and their magnitudes were listed. Here, these are represented through simple drawings in order to be clear the way they act.
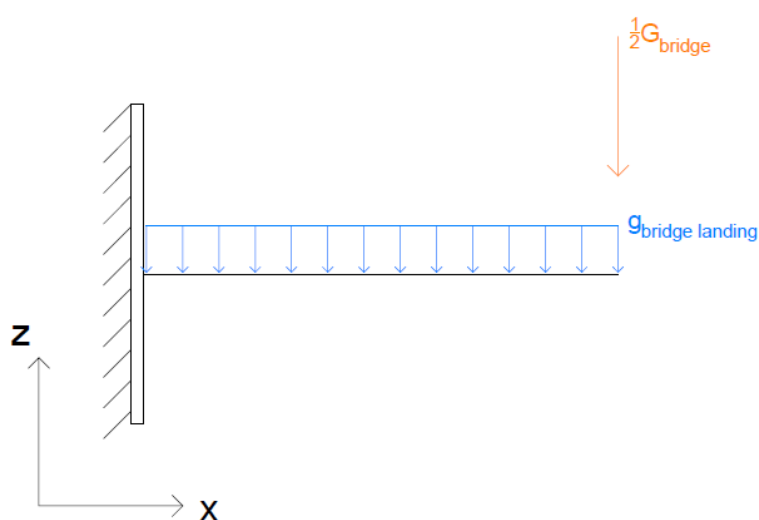

Figure A. 1 – Dead loads
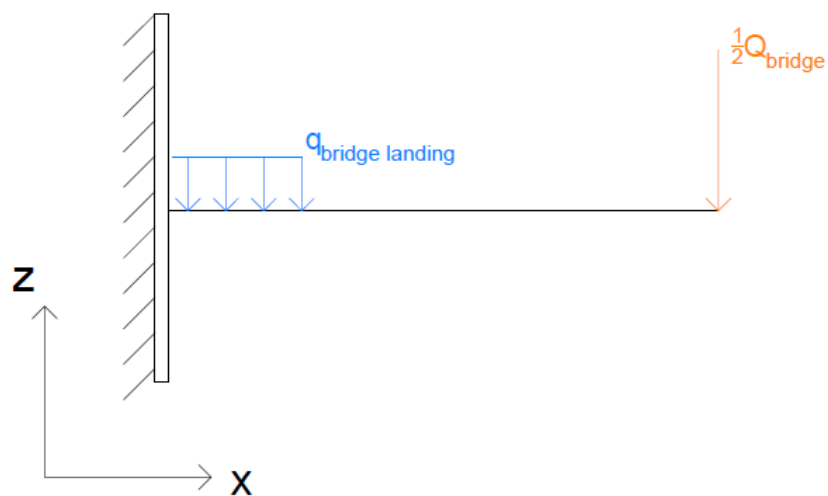
Figure A. 2 – Live loads
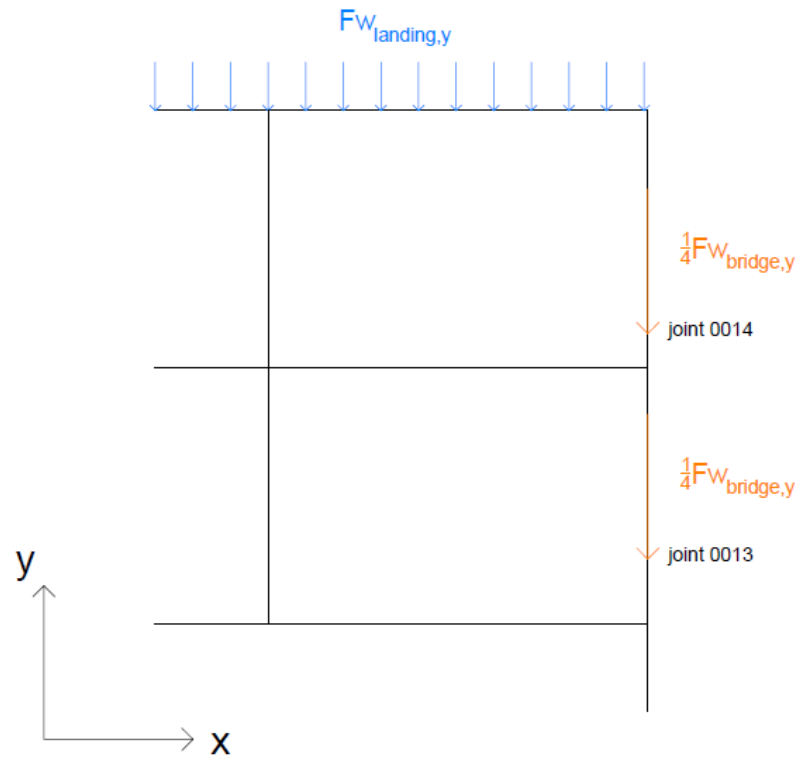
Figure A. 3 – Horizontal loads due to wind at negative y direction
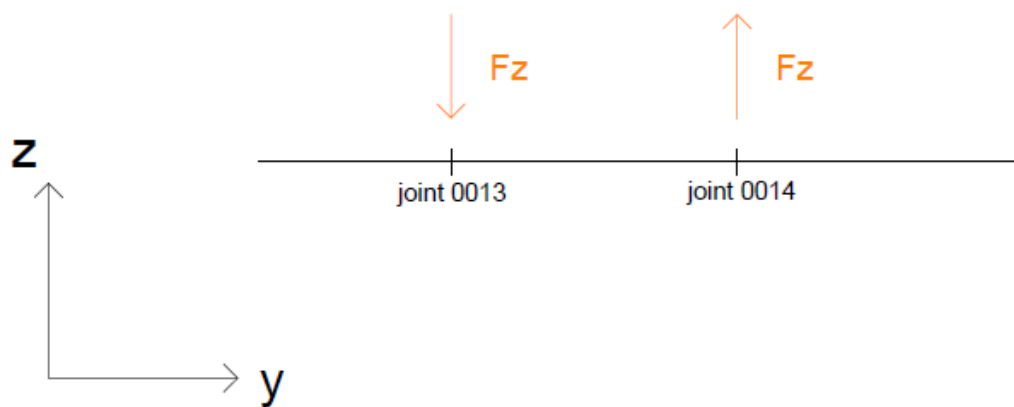
Figure A. 4 – Coupled vertical forces due to wind acting on the bridge
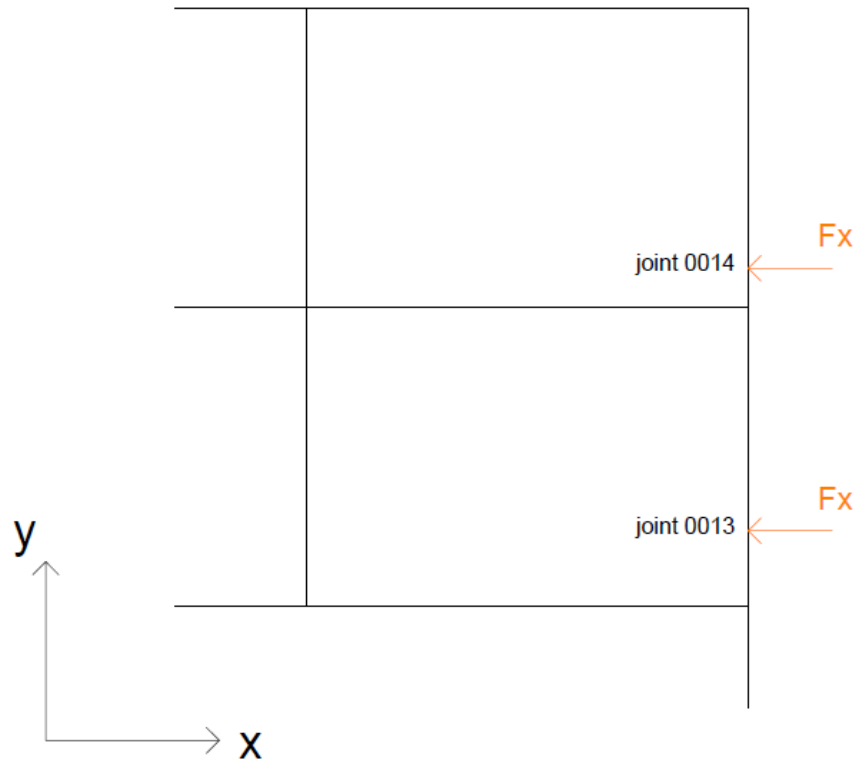
Figure A. 5 – Generated friction load at negative x direction
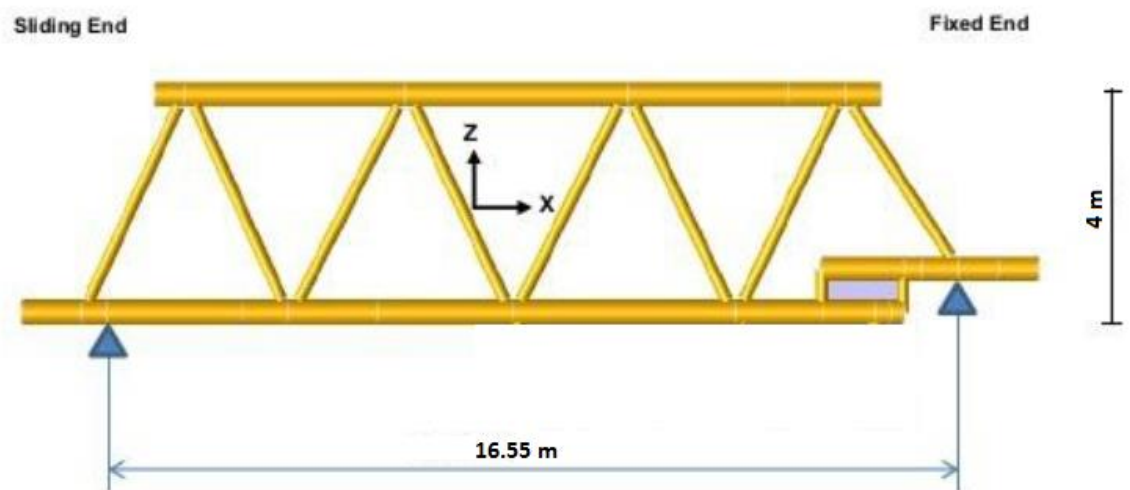
Figure A. 6 – Schematic overview of the bridge considered

Appendix B   Derivation of average wave period used in the base case

The average period of 5 s that was considered for performing the fatigue assessment of the bridge landing following the base case was derived by following the procedure below:

1) In the scatter diagram with the occurrences of the several (H_s, T_p) combinations, the peak period values are transformed to the mean zero-crossing ones (T_z), using the formula:
$$T_z = 0.777 \cdot T_p$$

2) For each mean zero-crossing wave period considered, the number of waves per seastate (3 hours storm) are determined, according to:
$$waves\ per\ seastate = \frac{3 * 60 * 60\ sec}{T_z}$$

3) The number of seastates per year is defined as:
$$seastates\ per\ year = (probability\ of\ occurence\ of\ Tp\ sector) \cdot 365\ days \cdot \frac{24\ hr}{3\ hr}$$

4) The number of waves per year for the certain T_z is calculated as:
$$waves\ per\ year\ for\ a\ T_z = \sum (waves\ per\ seastate) \cdot (seastates\ per\ year)$$

5) The number of waves for a certain T_z during the structure's service life of 25 years is defined as:
$$waves\ for\ a\ T_z\ in\ 25\ years = 25\ \cdot (waves\ per\ year\ for\ a\ T_z)$$

6) The total number of waves in the structure's service life of 25 years is derived as:
$$total\ number\ of\ waves\ in\ 25\ years = \sum (waves\ for\ a\ T_z\ in\ 25\ years)$$

7) Finally, the equivalent average period that can be considered can be defined by:
$$average\ wave\ period = \frac{25\ years}{total\ number\ of\ waves\ in\ 25\ years}$$

Appendix C   All the locations examined against fatigue

In chapter 5, the fatigue case was investigated, considering the base case. The results presented concerned the most prone member locations, in which the highest stress ranges were applied. Nevertheless, a much higher number of locations was considered before concluding into the most critical ones. All these locations and their applied stresses are demonstrated in this section. In the following figures all member locations that were considered to be examined against fatigue are highlighted.

Figure C. 1 – Top view of the bridge landing

Figure C. 2 – Cross sections A-A and B-B

In Table C. 1 below, the resultant stress ranges for the most critical local section detail of each member location considered are listed. These concern the base case, with the assumptions made as described in section 5.1. Moreover, the corresponding damage is also defined per location examined.

Table C. 1 – Resultant stress ranges of the most prone local section details for all member locations considered
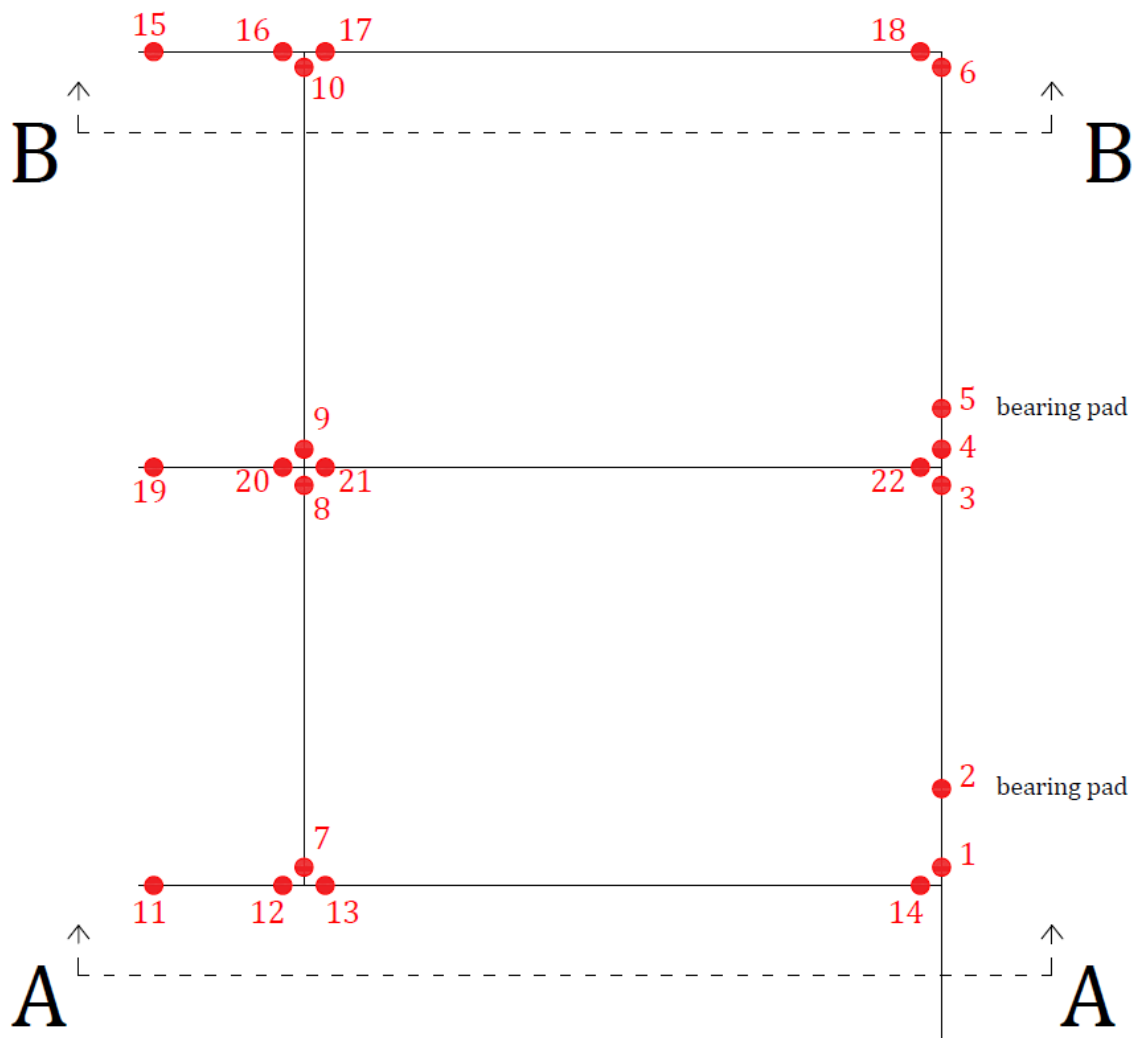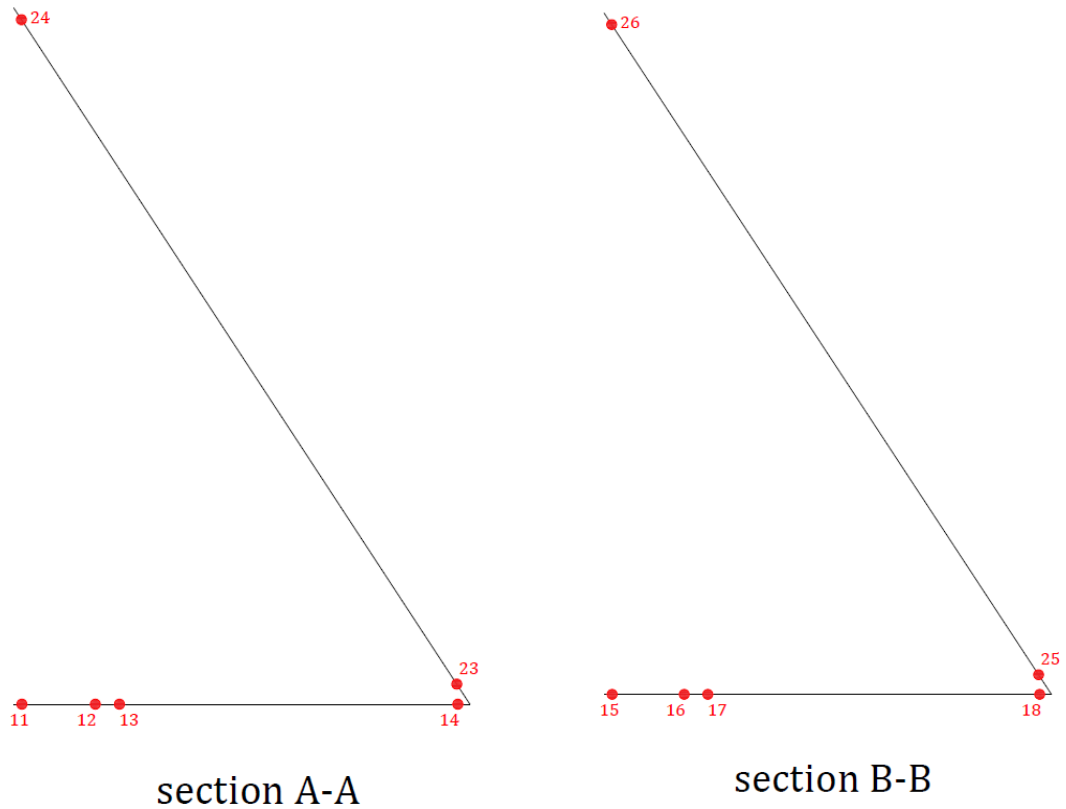
member location	section detail	$\Delta\sigma_{nom}$ (MPa)	SCF (-)	$\Delta\sigma_{hot\ spot}$ (MPa)	S-N curve	fatigue limit (MPa)	N (cycles)	damage for service life D (-)
1	7	92.37	1.0	92.37	G (toe cracking)	29.24	$2.99 \cdot 10^5$	526.60
2	1	59.42	1.0	59.42	F1	36.84	$2.25 \cdot 10^6$	70.08
3	1	66.59	1.0	66.59	W1	26.32	$5.83 \cdot 10^5$	270.38
4	1	69.49	1.0	69.49	W1	26.32	$5.13 \cdot 10^5$	307.34
5	1	37.44	1.0	37.44	F1	36.84	$1.1 \cdot 10^7$	14.28
6	2	36.13	1.0	36.13	G (toe cracking)	29.24	$5 \cdot 10^6$	31.52
7	7	0.99	1.0	0.99	W2	23.39	$5.94 \cdot 10^{13}$	≈ 0
8	8	0.94	1.0	0.94	W1	26.32	$1.38 \cdot 10^{14}$	≈ 0
9	7	3.32	1.0	3.32	W1	26.32	$2.48 \cdot 10^{11}$	≈ 0
10	1, 8	4.72	1.0	4.72	W2	23.39	$2.38 \cdot 10^{10}$	0.01
11	7	6.41	1.0	6.41	W3	21.05	$3.06 \cdot 10^9$	0.05
12	8	4.93	1.0	4.93	W1	26.32	$3.46 \cdot 10^{10}$	≈ 0
13	8	4.84	1.0	4.84	W1	26.32	$3.8 \cdot 10^{10}$	≈ 0
14	2, 7	22.18	1.0	22.18	B2	93.59	$1.34 \cdot 10^{10}$	0.01
15	7	3.62	1.0	3.62	W3	21.05	$5.34 \cdot 10^{10}$	≈ 0
16	7	7.94	1.0	7.94	B2	93.59	$2.27 \cdot 10^{12}$	≈ 0
17	7	8.49	1.0	8.49	B2	93.59	$1.62 \cdot 10^{12}$	≈ 0
18	1, 8	4.86	1.0	4.86	B2	93.59	$2.66 \cdot 10^{13}$	≈ 0
19	7	11.56	1.0	11.56	W3	21.05	$2.01 \cdot 10^8$	0.78
20	8	10.91	1.0	10.91	W3	21.05	$2.68 \cdot 10^8$	0.59
21	2	12.03	1.0	12.03	W1	26.32	$5.01 \cdot 10^8$	0.31
22	2, 7	14.57	1.0	14.57	W1	26.32	$1.92 \cdot 10^8$	0.82
23	1, 2, 3, 4	0.02	3.0	0.06	D	52.63	$5.12 \cdot 10^{21}$	≈ 0
24	1, 2, 3, 4	0.02	3.0	0.06	D	52.63	$5.12 \cdot 10^{21}$	≈ 0
25	1, 2, 3, 4	0.02	3.0	0.06	D	52.63	$5.12 \cdot 10^{21}$	≈ 0
26	1, 2, 3, 4	0.02	3.0	0.06	D	52.63	$5.12 \cdot 10^{21}$	≈ 0

The calculated damage indicates which member locations will fail due to fatigue, for the applied friction load, as described for the base case. It is apparent that member locations 1 to 6 are the ones that will fail, since the value of the accumulated damage for the service life of 25 years considered exceeds by far the limit value of 1 (values marked red). Furthermore, in all these locations the fatigue limit is below the applied stress range and therefore a detailed fatigue analysis should be performed. Regarding the labelling of the section detail locations, Figure C. 3 below illustrates the corresponding locations for both the wide flange and the tubular sections that are used for the bridge landing. Member locations 1 to 22 refer to wide flange sections (HEA or plate girder sections), whereas member locations 23 to 26 refer to tubular sections.
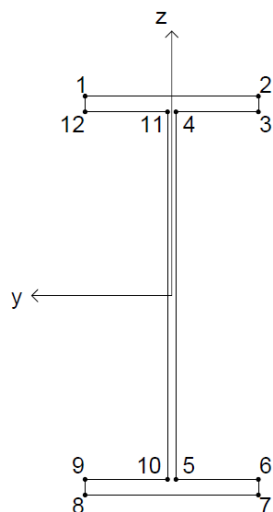
HEA and plate girder sections   tubular section
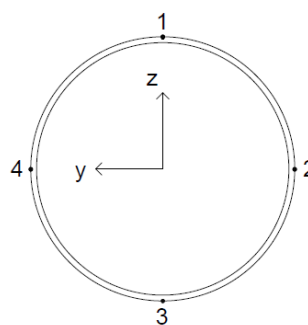
Figure C. 3 – Labelling of the multiple section detail locations considered

The most sensitive, with respect to fatigue, locations 1, 2, 3, 4, 5 and 6 are demonstrated in the following figures.

7) Locations 1 and 6: weld connection of member HE700A with plates at its ends

Figure C. 4 – Locations 1 and 6

8) <u>Locations 2 and 5</u>: weld attachment of bearing pads at the top flange of front member HE700A

Figure C. 5 – Locations 2 and 5

9) <u>Locations 3, 4</u>: transverse weld attachment of member HE400A at HE700A one

Figure C. 6 – Locations 3 and 4

Appendix D   Scatter diagrams of wave climate used

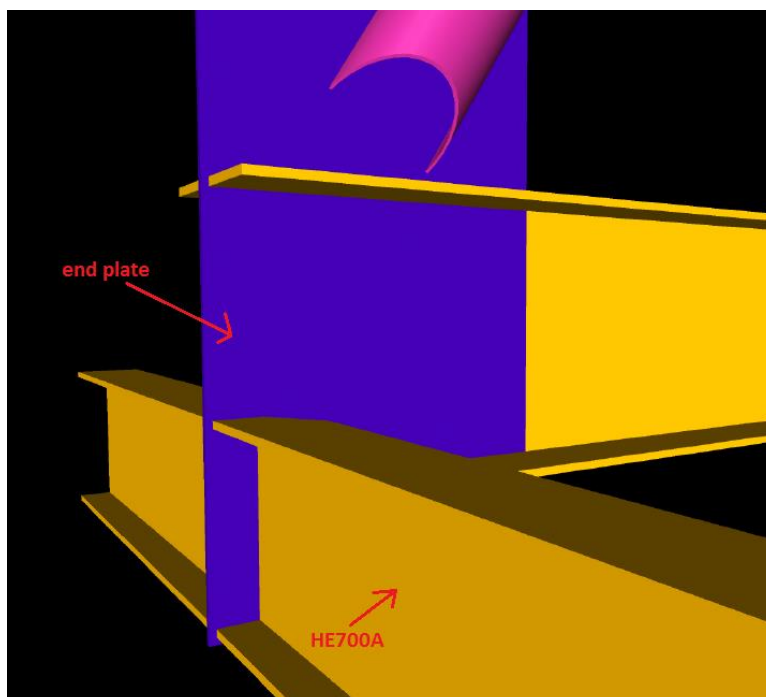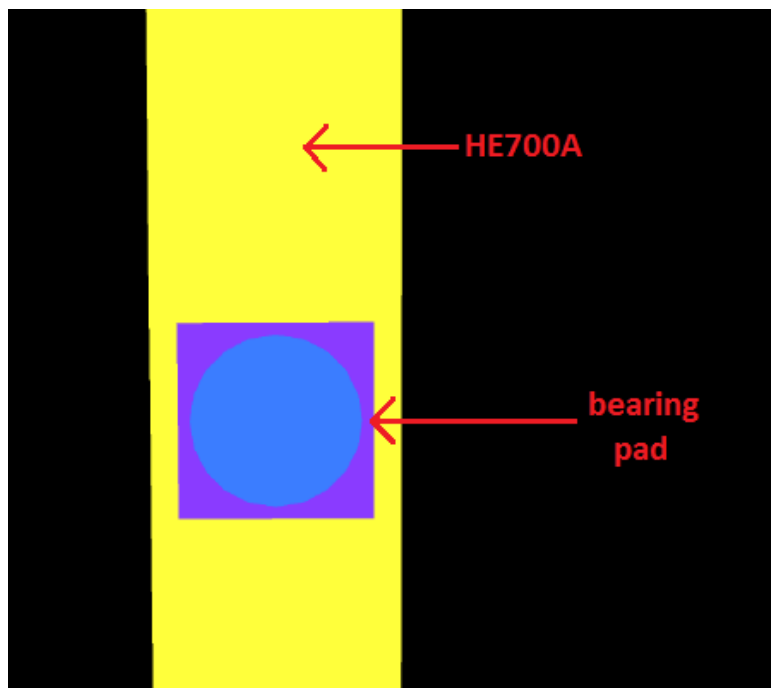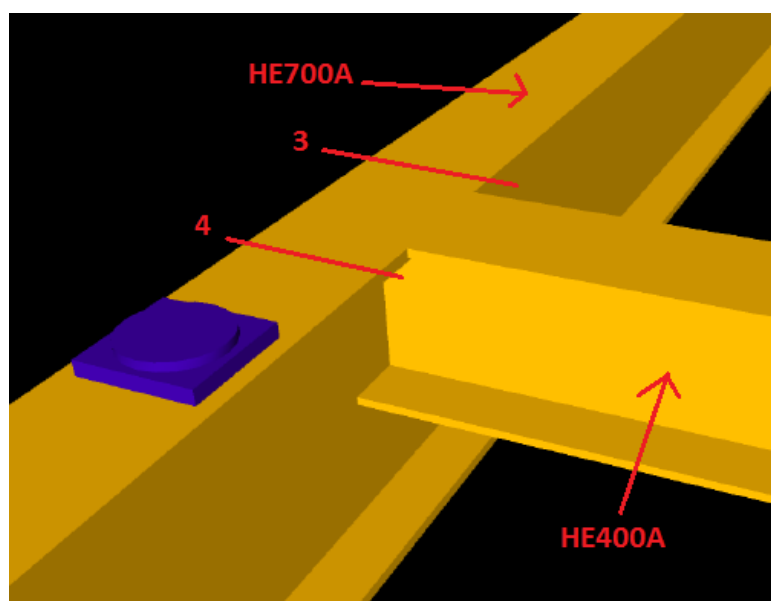| Hs		0–1	1–2	2–3	3–4	4–5	5–6	6–7	7–8	8–9	9–10	10–11	11–12	12–13	13–14	14–15	15–16	16–17	17–18	18–19	19–20	Total
8.5	9.0	0	0	0	0	0	0	0	0	0	0	0	0	0	0	0	0	0	0	0	0	0
8.0	8.5	0	0	0	0	0	0	0	0	0	0	0	0	0.002	0	0	0	0	0	0	0	0.002
7.5	8.0	0	0	0	0	0	0	0	0	0	0	0.002	0.006	0.004	0	0	0	0	0	0	0	0.012
7.0	7.5	0	0	0	0	0	0	0	0	0	0	0.004	0.006	0.006	0	0	0	0	0	0	0	0.016
6.5	7.0	0	0	0	0	0	0	0	0	0	0.002	0.010	0.012	0.004	0	0	0	0	0	0	0	0.028
6.0	6.5	0	0	0	0	0	0	0	0	0	0.008	0.034	0.026	0.004	0	0	0	0	0	0	0	0.073
5.5	6.0	0	0	0	0	0	0	0	0	0	0.040	0.111	0.026	0.010	0	0	0	0	0	0	0	0.187
5.0	5.5	0	0	0	0	0	0	0	0	0.012	0.187	0.131	0.020	0.004	0	0	0	0	0	0	0	0.354
4.5	5.0	0	0	0	0	0	0	0	0.002	0.141	0.393	0.123	0.026	0.006	0	0	0	0	0	0	0	0.691
4.0	4.5	0	0	0	0	0	0	0	0.030	0.630	0.367	0.091	0.030	0.004	0.004	0	0	0	0	0	0	1.156
3.5	4.0	0	0	0	0	0	0	0.004	0.322	1.186	0.316	0.089	0.022	0.008	0.006	0.004	0	0	0	0	0	1.957
3.0	3.5	0	0	0	0	0	0	0.103	1.770	1.156	0.296	0.073	0.026	0.002	0.010	0.016	0.006	0	0	0	0	3.457
2.5	3.0	0	0	0	0	0	0.030	1.025	3.232	1.023	0.316	0.089	0.018	0.004	0.026	0.010	0	0	0	0	0	5.773
2.0	2.5	0	0	0	0	0.008	0.860	3.908	2.805	1.045	0.332	0.121	0.060	0.042	0.048	0.018	0.006	0.002	0	0	0	9.256
1.5	2.0	0	0	0	0.002	0.803	4.553	4.684	2.632	1.077	0.322	0.173	0.117	0.050	0.026	0.002	0	0	0	0	0	14.441
1.0	1.5	0	0	0	0.628	6.441	4.738	4.555	2.475	1.192	0.582	0.296	0.171	0.044	0.032	0.016	0.004	0.004	0.004	0.004	0	21.186
0.5	1.0	0	0.006	0.731	8.032	4.627	5.358	3.949	1.617	1.027	0.735	0.439	0.149	0.064	0.127	0.103	0.097	0.069	0.044	0.012	0	27.185
0.0	0.5	0	0.548	3.461	2.984	2.265	1.416	0.785	0.646	0.431	0.469	0.211	0.159	0.191	0.240	0.205	0.103	0.062	0.032	0.016	0	14.226
Total		0	0.554	4.192	11.646	14.145	16.954	19.012	15.530	8.920	4.365	1.995	0.876	0.451	0.520	0.375	0.215	0.137	0.081	0.032	0	100

Figure D. 1 – Percentage of occurrence of the several significant wave height and peak period combinations

Hs		348.75–11.25	11.25–33.75	33.75–56.25	56.25–78.75	78.75–101.25	101.25–123.75	123.75–146.25	146.25–168.75	168.75–191.25	191.25–213.75	213.75–236.25	236.25–258.75	258.75–281.25	281.25–303.75	303.75–326.25	326.25–348.75	Total
8.5	9.0	0	0	0	0	0	0	0	0	0	0	0	0	0	0	0	0	0
8.0	8.5	0	0	0	0	0	0	0	0	0	0	0	0	0	0	0	0.002	0.002
7.5	8.0	0	0	0	0	0	0	0	0	0	0	0	0	0.002	0.002	0.004	0.004	0.012
7.0	7.5	0	0	0	0	0	0	0	0	0	0	0	0	0	0	0.010	0.006	0.016
6.5	7.0	0	0	0	0	0	0	0	0	0	0	0	0	0.002	0.006	0.014	0.006	0.028
6.0	6.5	0	0	0	0	0	0	0	0	0	0	0	0	0.004	0.018	0.032	0.018	0.073
5.5	6.0	0	0	0	0	0	0	0	0	0	0	0	0	0.014	0.036	0.079	0.058	0.187
5.0	5.5	0	0	0	0	0	0	0	0	0	0	0	0.002	0.056	0.058	0.123	0.115	0.354
4.5	5.0	0.002	0	0	0	0	0	0	0	0	0	0	0.012	0.066	0.171	0.193	0.246	0.691
4.0	4.5	0.012	0.010	0	0	0	0	0	0	0	0	0.008	0.050	0.193	0.338	0.264	0.280	1.156
3.5	4.0	0.010	0.006	0	0	0	0	0	0	0	0	0.008	0.135	0.439	0.421	0.467	0.471	1.957
3.0	3.5	0.056	0.046	0.004	0.032	0.006	0	0	0	0	0	0.030	0.489	0.769	0.614	0.665	0.745	3.457
2.5	3.0	0.203	0.069	0.038	0.062	0.050	0	0.004	0.006	0.002	0.014	0.089	0.985	1.027	0.946	1.019	1.259	5.773
2.0	2.5	0.304	0.121	0.095	0.211	0.250	0.036	0.006	0.002	0.040	0.054	0.298	1.583	1.450	1.309	1.506	1.991	9.256
1.5	2.0	0.572	0.318	0.276	0.578	0.719	0.242	0.044	0.040	0.111	0.173	0.646	1.963	1.963	1.750	1.965	3.081	14.441
1.0	1.5	1.269	0.636	0.568	1.075	1.408	0.592	0.304	0.179	0.264	0.507	1.138	2.444	2.338	2.062	2.205	4.198	21.186
0.5	1.0	2.428	1.174	1.011	1.502	2.185	1.333	0.773	0.592	0.524	0.797	1.337	2.765	2.259	1.792	2.424	4.289	27.185
0.0	0.5	1.484	0.930	0.765	0.709	0.985	0.683	0.409	0.322	0.238	0.228	0.405	1.083	1.297	1.148	1.665	1.877	14.226
Total		6.341	3.310	2.757	4.170	5.602	2.885	1.540	1.142	1.178	1.774	3.959	11.511	11.880	10.672	12.635	18.645	100

Figure D. 2 – Directional distribution of significant wave height

Appendix E   Coefficient of friction

Table E. 1 – Typical values of friction coefficient for the most common material combinations [25]

Materials and Material Combinations		Static Frictional Coefficient	
		Clean and Dry Surfaces	Lubricated and Greasy Surfaces
Aluminum	Aluminum	1.05 - 1.35	0.3
Aluminum-bronze	Steel	0.45	
Aluminum	Mild Steel	0.61	
Brake material[2]	Cast iron	0.4	
Brake material[2]	Cast iron (wet)	0.2	
Brass	Steel	0.35	0.19
Brass	Cast Iron	0.3	
Brick	Wood	0.6	
Bronze	Steel		0.16
Bronze	Cast Iron	0.22	
Bronze - sintered	Steel		0.13
Cadmium	Cadmium	0.5	0.05
Cadmium	Chromium	0.41	0.34
Cadmium	Mild Steel	0.46	
Cast Iron	Cast Iron	1.1, 0.15	0.07
Cast Iron	Oak	0.49	0.075
Cast iron	Mild Steel	0.4, 0.23	0.21, 0.133
Car tire	Asphalt	0.72	
Car tire	Grass	0.35	
Carbon (hard)	Carbon	0.16	0.12 - 0.14
Carbon	Steel	0.14	0.11 - 0.14
Chromium	Chromium	0.41	0.34
Copper-Lead alloy	Steel	0.22	
Copper	Copper	1	0.08
Copper	Cast Iron	1.05, 0.29	
Copper	Mild Steel	0.53, 0.36	0.18
Diamond	Diamond	0.1	0.05 - 0.1
Diamond	Metal	0.1 - 0.15	0.1

Glass	Glass	0.9 - 1.0, 0.4	0.1 - 0.6, 0.09-0.12
Glass	Metal	0.5 - 0.7	0.2 - 0.3
Glass	Nickel	0.78	0.56
Graphite	Steel	0.1	0.1
Graphite	Graphite (in vacuum)	0.5 - 0.8	
Graphite	Graphite	0.1	0.1
Hemp rope	Timber	0.5	
Horseshoe	Rubber	0.68	
Horseshoe	Concrete	0.58	
Ice	Ice	0.02 - 0.09	
Ice	Wood	0.05	
Ice	Steel	0.03	
Iron	Iron	1.0	0.15 - 0.20
Lead	Cast Iron	0.43[1]	
Leather	Oak	0.61, 052[1]	
Leather	Metal	0.4	0.2
Leather	Wood	0.3 - 0.4	
Leather	Clean Metal	0.6	
Leather fiber	Cast iron	0.31	
Leather fiber	Aluminum	0.30	
Magnesium	Magnesium	0.6	0.08
Masonry	Brick	0.6 - 0.7	
Nickel	Nickel	0.7 - 1.1, 0.53	0.28, 0.12
Nickel	Mild Steel	0.64	0.178
Nylon	Nylon	0.15 - 0.25	
Oak	Oak (parallel grain)	0.62, 0.48	
Oak	Oak (cross grain)	0.54, 0.32	0.072
Paper	Cast Iron	0.20	
Phosphor-bronze	Steel	0.35	
Platinum	Platinum	1.2	0.25
Plexiglas	Plexiglas	0.8	0.8
Plexiglas	Steel	0.4-0.5	0.4 - 0.5

Polystyrene	Polystyrene	0.5	0.5
Polystyrene	Steel	0.3-0.35	0.3 - 0.35
Polythene	Steel	0.2	0.2
Rubber	Rubber	1.16	
Rubber	Cardboard	0.5 - 0.8	
Rubber	Dry Asphalt	0.9 (0.5 - 0.8)	
Rubber	Wet Asphalt	0.25 - 0.75	
Rubber	Dry Concrete	0.6 - 0.85	
Rubber	Wet Concrete	0.45 - 0.75	
Silver	Silver	1.4	0.55
Sapphire	Sapphire	0.2	0.2
Silver	Silver	1.4	0.55
Skin	Metals	0.8 - 1.0	
Steel	Steel	0.5 - 0.8	0.16
Straw Fiber	Cast Iron	0.26	
Straw Fiber	Aluminum	0.27	
Tarred fiber	Cast Iron	0.15	
Tarred fiber	Aluminum	0.18	
Polytetrafluoroethylene (PTFE)	Polytetrafluoroethylene (PTFE)	0.04	0.04, 0.04
Polytetrafluoroethylene (PTFE)	Steel	0.05 - 0.2	
Tungsten Carbide	Steel	0.4-0.6	0.1 - 0.2
Tungsten Carbide	Tungsten Carbide	0.2 - 0.25	0.12
Tungsten Carbide	Copper	0.35	
Tungsten Carbide	Iron	0.8	
Tin	Cast Iron	0.32	
Tire, dry	Road, dry	1	
Tire, wet	Road, wet	0.2	
Wood	Clean Wood	0.25 - 0.5	
Wood	Wet Wood	0.2	
Wood	Clean Metal	0.2 - 0.6	

Wood	Wet Metals	0.2	
Wood	Stone	0.2 - 0.4	
Wood	Concrete	0.62	
Wood	Brick	0.6	
Wood - waxed	Wet snow	0.14, 0.1	
Wood - waxed	Dry snow	0.04	
Zinc	Cast Iron	0.85, 0.21	
Zinc	Zinc	0.6	0.04

Appendix F   Stresses on the throat plane of fillet welds

This section provides insight into the way that the stresses at the throat plane of the fillet welds were defined. It, therefore, concerns both section 4.6 and the results of Table 5-4 of section 5.5.3 regarding weld root cracking.

1) Fillet welds in either (a) connecting a HEA's end to a plate or (b) connecting two HEA members perpendicularly

The following figure illustrates such situations, where fillet welds are used circumferentially to the section of the HEA member.
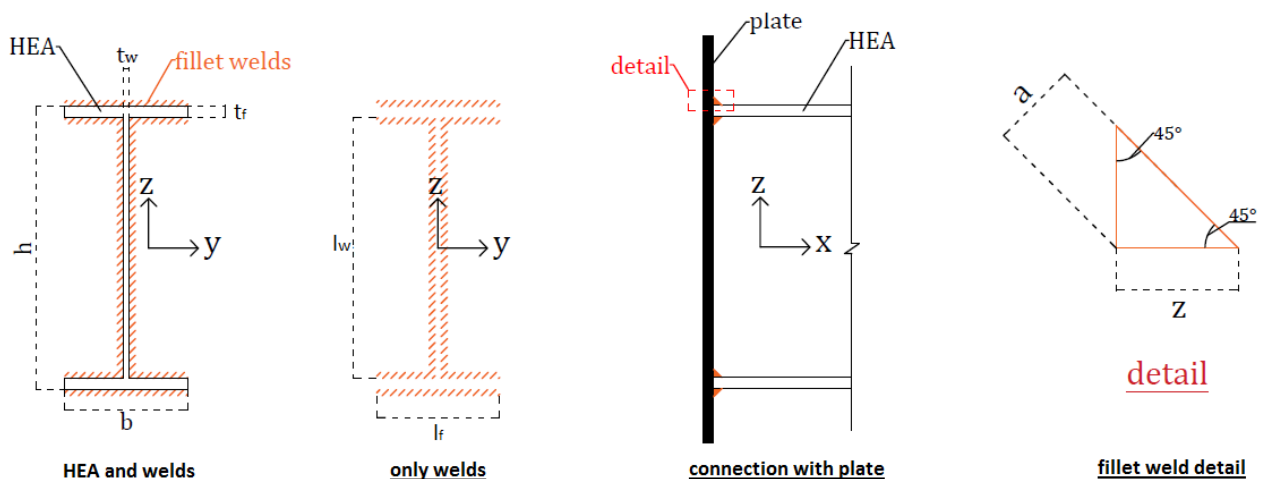

HEA and welds   **only welds**   **connection with plate**   **fillet weld detail**

Figure F. 1 – Weld attachment of HEA section to end plate

The weld properties were first defined according to the following formulas:

- area of flange welds:
$$A_f = 2 \cdot a_f \cdot l_f$$

- area of web welds:
$$A_w = 2 \cdot a_w \cdot l_w$$

- total area of weld:
$$A_{tot} = 2 \cdot A_f + A_w$$

- moment of inertia over y:

$$I_y = 4 \cdot \frac{l_f \cdot a_f^3}{12} + 2 \cdot \left\{ l_f \cdot a_f \cdot \left(\frac{h + a_f}{2} \right)^2 \right\} + 2 \cdot \left\{ l_f \cdot a_f \cdot \left(\frac{h - a_f}{2} \right)^2 \right\} + 2 \cdot \frac{a_w \cdot l_w^3}{12}$$

- moment of inertia over z:

$$I_z = 4 \cdot \frac{a_f \cdot l_f^3}{12} + 2 \cdot \left\{ l_w \cdot a_w \cdot \left(\frac{t_w + a_w}{2} \right)^2 \right\} + 2 \cdot \frac{l_w \cdot a_w^3}{12}$$

where: h is the total height of the HEA section

       b is the flange width of the HEA section

       t_w is the web thickness of the HEA section

       t_f is the flange thickness of the HEA section

       z_f is the leg size of the fillet weld used in the flange connections

       $a_f = \frac{z_f}{\sqrt{2}}$ is the throat size of the fillet weld used in the flange connections

       $l_f = b$ is the length of the welds used in the flanges

       z_w is the leg size of the fillet weld used in the web connections

       $a_w = \frac{z_w}{\sqrt{2}}$ is the throat size of the fillet weld used in the web connections

       l_w=h   is the length of the welds used in the web

After defining the weld properties, the corresponding to the throat plane stresses were determined, considering the end forces and moments applied. The following apply:

- maximum normal to the throat plane stresses:

$$\sigma_\perp{}^{web} = \frac{\frac{\sqrt{2}}{2} \cdot F_x}{A_{tot}} + \frac{M_y}{I_y} \cdot \frac{(h - 2 \cdot t_f)}{2} + \frac{M_z}{I_z} \cdot \frac{t_w}{2}$$

$$\sigma_\perp{}^{flange} = \frac{\frac{\sqrt{2}}{2} \cdot F_x}{A_{tot}} + \frac{M_y}{I_y} \cdot \frac{h}{2} + \frac{M_z}{I_z} \cdot \frac{b}{2}$$

- shear stresses in the throat plane acting parallel to the longitudinal axis of the weld:

$$\tau_{||}{}^{flange} = \frac{F_y}{2 \cdot A_f}$$

$$\tau_{||}{}^{web} = \frac{F_z}{A_w}$$

- shear stresses in the throat plane acting perpendicular to the longitudinal axis of the weld:

$$\tau_{\perp d}{}^{flange} = \tau_{\perp d}{}^{web} = \frac{\frac{\sqrt{2}}{2} \cdot F_x}{A_{tot}}$$

where: F_x is the axial force applied at that end

           F_y is the horizontal shear force applied at that end

           F_z is the vertical shear force applied at that end

           M_y is the in-plane bending moment applied at that end

           M_z is the out-of-plane bending moment applied at that end

           $\frac{\sqrt{2}}{2}$ is the factor corresponding to either the $\sin 45°$ or $\cos 45°$ for analysing the applied axial force into the throat plane of the fillet weld

2)   Fillet welds connecting the bearing pads at the top flange of the HE700A section

This situation is demonstrated in Figure F. 2 below, where fillet welds are used circumferentially to the bearing pad in order to be attached at the top flange of the HEA section.
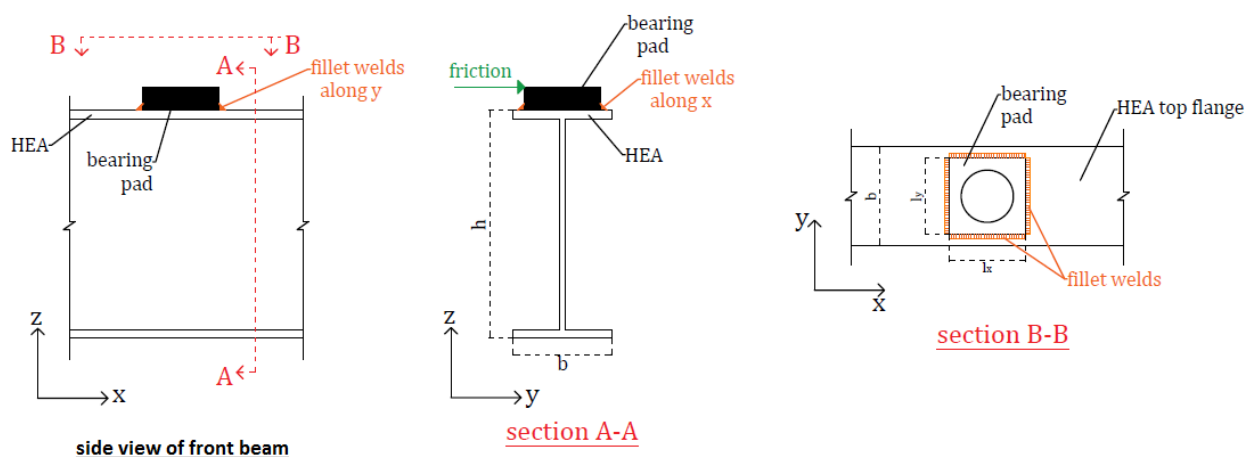

Figure F. 2 – Weld attachment of bearing pad at the top flange of HEA

In this situation, the only load affecting the welds is the generated friction that acts at the bearing pad. According to the above figure, friction acts along y-axis, thus affecting the fillet welds along y. The corresponding resultant stresses in the throat plane of the fillet weld are shear ones acting parallel to the longitudinal axis of the weld. Thus, the following apply:

$$\tau_{\parallel}{}^{y-welds} = \frac{friction}{2 \cdot A_y}$$

where: $friction$ is the generated friction

           $A_y = a_y \cdot l_y$ is the area of the welds along the y axis

           $a_y = \frac{z_y}{\sqrt{2}}$ is the throat size of the fillet welds used along the y axis

           z_y is the leg size of the fillet welds used along the y axis

           l_y is the length of the welds used along the y axis